A Palaeomagnetic study of selected formations in the Waterberg Group, South Africa

by

Leonie Pauline Maré

Submitted in partial fulfilment of the requirements for the degree

MASTER OF SCIENCE

in the Faculty of Natural & Agricultural Science

University of Pretoria

Pretoria

October 2003

ABSTRACT

A palaeomagnetic study of the Waterberg Group (Jones and McElhinny, 1967) did not find a consistent direction. However, a pattern was identified and interpreted in terms of apparent polar wander during the deposition and consolidation of the Waterberg sediments. These pole positions indicated that the Waterberg Group sedimentation commenced during emplacement of the Bushveld Complex, and intermittently continued through numerous tectonic events in the pre-existing Transvaal Basin to just before the Umkondo thermal event.

The Swaershoek Formation as the basal unit of the Waterberg Group in the Nylstroom Protobasin has been tentatively correlated with the Wilge River Formation in the Middelburg Basin. A palaeomagnetic study has been conducted on the Swaershoek and Wilge River Formations in an attempt to re-determine the palaeomagnetic pole positions for these two Formations and to confirm the said geological correlation. A total of 49 sites across both basins were sampled, both within the sediments as well as in the associated diabase intrusions. Despite generally weak results, the calculated pole positions for the Swaershoek Formation (37.1° S, 335.9° E and A_{95}: 17.4°) and the Wilge River Formation (31.9° S, 332.7° E and A_{95}: 20.5°) correlate very well, thereby confirming the association made between these two formations.

The intrusive diabase in both basins was sampled to test for thermal overprinting of the calculated pole positions of the sediments. Although the calculated pole positions for the diabase intrusion in the Nylstroom Protobasin (63.3° S, 233.2° E and A_{95}: 35.7°) is very weak, it correlates well with the diabase in the Middelburg Basin (69.3° S, 208.5° E and A_{95}: 14.2°). These two poles correlate very well with previous studies on post-Waterberg diabase (Jones and McElhinny, 1966) as well as on the Umkondo diabase (McElhinny and Opdyke, 1964). The pole positions from the Waterberg sediments and associated diabase are sufficiently displaced from each other to rule out any overprinting by these intrusions.

Recent results from the Blouberg area (Bumby *et al.*, 2001) indicate the Soutpansberg Group to be younger than the Waterberg Group. In an attempt to refine the Apparent Polar Wander Path (APWP) for the middle Proterozoic, another 6 sites from the Mogalakwena Formation (Waterberg Group) were sampled. Bumby *et al.* (2001) suggested that the Mogalakwena Formation pre-date the Wyllies Poort Formation (Soutpansberg Group). The calculated pole position for the Mogalakwena Formation was very weak, but correlated fairly well with a pole position (Group 2, McElhinny, 1968) from the Wyllies Poort Formation in the Soutpansberg Group. The location of the Mogalakwena Formation pole (36.1° S, 207.3° E and A_{95}: 27.6°) on the APWP for Southern Africa confirms the Waterberg Group to be older than the Soutpansberg Group.

OPSOMMING

'n Palaeomagnetiese studie deur Jones en McElhinny (1967) kon nie 'n enkel riginting vir die Waterberg Groep oplewer nie. 'n Patroon is egter ge-identifiseer in terme van pooldwaling tydens die neerlegging en konsolidasie van die Waterberg sedimente. Hierdie poolrigtings dui daarop dat neerlegging van die Waterberg Groep sedimente ontstaan het tydens die indringing van die Bosveld Kompleks, en onderbroke voort geduur het ten tye van verskeie tektoniese gebeure in die bestaande Transvaal Kom tot net voor die Umkondo termiese gebeurtenis.

Die Swaershoek Formasie, as basis eenheid van die Waterberg Groep in die Nylstroomprotokom, word tentatief met die Wilgerivier Formasie in die Middelburgkom gekorreleer. A palaeomagnetiese studie is op hierdie twee formasies uitgevoer in 'n poging om die genoemde geologiese korrelasie te bevestig. In totaal is 49 lokaliteite verspreid oor beide komme bemonster. Rotsmonsters van beide die sedimente sowel as die geassosieerde diabaas intrusies is geneem. Ten spyte daarvan dat die resultate oor die algemeen swak is, korreleer die berekende poolposisies vir die Swaershoek Formasie (37.1° S, 335.9° E en A_{95}:17.4°) en die Wilgerivier Formasie (31.9° S, 332.7° E en A_{95}:20.5°) baie goed. Hierdie goeie korrelasie bevestig die verwantskap wat tussen die twee formasies bestaan.

Die intrusiewe diabaas van beide komme is gemonster om te toets vir enige termiese poolherskrywing van die berekende poolrigtings van sedimente. Die berekende poolposisie van die diabaas intrusie in die Nylstroomprotokom (63.3° S, 233.2° E en A_{95}: 35.7°) is baie swak, maar vergelyk goed met die diabaas in die Middelburgkom (69.3° S, 208.5° E en A_{95}: 14.2°). Beide hierdie poolposisies stem baie goed ooreen met vorige studies op na-Waterbergse diabaas (Jones en McElhinny, 1966) sowel as op die Umkondo diabaas (McElhinny en Opdyke, 1964). Die poolposisies van die Waterberg sedimente en die geassosieerde diabaas is genoegsaam van mekaar verwyder om enige poolherskrywing deur hierdie intrusies uit te skakel.

'n Onlangse studie in die Blouberg omgewing (Bumby *et al.*, 2001) dui daarop dat die Soutpansberg Groep jonger is as die Waterberg Groep. In 'n poging om die pooldwalingskurwe (APWP) vir die middel Proterozoikuur te verfyn, is 6 addisionele lokaliteite van die Mogalakwena Formasie (Waterberg Groep) bemonster. Bumby *et al.* (2001) stel voor dat die Mogalakwena Formasie ouer is as die Wyllies Poort Formasie (Soutpansberg Groep). Die berekende poolposisie vir hierdie formasie was weereens baie swak, maar korreleer redelik goed met 'n poolposisie (groep 2, McElhinny, 1968) vir die Willies Poort Formasie in die Soutpansberg Groep. Die posisie van die Mogalakwena Formasie pool (36.1° S, 207.3° E en A_{95}: 27.6°) op die pooldwalingskurwe (APWP) vir suidelike Afrika bevestig dat die Waterberg Groep ouer is as die Soutpansberg Groep.

CONTENTS

LIST OF FIGURES

LIST OF TABLES

1. INTRODUCTION

The primary objective of palaeomagnetic research is to obtain a record of past configurations of the geomagnetic field. To determine the Earth's history of continental aggregation, mobile belt formation and continental dispersal, palaeomagnetic data are needed from rocks of known age from as many crustal domains as possible (Butler, 1992). For this purpose the palaeomagnetic pole position, which is the geographical location of the projection of the site-mean declination and inclination onto the Earth's surface, is calculated. By integrating palaeomagnetic poles from rocks of varying known geological age from numerous sites on the Earth an Apparent Polar Wandering Path (APWP) for continent and/or mobile belt activities through time can be derived (Butler, 1992).

The Waterberg Group occurs in the Limpopo, Northwest, Gauteng and Mpumalanga Provinces in South Africa, as well as in the eastern part of Botswana (Fig. 1.1). According to Callaghan (1993) the main depository evolved as a continental, fault-bounded basin in the northern part of the Kaapvaal Craton. Callaghan (1993) further indicated that the Main Basin is bounded in the south by the Murchison fault zone and in the north by the Melinda fault zone (Fig. 1.1).

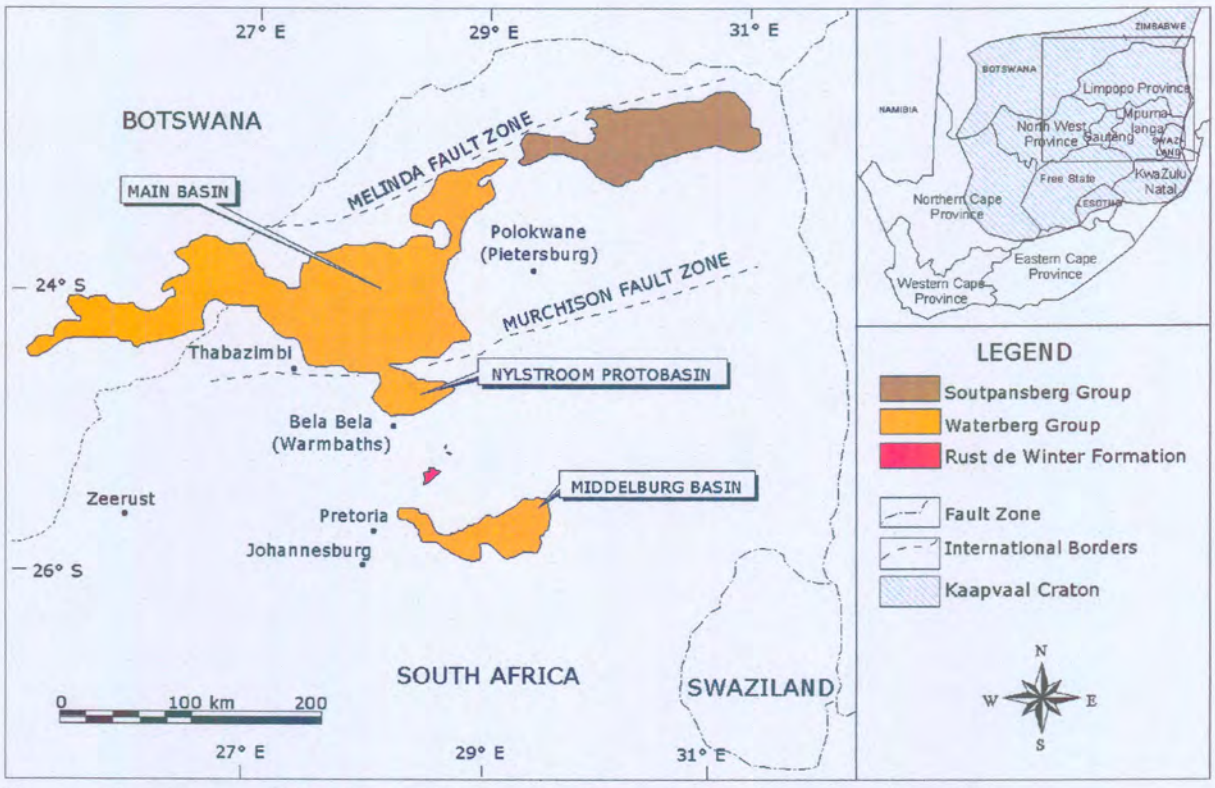

Figure 1.1: Locality map of Waterberg and Soutpansberg Groups (modified from Callaghan, 1987).

The Waterberg Group consists of twelve formations, some of which grade laterally into others (Callaghan *et al.*, 1991). The main depository hosts eleven formations (Fig. 1.2) that are grouped into the Nylstroom, Matlabas and Kransberg subgroups (Fig. 1.3) (SACS, 1980). The twelfth Formation is situated in the Middelburg Basin some distance to the south.

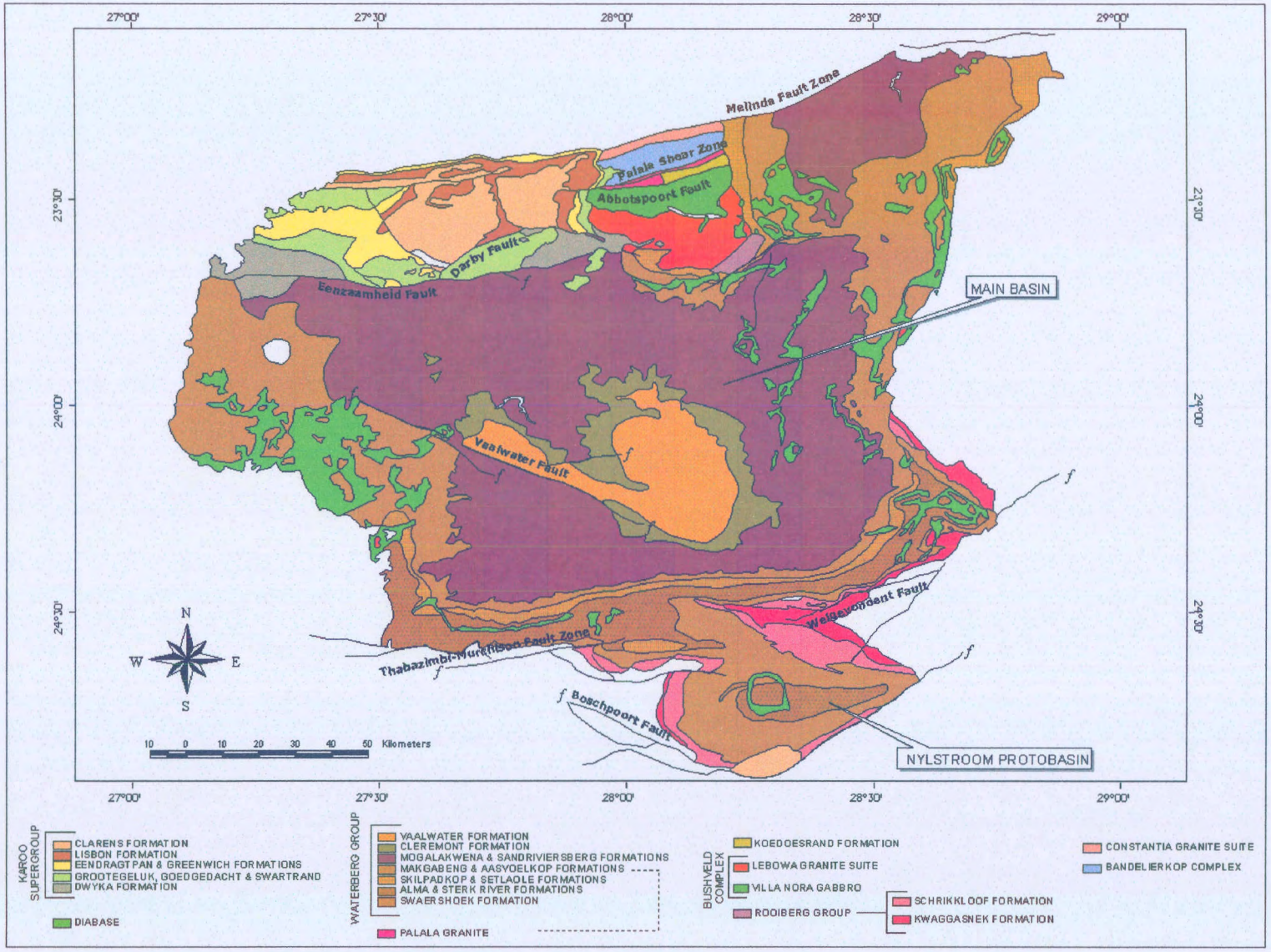

Figure 1.2: Distribution of the eleven lithostratigraphic units in the main Waterberg Basin (modified from the 1:1 000 000 geological map of the Republic of South Africa, 1997).

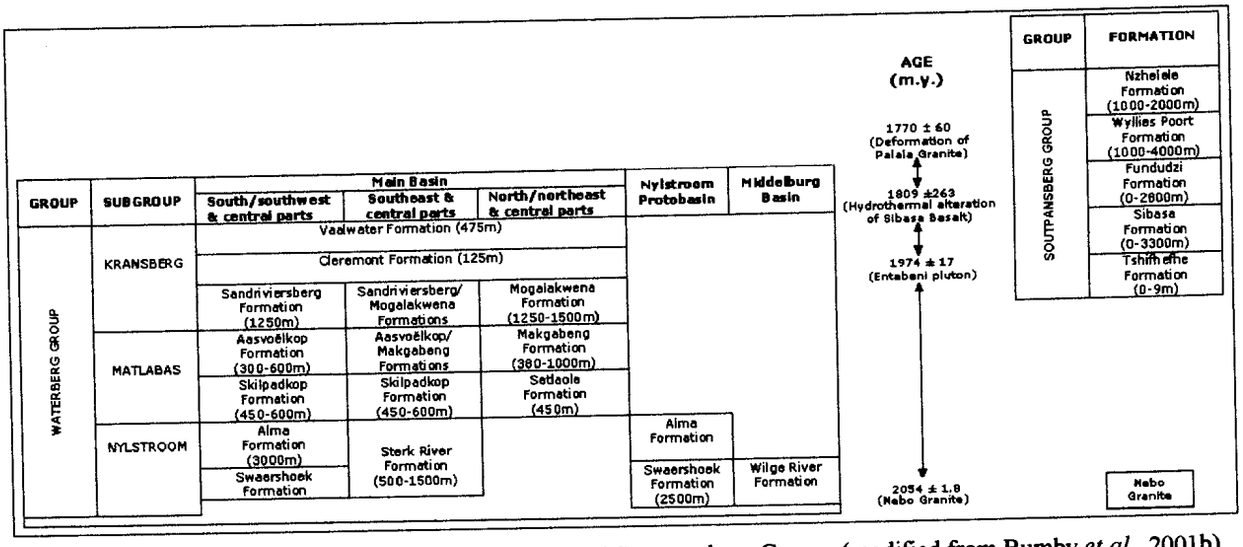

Figure 1.3: Stratigraphic subdivision of the Waterberg and Soutpansberg Groups (modified from Bumby *et al.*, 2001b).

The Waterberg Group is Palaeoproterozoic (Mokolian) in age and is generally regarded as being 1900-1700 Ma old (SACS, 1980). The Nebo Granites from the Lebowa Granite Suite in the Bushveld Complex that were dated by Walraven *et al.* (1993) as 2054.4 ± 1.8 Ma., yield the lower limiting date of the Waterberg Group. The Palala Granite is sheared by the Abbotspoort fault (Fig. 1.2), and the age of the deformation (but not of the intrusion) of the Palala Granite is well established at 1770 ± 60 Ma. (Walraven *et al.*, 1983; Barton and McCourt, 1983, Burger and Coertze, 1974). The Abbotspoort fault does not cut the Makgabeng Formation or the Mogalakwena Formation (Jansen, 1982) indicating that these Formations must be somewhat younger than the deformation, but how much younger is not known. To date the deformation of the Palala Granite was regarded as the upper limiting age of the Waterberg Group.

Previously, the Soutpansberg succession (Fig. 1.1) was regarded as part of the Waterberg sedimentary cycle (Van Eeden, 1972). However, according to Jansen (1976) the Soutpansberg succession must be regarded as an independent Group representing accumulation over a much larger time interval, from middle- to post-Waterberg. In a recent study by Bumby *et al.* (2001b) it was determined, both by field and geochemical data from the Blouberg area that the Mogalakwena Formation pre-dates the Wyllies Poort Formation. The study by Bumby *et al.* (2001b) demonstrates that the Sibasa Formation, Soutpansberg Group also post-dates the Mogalakwena Formation. The Sibasa Formation has been dated by Cheney *et al.* (1990) between 1974-1800 Ma. (Rb-Sr whole rock). Depending on the accuracy of such dates, this work suggests that the Waterberg Group may be older than previously thought.

Jansen (1982) describes the Swaershoek Formation as the basal unit of the Waterberg Group in the Nylstroom Protobasin, and correlates it with the Wilge River Formation in the Middelburg Basin. Both the Swaershoek and the Wilge River Formations are confined within the limits of the Transvaal Basin (Coertze *et al.*, 1977). The composition of pebbles and fragments in the arenaceous beds of both the Swaershoek and Wilge River Formations indicate the Transvaal Group as the main source area (Jansen, 1982; Visser *et al.*, 1961).

In a palaeomagnetic study of the Waterberg sediments (12 sites from four different areas), Jones and McElhinny (1967) did not find a consistent direction. They however identified a pattern that was interpreted in terms of apparent polar

wander during the deposition and consolidation of the Waterberg sediments. Allsopp *et al.* (1989) noted that these pole positions showed that deposition of the Waterberg Group commenced during emplacement of the Bushveld Complex, and intermittently continued through numerous tectonic events in the Transvaal Basin to just before the Umkondo thermal event, dated at 1080 +140/-25 Ma. However, Jones and McElhinny's (1967) sampling sites were spread over different stratigraphic units including the Middelburg Basin, the Nylstroom Protobasin as well as the Soutpansberg Group. Allsopp *et al.* (1989) suggested that the results of Jones and McElhinny (1967) should be viewed as preliminary, and that a major, detailed palaeomagnetic study of the Waterberg sediments would serve to test the different depositional models.

The aim of this study is to start this process by re-determining the palaeomagnetic correlation between the basal Swaershoek Formation in the Nylstroom Protobasin and the Wilge River Formation in the Middelburg Basin if any. Taking into account the recently determined stratigraphic relationship between the Waterberg and Soutpansberg Groups (Bumby *et al.*, 2001b), the secondary aim of this study is to calculate the palaeomagnetic pole position for the Mogalakwena Formation and correlate it with results from the Soutpansberg Group.

2. COLLECTION AND PREPARATION OF ROCK SAMPLES

A. The distribution of sampling sites

There are several goals in sampling rock units. One is to average the errors involved in the sampling process itself. Another is to assess the reliability of the geological recording medium. In addition, we often wish to average the scatter caused by secular variation of the geomagnetic field in order to estimate the time-averaged palaeomagnetic field direction representative of the time that the rock unit acquired its magnetization (Tauxe, 2002). The proper number of sites for a palaeomagnetic study is a matter of debate, but according to Butler (1992) ten or more sites are required for reasonable averaging of geomagnetic secular variation and for estimating dispersion of site-mean Virtual Geomagnetic Poles (VGP's). Tauxe (2002) suggests that the number of samples taken should be tailored to the particular project at hand. If one wishes to know polarity, perhaps three samples would be sufficient (these would be taken primarily to assess "geological noise"). If, on the other hand, one wished to make inferences about secular variation of the geomagnetic field, more samples would be necessary to suppress sampling noise. In order to determine the time-averaged palaeomagnetic field direction, the secular variation of the geomagnetic field (palaeomagnetic "noise") needs to be averaged (Tauxe, 2002). According to Tauxe (2002) a good rule of thumb is about ten sites (each with nine to ten samples).

Figure 2.1 is a simplified geological map of the Waterberg Group indicating all the sampling sites from this study. Sampling was restricted to streambeds where possible or low-lying rock outcrops and this, together with the exclusion of conglomerate layers for sampling, explain the uneven distribution of the sampling sites for this study. Samples were drilled a few metres apart at each site so that possible components due to lightning would vary in direction and magnitude (Gough, 1967).

Cores were drilled at 14 sites in the Swaershoek Formation (Nylstroom Protobasin), 19 sites in the Wilge River Formation (Middelburg Basin) and an additional 6 sites in the Mogalakwena Formation (Main Basin). The intrusive rocks in both the Swaershoek- and Wilge River Formations were also sampled to test for magnetic overprinting. Cores were drilled at 8 sites in the Wilge River diabase, while in the Swaershoek Formation cores were drilled at 6 diabase sites and 2 trachytic lava sites.

B. Sampling techniques

Cores were drilled in the field with a portable drill. The power source for this drill is a small two-stroke petrol engine, such as is used for portable chainsaws. It was modified to take a tubular drill bit and is water fed for cooling. The cores obtained were up to 200mm in length with a diameter of 25mm.

The samples were orientated in situ in the geographical framework by means of a sun compass as described by Creer and Sanver (1967), as well as with magnetic compass. During the sampling of the Swaershoek Formation the weather was overcast for several days resulting in some samples being orientated only by magnetic compass. Due to the very low magnetic intensity of the sediments, any

deflection of the compass reading would have been minimal. The sun compass is both fast and precise, being accurate to within 1 degree if the time is known within two minutes and the location within 0.5 degrees (Tarling, 1971).

According to Butler (1992) the collection of at least six to eight separately oriented samples from a site spread over 5 to 10m of outcrop is sufficient to evaluate within-site homogeneity of the Normal Remanent Magnetization (NRM). The number of cores drilled at each site for this study varied between five where the outcrop was limited, and eight.

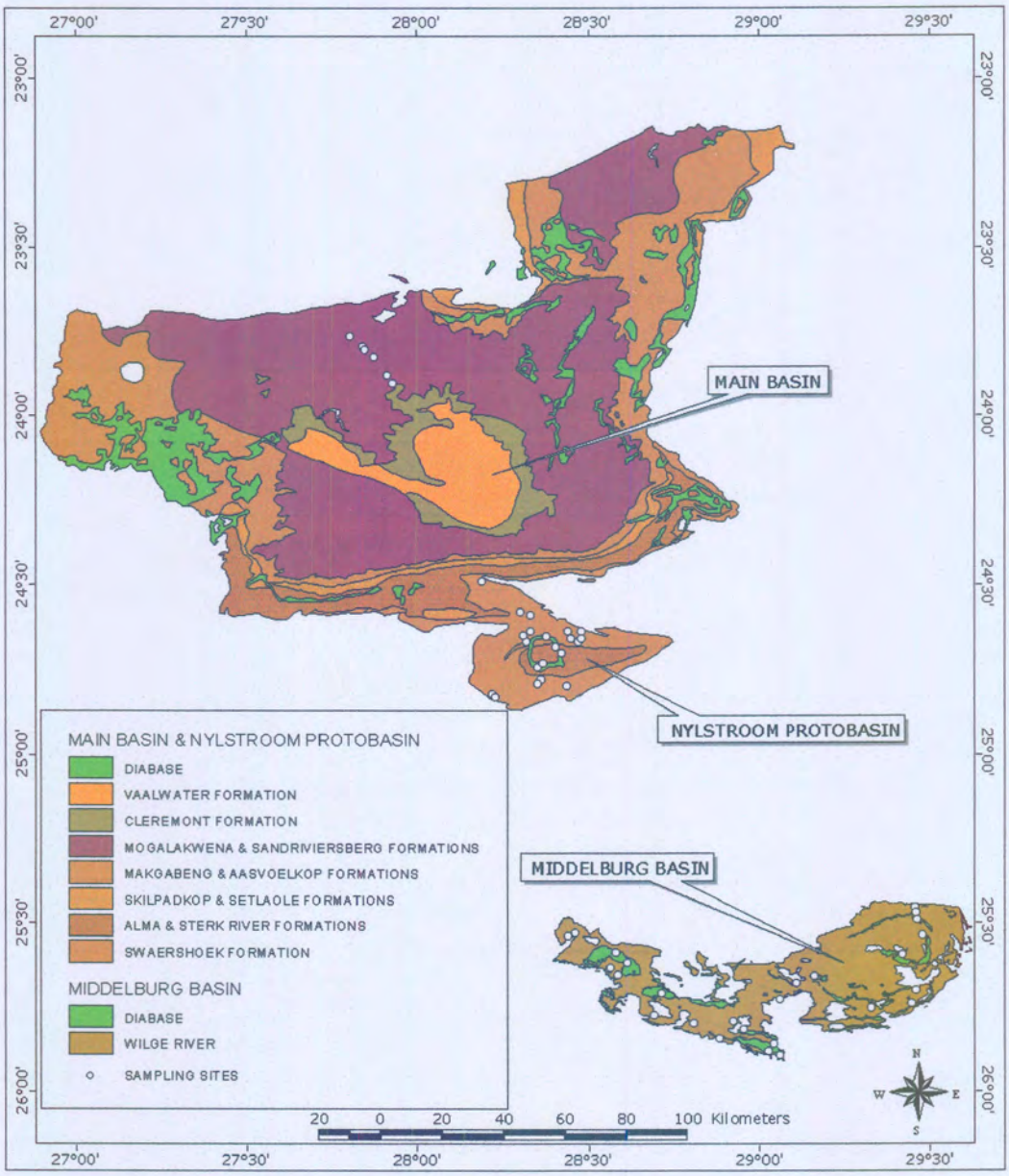

Figure 2.1: Simplified geological map of the Waterberg Group indicating the locations of all the sampling sites from this study.

C. Sample preparation

Initial laboratory procedures comprised the careful marking of the separate specimen names on each core sample. The core samples were then cut into 25mm length specimens with a non-magnetic diamond edged blade. This size (~10cc) is the standard size that most palaeomagnetic measuring equipment is designed and calibrated for. Thin sections were made from the remaining specimens for petrological and mineralogical investigations.

D. Measurement of the bedding dip and dip directions

Dip and dip direction of the sedimentary layering was measured at each sampling site where possible. In the remaining cases the regional dip and dip directions were instead taken from the 1:250 000 geological sheets (Brandl, G., 1993 and Walraven, F., 1978). In the case of the Swaershoek Formation the published dips from Jansen (1970) were also used.

3. LABORATORY MEASUREMENTS AND PROCEDURES

A. Laboratory Instruments

Bulk susceptibility measurements were made on these specimens using a low-field susceptibility bridge attached to the Digico system (Fuller, 1967). This bridge method makes use of the change in inductance of air-cored coils brought about by the introduction of a rock specimen. The fractional change of inductance ($\Delta L/L$) is linearly proportional to the susceptibility of the specimen and the volume ratio of the specimen to air space (p). The measurement of each specimen is repeated three times to determine its repeatability whereupon an average susceptibility value is calculated. This instrument was calibrated using a calibration specimen with known susceptibility value.

The anisotropy of magnetic susceptibility (AMS) was measured with a Digico Minisep system. The specimen, rotating at 7 Hz about a vertical axis, is surrounded by two coils with their axes horizontal and mutually perpendicular. One coil carries alternating current at a frequency of ~10 kHz, generating an applied field of ~0.5 mT root-mean-square (r.m.s.) at the specimen, and the other is the pick-up coil (Rathore, 1975). If the specimen is anisotropic in the plane perpendicular to the rotation axis a sinusoidal signal, proportional in amplitude to the difference in the principal susceptibilities in the horizontal plane in the specimen, is generated in the pick-up coil at twice the specimen rotation frequency. After measurements have been made with the specimen in three different orthogonal positions, phase and amplitude data of the sin 2θ components are used, in conjunction with a measurement of the axial susceptibility of the specimen, to compute the magnitudes of the maximum, intermediate and minimum susceptibilities and the orientation of the principal axes of the ellipsoid relative to a fiducial (reference direction) on the rotating shaft of the specimen.

The normal remanent magnetization (NRM) of specimens was measured using a Digico "Complete Results" fluxgate spinner magnetometer. This instrument spins a core specimen at 7 Hz to produce an output signal, the amplitude of which is proportional to the intensity of magnetization of the specimen. The phase of this signal relative to a fiducial on the rotating shaft, indicates the angle of the vector of magnetization in a plane perpendicular to the axis of rotation. Six successive measurements were made with the specimen in different orthogonal positions in the sample holder; this allowed the three orthogonal components of the remanent magnetization vector to be determined. The manufacturers of this instrument claim a sensitivity of 0.01×10^{-3} A/m. In practice, however, it was found that to measure a reliable direction of magnetization to within one degree a minimum intensity of magnetization of 0.5×10^{-3} A/m was required.

Progressive alternating-field (AF) demagnetization of specimens was done with an apparatus built at the Council for Geoscience following a description by McElhinny (1964a). The specimens were tumbled with a three-axis tumbler situated in the centre of a coil, through which a decaying 50 Hz current flowed which demagnetised all magnetic domains with coercivities below the maximum field

produced by the peak current. The whole apparatus is contained in Helmholtz coils that annul the earth's magnetic field at the tumbler and thus prevent specimens from acquiring an anhysteretic remanent magnetization (ARM) (Patton and Fitch, 1962). This demagnetization apparatus is capable of creating a peak alternating demagnetization field of 120 mT.

Progressive thermal demagnetization of specimens was done using the TSD-1 Thermal Demagnetiser from Schonstedt Instrument Co. This instrument provides progressive thermal demagnetization of specimens by heating them to any temperature up to 800° C and then cooling them in a zero magnetic field environment. The shield assembly attenuates external fields so that the instrument can be operated in normal laboratory environments. There are two separate chambers, one for heating and one for cooling. They are arranged coaxially so that as soon as specimens in the furnace chamber reach thermal equilibrium, the specimen holder can be pushed directly into the cooling chamber. Complete chamber isolation and individual controls allow one specimen batch to be blower cooled while another is being heated. An analogue proportional power controller affords temperature accuracy of 20° C with a repeatability of 5° C.

B. Laboratory Procedures

The bulk susceptibility and natural remanent magnetization (NRM) of each specimen was first measured, followed by statistical analysis of the susceptibility distribution and the NRM directions. Subsequently progressive AF demagnetization of a few pilot specimens was done and the remanent magnetization direction determined after each step. Components of magnetization were isolated from directions obtained from AF and thermal demagnetization by looking at the orthogonal vector plots, more commonly known as Zijderveld diagrams (Zijderveld, 1967), and by the use of principal component analysis as described by Kirschvink (1980). The program primarily used is modified after Kirschvink (1980) and employs a least-squares method for isolating demagnetization vectors and planes. It was found that this technique worked very well for most specimens analyzed. The Kirschvink program however was not very effective at isolating components that had small amounts of superimposed noise, or for isolating directions in specimens that had a very high NRM intensity relative to other demagnetization steps (e.g. a mean destructive field of less than 10 mT). In such a case, the Kirschvink programme weighted the chosen magnetic vector strongly toward the NRM direction, even if there were obvious (but weaker) components. A second program developed by Torsvik *et al.* (1996) makes use of "line-find" routines as described by Kent *et al.* (1983). This program was more effective at overcoming this second problem and was used in cases where the Kirschvink programme did not give suitable results.

Rocks with multiple components of NRM with severely overlapping spectra of blocking temperature or coercivity spectra often yield arcs or remagnetization circles during progressive demagnetization (Halls, 1975). A single great circle on its own provides insufficient information to estimate the

direction of the hidden component, but if more than one great circle is available (say from different specimens) and these great circles converge, then an estimate may be obtained. Furthermore, if a direct estimate is independently available through a stable endpoint obtained from another specimen, then this may also be used to access the information available in a great circle (Jones *et al.*, 1975; Halls, 1976 and 1977; McFadden, 1977; Bailey *et al.*, 1984). Due to the errors present in all palaeomagnetic data, however, the intersecting great circles invariably form a cluster of intersection points instead of one common point (Onstott, 1980). The axes perpendicular to these remagnetization circles in turn will tend to be dispersed around a great circle plane perpendicular to the cluster of intersection directions (Halls, 1976). Onstott (1980) proposes that the distribution of perpendicular axes about and along the great circle plane is approximately a Bingham distribution (Bingham, 1964). Quite a number of samples from this study contained multiple components as described above, and these were analyzed with a program (IAPD2000) developed by Torsvik *et al.* (1996).

It was found that in the majority of sandstone specimens progressive AF demagnetization was unable to successfully delineate the magnetic components. Thus, the remaining specimens were subjected to progressive thermal demagnetization up to temperatures of 800° C. The specimens were demagnetized thermally in steps of 100° C, and as each Curie point was approached, this was reduced to intervals of 20° C. The remanent magnetization was measured after each step and vector analysis applied.

All the specimens were also subjected to anisotropy of magnetic susceptibility (AMS) measurements. Graham (1954) first discussed the use of magnetic anisotropy in petrofabric analysis, but its application to geological problems has attracted growing interest only in the last two decades (Borradaile, 1988; and references therein). Magnetic susceptibility, K, is defined by M=KH, where M is the induced magnetism of the rock, and H is the inducing magnetic field. Magnetic susceptibility within a solid material varies with direction and is expressed by a second order symmetric tensor (ellipsoid) with maximum (K1), intermediate (K2) and minimum (K3) susceptibility axes (Nye, 1957).

The causes of AMS in rocks may be due to any one or a combination of the following effects (Stacey 1960; Park *et al.* 1988; Hargraves *et al.* 1991): (1) intra-crystalline anisotropy (magnetic hard or soft directions), (2) shape of individual magnetic grains (long axis coinciding with its maximum susceptibility), (3) distribution of magnetic minerals within the sample (distribution anisotropy), (4) alignment of magnetic domains (domain anisotropy), and (5) deformation of crystal lattices (stress-induced anisotropy). AMS may be used to identify preferred orientations in the rock, which may be caused by flow or by weak tectonic load. Where magnetic minerals align parallel to the flow direction, the long axis of the AMS ellipsoid (K1) indicates this direction (Owens 1974).

Four parameters are used to describe the observed magnetic anisotropy: (1) The bulk (mean) susceptibility of the sample, K=(K1 + K2 + K3)/3; (2) the total anisotropy, H=100(K1 - K3)/K (after Owens, 1974); (3) the degree of lineation, L= K1/K2 (Balsley and Buddington, 1960); and (4) the

degree of foliation, F=K2/K3 (Hrouda and Janak, 1976). A graph of L versus F reveals whether the preferred orientation of grains results in a prolate (L>F) or oblate (F>L) AMS ellipsoid (Flinn, 1962).

The purpose of the study of the magnetic anisotropy of sediments is to obtain some information on the deposition process of ferromagnetic grains. It has been found (Hrouda, 1982) that the process of orientation of ferromagnetic minerals is affected by several factors. The first and most important factor is the Earth's gravity field, the action of which causes the mineral particles to be deposited with their larger surfaces lying flat, parallel to the depositional surface on the bottom of the sedimentation basin. If the bottom is gently sloped, the grains may roll along the bottom and orientate their longer axes parallel to the contour line. On steeper slopes the long axes of grains become oriented parallel to the dip direction. The second important factor is the water current that tends to orientate the longer axes of grains parallel to the flow line. If the current is strong, some grains may roll and orientate their longer axes perpendicular to the current direction. The third important factor is the geomagnetic field, which orientates the longer axes of the ferromagnetic grains parallel to the local magnetic meridian.

Through experiments it has been found that the preferred orientation of ferromagnetic minerals in sedimentary rocks is controlled primarily by the hydrodynamic factors, while the geomagnetic field only influences grains smaller than 0.03 mm. The minimum susceptibility directions have been found to be perpendicular to the bedding under all the sedimentary regimes. Small deviations have been recorded in the case of sedimentation on a slope, but for practical purposes they can be ignored (usually they are less than 10°). These experiments are reported in papers by Rees (1966, 1968, and 1971), Hamilton and Loveland (1967), Hamilton *et al.* (1968) and Rees and Woodall (1975).

If a magnetically isotropic mineral of the magnetite type represents the ferromagnetic fraction, the magnetic lineation is usually parallel to the current direction and plunges slightly against the current. If the carrier of rock magnetism is haematite, the intermediate susceptibility direction is parallel to the water current (Hrouda and Janak, 1971; van den Ende, 1975).

Curie temperatures of ferromagnetic minerals can be determined from strong-field thermomagnetic experiments in which magnetization of a sample exposed to a strong magnetic field (>1000Oe = 100mT) is monitored while temperature is increased (Butler, 1992). For samples with magnetization dominated by the ferromagnetic minerals (rather than paramagnetic and/or diamagnetic minerals), measured strong-field magnetization approximates $\mathbf{J}_s$ of the ferromagnetic mineral(s). Curie temperatures (T_C) are determined as the points of major decrease in $\mathbf{J}_s$.

Strong-field thermomagnetic analysis was performed on selected specimens from all the different formations with a Curie balance designed and built at the Norwegian Geological Survey.

C. Statistical analysis of results

The statistical analysis of palaeomagnetic data is required for determining a mean direction from a set of observed directions. This method should provide some measure of uncertainty in the mean direction. Additionally, we need methods for testing the significance of field tests of palaeomagnetic stability. Any statistical method for determining a mean (and confidence limit) from a set of observations is based on a probability density function. This function describes the distribution of observations for a hypothetical, infinite set of observations called a population.

The Fisher distribution

A probability density function applicable to palaeomagnetic directions was developed by the British statistician R.A. Fisher (1953) and is known as the Fisher distribution. Each direction is given unit weight and is represented by a point on a sphere of unit radius. The Fisher distribution function $P_{dA}(\theta)$ gives the probability per unit angular area of finding a direction within an angular area, dA, centered at an angle θ from the true mean. Directions are distributed according to the probability density function

$$P_{dA}(\theta) = [\kappa/(4\pi\sinh(\kappa))]\exp(\kappa\cos\theta)$$

where θ is the angle from true direction (=0 at true mean), and κ is the precision parameter. The notation $P_{dA}(\theta)$ is used to emphasize that this is a probability per unit angular area.

The distribution of directions is azimuthally symmetric about the true mean. κ is a measure of the concentration of the distribution about the true mean direction. κ is 0 for a distribution of directions that is uniform over the sphere (random) and approaches ∞ for directions concentrated at a point.

The angle from the true mean within which a chosen percentage of directions lie can also be calculated from the Fisher distribution. The angle analogous to the standard deviation of the normal distribution is

$$\theta_{63}=81°/\sqrt{\kappa}$$

This angle is often called the angular standard deviation (Irving, 1964). The final critical angle of interest is that containing 95% of directions and given by

$$\theta_{95}=140°/\sqrt{\kappa}$$

Computing a mean direction

The above equations apply to a population of directions that is distributed according to the Fisher probability density function. But we commonly have only a small sample of directions (e.g., a data set of ten directions) for which we must calculate (1) a mean direction, (2) a statistic indicating the amount of scatter of the directions, and (3) a confidence limit for the calculated mean direction. By employing the Fisher distribution, the following calculation scheme can provide the desired quantities.

The mean of a set of directions is found simply by vector addition (McElhinny, 1973). To compute the mean direction from a set of N unit vectors, the direction cosines of the individual vectors are first determined by

$$l_i=\cos I_I\cos D_I\ ;\quad m_i=\cos I_I\cos D_I\ ;\quad n_i=\cos I_I\cos D_I$$

where D_I is the declination of the i vector; I_I is the inclination of the i vector; and l_I, m_I, and n_I are the direction cosines of the i vector with respect to north, east, and down directions (Tarling, 1971). The direction cosines, l, m, and n, of the mean direction are then given by

$$l=\sum l_i/R \; ; \quad m=\sum m_i/R \; ; \quad n=\sum n_i/R$$

where **R** is the resultant vector with length R given by

$$R^2=(\sum l_I)^2+(\sum m_I)^2+(\sum n_I)^2$$

According to Tarling (1971) the declination and inclination of the mean direction can thus be computed by

$$D_m=\tan^{-1}(m/l) \text{ and } I_m=\sin^{-1}(n)$$

Dispersion estimates

Having calculated the mean direction, the next objective is to determine a statistic that can provide a measure of the dispersion of the population of directions from which the sample data set was drawn. One measure of the dispersion of a population of directions is the precision parameter, κ. From a finite set of directions, κ is unknown, but a best estimate (k) of κ can be calculated by

$$k=(N-1)/(N-R)$$

with N the number of observations (Fisher, 1953). It can readily be seen that k increases as R approaches N for a tightly clustered set of directions.

The reliability of the mean direction can also be defined by measuring the radius (α) of a circle on the surface of the sphere, centered on the observed mean direction, within which there is a particular probability (ρ) of the true mean direction lying in this cone of confidence. The radius (α) can, according to Irving (1964), be expressed as

$$\alpha=\cos^{-1}(1-(N-R)/R)[\,\rho^{-(1/(N-1))}-1]$$

where ρ was taken, in most palaeomagnetic studies (Tarling, 1971), to be 0.05, so that there is a 20 to 1 chance of the true mean lying within α_{95} degrees of the observed mean.

By making use of the above-described methods the directions of magnetization of specimens were first averaged to give a sample mean. Sample means were then, in turn, combined to yield site mean directions, which were then combined to give the group overall mean directions. Watson's (1956) test for randomness of directions was then applied at sample and site levels. Sample or site mean directions, which were not significant at 95% probability, were rejected. The estimate k of the precision parameter κ and the radius (α_{95}) of the circle of confidence were calculated for each site, as well as for the different formation directions. The palaeomagnetic pole positions corresponding to group mean magnetization directions were calculated using the conventional premise that the Earth's field is that of a geocentric dipole (McElhinny, 1973). The polar error (dp, dm) is termed the oval of 95% confidence about the pole position. This was calculated from an equation given by McElhinny (1973).

C. Theoretic Background on Magnetization of Sediments

Although the magnetization of most red sediments probably arises from chemical remanent magnetization (CRM) (Collinson, 1965a), it is known however that detrital remanent magnetization (DRM) is a naturally occurring process, capable of explaining the observed remanent magnetization of some sediments (McElhinny, 1973). DRM describes the process of alignment of magnetic particles by an applied field as they fall through water and the rotation of such particles into the field direction when they are in the water-filled interstitial holes of wet sediment. The former, acquired at deposition due to particle alignment during sedimentation, is termed depositional DRM (dDRM), whilst the latter, due to particle rotation after deposition but prior to consolidation, is termed post-depositional DRM or pDRM (McElhinny, 1973). The depositional process has been investigated under controlled laboratory conditions by Johnson *et al.* (1948), King (1955) and Griffiths *et al.* (1960) and the post-depositional process by Irving and Major (1964). Nagata (1961), Stacey (1963), Collinson (1965b) and King and Rees (1966) have considered theoretically the alignment of magnetic particles as they fall through water.

Sedimentary rocks contain various kinds of magnetic minerals derived primarily from the physical and chemical weathering of igneous rocks (O'Reilly, 1984). Alteration of the magnetic minerals during weathering, transportation, sedimentation, and diagenesis may produce a mineral assemblage in a highly oxidized state. Then the ultimately stable iron oxide, haematite α-Fe_2O_3, can be the principal magnetic constituent of sedimentary rocks. Non-magnetic minerals in the source rocks may also be the origin of haematite (or magnetite) in sediments, either by direct transformation or via iron-bearing solutions (O'Reilly, 1984). Red sandstone and red beds are particularly useful carriers of palaeomagnetic information, and they commonly contain a few percent of haematite, and the remanence is rather weak, of the order of $10^{-2} \sim 10^{-3}$ A/m, while the coercive force is very high (Creer *et al.*, 1975). Grains of specular haematite that may thus possibly have originated when they settled in the water on deposition sometimes give the main magnetic property in rocks. In some rocks fine-grained haematite is present in the pigment which gives the characteristic red colour and stable magnetic remanence. Haematite is also present in red beds in the form of black grains of specularite, possibly resulting from the martitization or maghemitization/inversion of detrital magnetite particles. Unaltered magnetite is sometimes present but the contents in the sediment decrease with increasing age (O'Reilly, 1984).

Maghemite α-Fe_2O_3 occurs chiefly as the oxidation product of titanomagnetites and as such is thought to be responsible for the strong magnetization of lodestone. Although it has been rarely reported in red beds, maghemite may occur on a worldwide scale in laterites. Strictly, these are not sediments as they are produced by intense weathering of rocks when the silica is removed, leaving a residue rich in Al and Fe oxide (Creer *et al.*, 1975).

Ferric oxyhydroxides such as goethite α-FeOOH, occur in red beds and are thought to be responsible for the unstable magnetization of some rocks (Creer *et al.*, 1975).

The vector sum of dDRM and pDRM exhibits the actual remanent magnetization of the sediment (DRM). The best evidence for timing of remanence acquisition comes from field tests of palaeomagnetic stability. The consensus view is that red sediments with uncomplicated, high-stability characteristic remanent magnetization (ChRM) probably acquired this magnetization by processes that occurred within 1000 years after deposition. Palaeomagnetic data from these red sediments are useful for magnetic polarity stratigraphy and for determination of palaeomagnetic poles (Butler, 1992).

4. PREVIOUS PALAEOMAGNETIC STUDIES ON THE WATERBERG GROUP

In 1967 Jones and McElhinny published the results from a joint palaeomagnetic study on the Waterberg red beds. The aim of their study was to correlate the Waterberg and Umkondo Groups (then known as Systems), by determining the palaeomagnetic pole position of the Waterberg Group.

Samples were collected from twelve sites in the Waterberg succession in four localities (Fig. 4.1). Specimens from each site were subjected to both stepwise thermal and alternating field demagnetization. The site mean directions after both thermal and magnetic cleaning were usually well grouped away from the direction of the earth's magnetic field. After the stratum was restored to the horizontal at each site, the directions of magnetization fell into three groups.

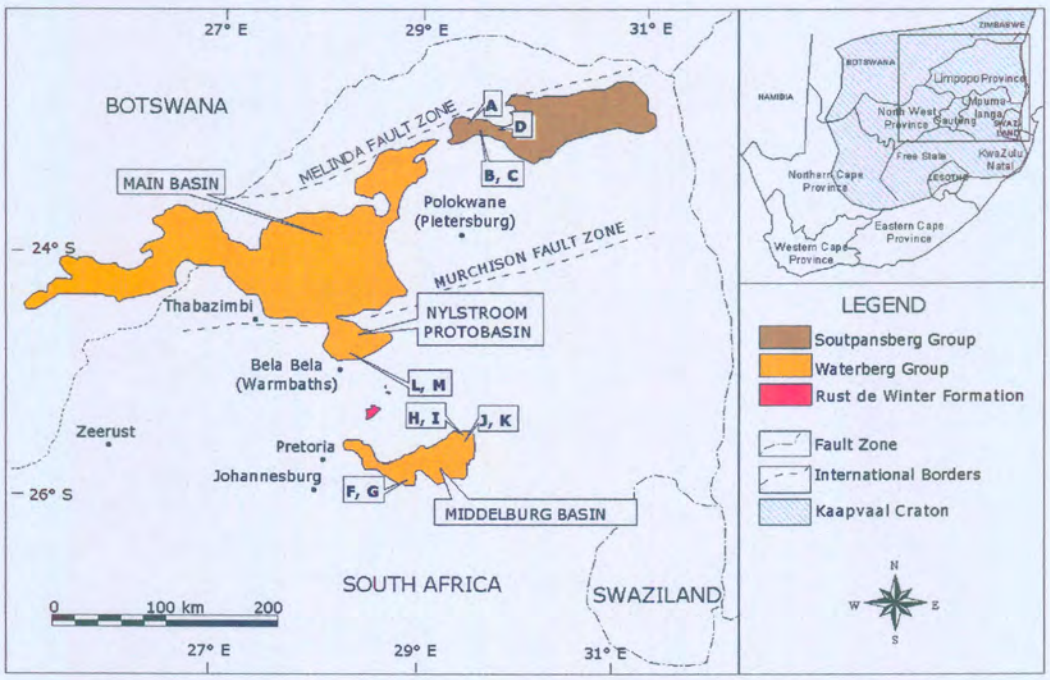

Figure 4.1: Locality map of Waterberg and Soutpansberg Groups (modified from Callaghan, 1987). Sampling sites from previous palaeomagnetic study indicated.

The authors (Jones and McElhinny, 1967) suggested that these results represent a pattern of polar wandering that occurred during the deposition and consolidation of the Waterberg Group. Their suggested path is shown in Fig. 4.2a. The most recent polar wandering path of selected pole positions from southern Africa is shown in Fig. 4.2b.

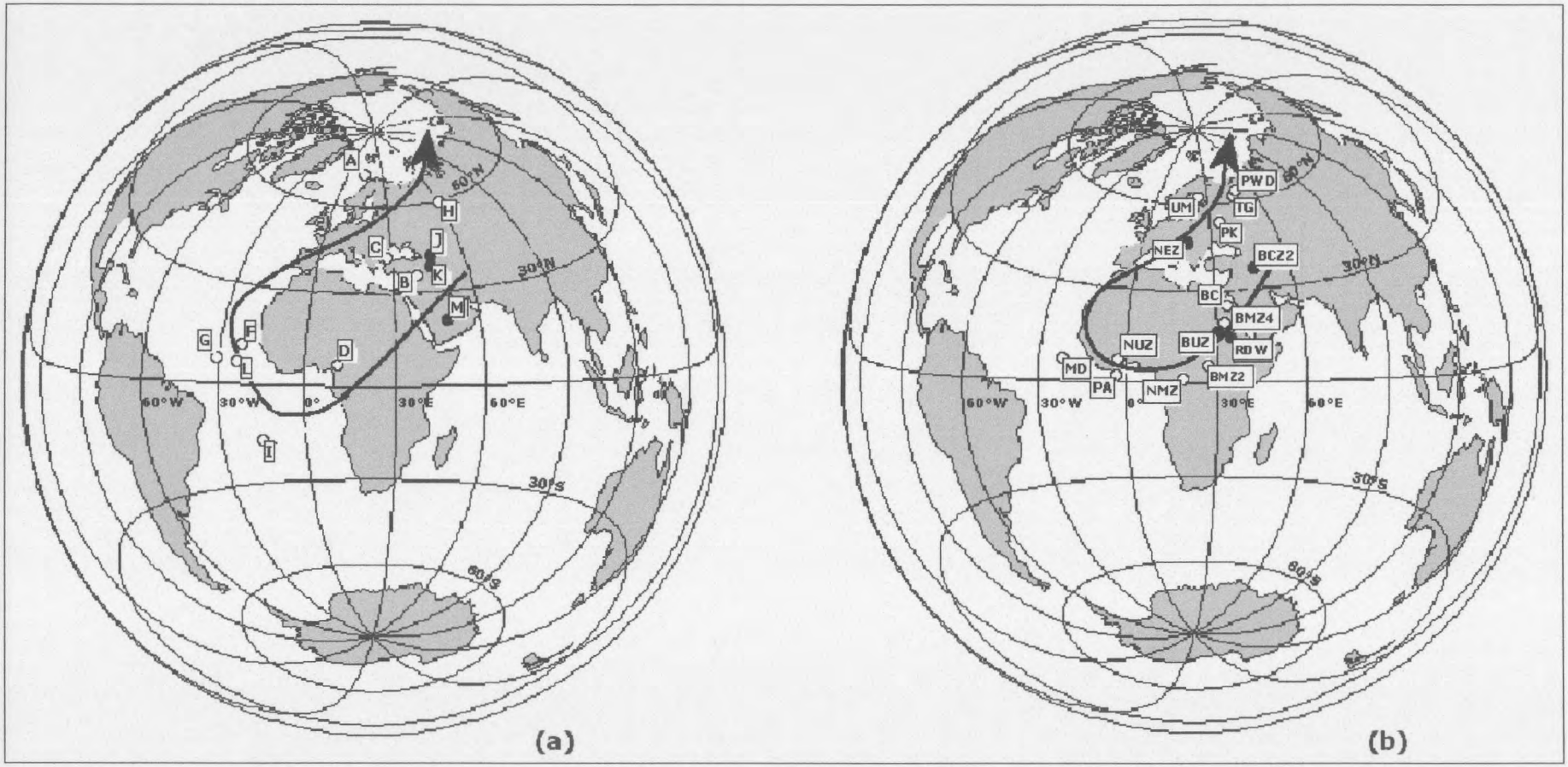

Figure 4.2: (a) APWP with virtual pole positions A-M from previous Waterberg Group study (Jones and McElhinny, 1967). (b) APWP for Africa with selected pole positions shown from Southern Africa for ca. 2070-1070 Ma. A detail of pole positions follows.

The palaeomagnetic pole positions as indicated in figure 4.2(b) are as follows: **BC** (2050 Ma) – Bushveld Complex (Gough and Van Niekerk, 1959,); **BMZ2** – subzone B, main zone (Hattingh, 1986b); **BMZ4** – subzone C, main zone (Hattingh, 1986b); **BCZ3** – critical zone, Bushveld Complex (Hattingh, 1986a); **BUZ** – Bushveld Complex Upper Zone (Hattingh, 1989); **NMZ** – Northern Bushveld Complex, main zone (Hattingh and Pauls, 1994); **NUZ** – Northern Bushveld Complex, upper zone (Hattingh and Pauls, 1994); **RDW** (2025 Ma) – Rust de Winter Formation (Morgan and Briden, 1981 and Walraven, 1981); **PA** – Phalaborwa syenite and dolerites (Morgan and Briden, 1981); **MD** (1830 Ma) – Mashonaland dolerites (McElhinny and Opdyke, 1964, Bates and Jones, 1996). Rock age from Morgan and Briden (1981); **NEZ** (1240 Ma) – Namaqua Eastern Zone (Evans *et al.*, 2002); **PK** – Premier Mine Kimberlite (Jones, 1968); **UM** (1080 Ma) – Umkondo igneous events (Hargraves, Hattingh and Onstott, 1994, Allsopp *et al.*, 1989); **PWD** (1090 Ma) – Post-Waterberg dolerite (Jones and McElhinny, 1966, Allsopp *et al.*, 1967, 1989); **TG** (1072 Ma) – Timbavati gabbro (Hargraves, Hattingh and Onstott, 1994).

Through continued research by different scientists the Waterberg Group has been divided into its presently defined stratigraphic units, given in SACS (1980). Figure 4.3 depicts the stratigraphic positions of the twelve sampling sites from Jones and McElhinny's (1967) study according to their presently defined stratigraphic positions. From figure 4.3 it is clear that most of their sampling sites (sites F, G, H, I, J, K and M) were located within the lower Waterberg Group (Swaershoek and Wilgerivier formations), while the rest (sites A, B, C and D) were located in the Soutpansberg Group.

Jones and McElhinny (1967) grouped the sites into three stratigraphic groups according to their pole positions: Site J, K and M from the base of the succession as group 1, while sites F, G, L and I which are certainly higher horizons than group 1 (but still in the Lower Waterberg) form group 2. Site A and H were grouped together as group 3, but it is clear from figure 4.3 that these two sites are not just of different stratigraphic age, but also from different stratigraphic units.

In a later publication McElhinny (1968) regrouped the results into five groups. Sites A and H formed group 1, sites B and C formed group 2, while sites F, G, L and I form group 3. McElhinny gave the samples from site D unit weight and calculated a pole position for this single site, and regarded it as group 4. Site J, K and M were grouped together to form group 5.

Some doubt exists regarding the statistical validity of the previous authors' calculated pole positions, since McElhinny (1973) himself suggested that poles calculated from fewer than three sites could only be regarded as virtual palaeomagnetic poles.

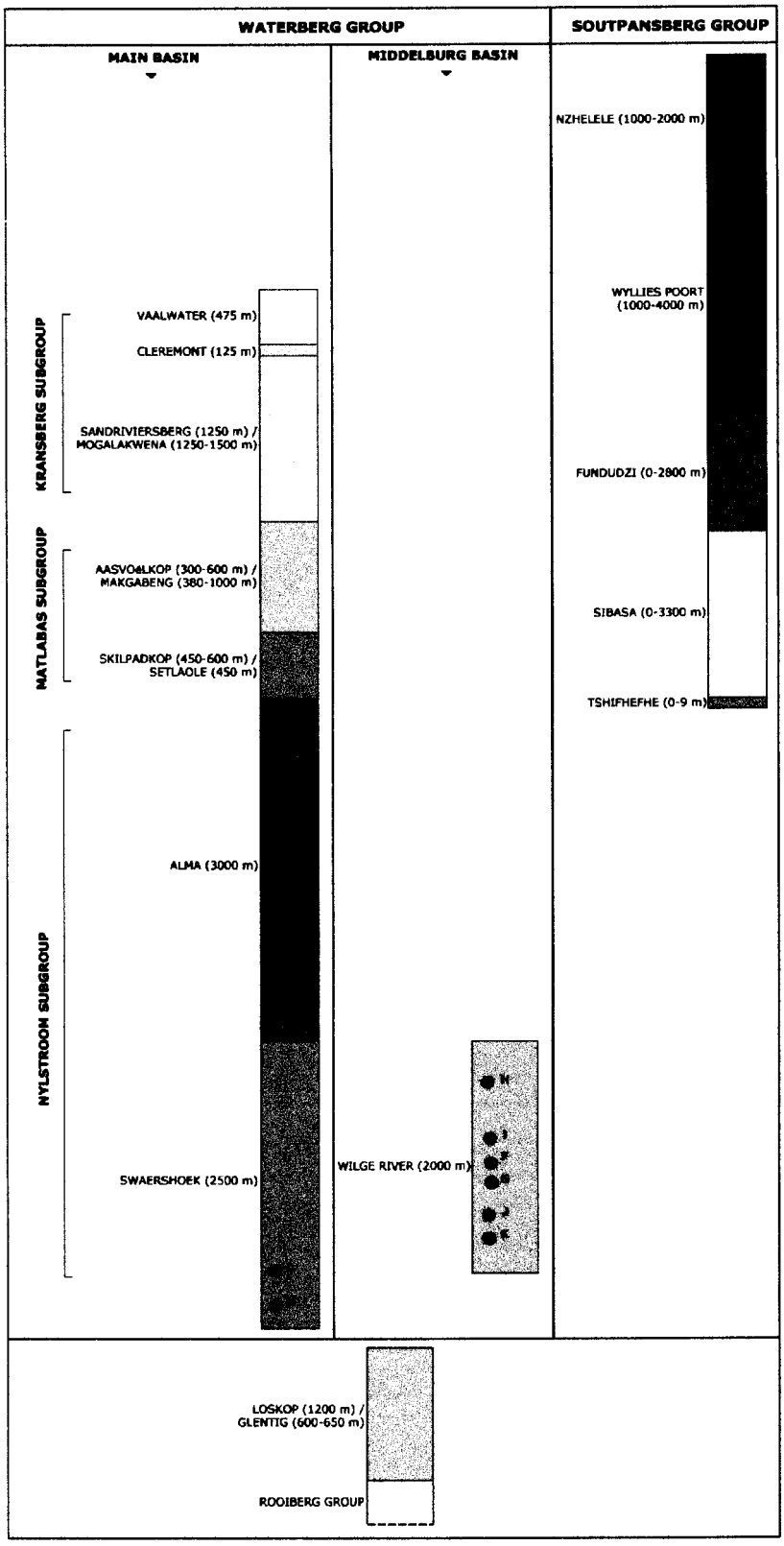

Figure 4.3: Stratigraphic subdivision of Waterberg and Soutpansberg Groups indicating the stratigraphic positions of the sampling sites (Jones and McElhinny, 1967). Formations are shown according to structural thickness (SACS, 1980).

The pole positions indicated by both the studies of Jones and McElhinny (1967) and McElhinny (1968) indicate that deposition of the Waterberg Group commenced during emplacement of the Bushveld Complex, and intermittently continued through numerous tectonic events in the pre-existing Transvaal basin to just before the Umkondo thermal event (Allsopp *et al.*, 1989). However, Jones and McElhinny's (1967) sampling site were spread over different stratigraphic units including the Middelburg Basin, the Nylstroom Protobasin as well as the Soutpansberg Group. Allsopp *et al.* (1989) suggested that the results of Jones and McElhinny (1967) should be viewed as preliminary, and that a major, detailed palaeomagnetic study of the Waterberg sediments would serve to test the different depositional models.

5. THE PALAEOMAGNETISM OF THE SWAERSHOEK FORMATION

A. Geology.

Jansen (1982) describes the Swaershoek Formation as the basal unit of the Waterberg Group in the Main Basin (Figure 5.1). It occurs largely in the Nylstroom Protobasin and Alma trough of the Main Basin (Coertze *et al.*, 1977). The Swaershoek Formation is lenticular on a regional scale, showing a rapid thickness variation from 2500m (Figure 5.2) in the central portion of the Nylstroom Protobasin (De Vries, 1970) to a few hundred meters or less at the present day edges of the basin.

The geographic distribution of this formation differs considerably from those higher up in the succession (Jansen, 1982). Earliest Swaershoek sedimentation is thought to have been penecontemporaneous with the intrusion of Bushveld granites (Du Plessis, 1972, Coertze *et al.*, 1977, Cheney and Twist, 1986). The Swaershoek Formation is informally divided into an upper and lower part by several authors. The lower portion has a much smaller aerial extent, includes a quartz porphyry and has no Bushveld granite clasts; the upper portion has a thick lava at its base and several other lava flows higher up (Jansen, 1982). Meinster (1971) describes the lower part as usually being moderately to intensely sheared and jointed. The Swaershoek Formation consists largely of arenite and it is distinguished from underlying rocks by its siliciclastic nature. Du Plessis (1972) showed that the lower Swaershoek Formation is conformable with the Rooiberg rhyolites in the Modimolle (Nylstroom) area. Cheney and Twist (1986) put forward a strong argument that this lower portion of the Swaershoek Formation is a correlation of the Loskop and Glentig Formations, which are generally regarded as being late-Transvaal in age (SACS, 1980).

In the southwestern part of the basin the upper Swaershoek Formation unconformably overlies Rooiberg rhyolite. Where the rhyolite has been completely eroded away prior to the deposition of the Waterberg sediments, the upper Swaershoek unconformably overlies Bushveld granite (Meinster, 1975).

The Swaershoek Formation consists mainly of reddish sandstone with minor intercalations of conglomerate, purple and red-brown shale, and red amygdaloidal lava. The rudites consist of small pebbles to boulders of rhyolite, arenite, vein quartz, chert, iron-formation, jasper, rudite and lutite. The rudites are coarsely bedded with beds ranging from 3 to 6m in thickness (Tankard *et al.*, 1982), with an average of 5m (De Vries, 1970). The top of the Swaershoek Formation is defined by a 5m thick pebble rudite that is persistent over a large area. Ripple marks and small-scale trough cross-beds are common in the arenites (De Vries, 1970). Cross-beds may show intraformational deformation (Meinster, 1970). The rudites are generally massive.

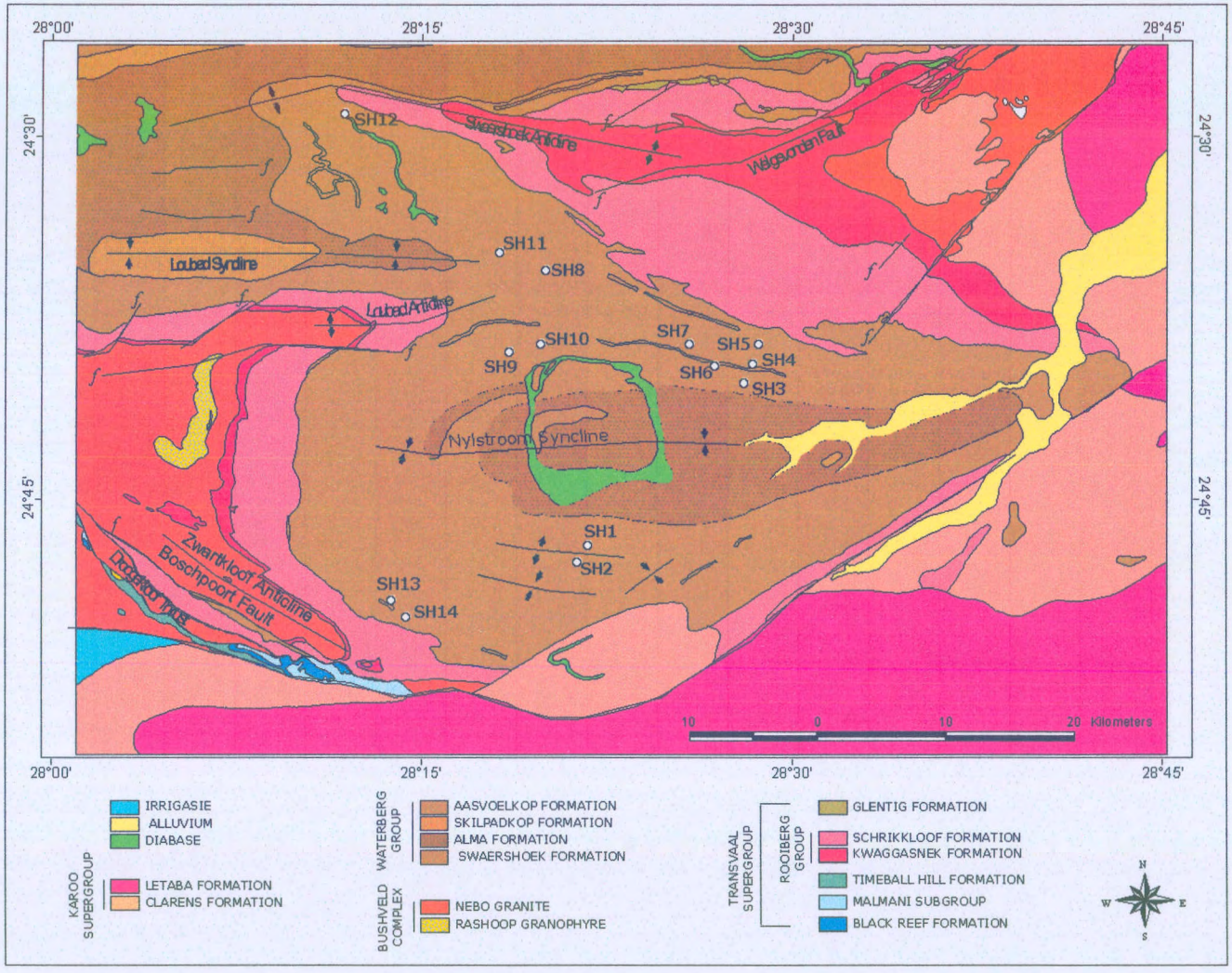

Figure 5.1: Distribution of lithostratigraphic units in the Nylstroom basin indicating the sampling sites on the Swaershoek Formation (modified from the 2428 Nylstroom 1:250 000 geological series, compiled by Du Plessis, 1978).

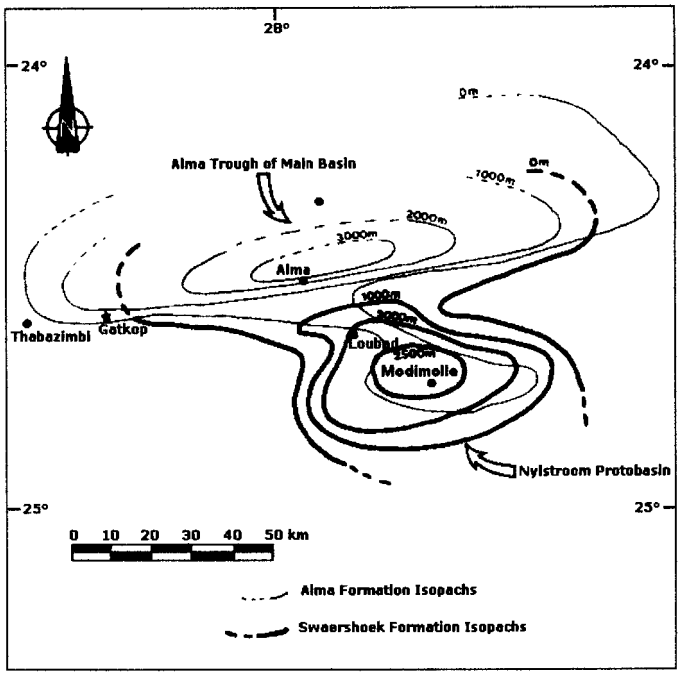

Figure 5.2: Isopach map of the Swaershoek and Alma Formations (from Callaghan, 1987; modified after Jansen, 1982).

Lutites may attain a thickness of 250m in places. Lavas occur throughout the succession except in the lowermost beds. They have been intensely altered, and Jansen (1982) suggested that they might have a trachytic composition. The lavas are typically amygdaloidal and occur in flows of 10-30m thick. Lenticular quartz porphyry flows are exposed in the lowermost beds of the Swaershoek Formation.

The Swaershoek Formation as well as its correlate the Wilge River Formation (Middelburg Basin) shows a greater similarity in geographic distribution with the Rooiberg Group than with the overlying Waterberg sedimentary rocks (Van Biljon, 1976, Coertze *et al.*, 1977 and Callaghan, 1987). Both are confined within the limits of the Transvaal Basin (Coertze *et al.*, 1977). The genesis of the Nylstroom basin has been interpreted as being due to upper crustal warping, whilst the Alma trough has been interpreted as the result of deep seated faulting (Jansen, 1975 and Coertze *et al.*, 1977). On this evidence Callaghan (1987) suggested that both formations might belong to the terminal phase of sedimentation of the Transvaal Sequence.

Most of the sediments were deposited in very shallow water, with continental alluvial conditions prevailing during Swaershoek times (Jansen, 1982). The differences in thickness at many localities, the presence of local sedimentary unconformities and the large number of conglomerate bands of rather small extent, indicate that the basal portion of the Swaershoek Formation represents rapid sedimentation upon a locally highly irregular topography (Callaghan *et al.*, 1991). The Wilge River Formation was deposited by wet alluvial fans and fan deltas which may have prograded into a lacustrine basin where weak tides reworked the sediments (Vos and Eriksson, 1977; Van der Neut *et al.*, 1991).

The dominant structure of the Nylstroom protobasin is the Nylstroom syncline (Fig. 5.1), which developed during and after the formation of the protobasin (Jansen, 1982). In the western part it is a brachysyncline almost circular in shape, which grades to the east into an elongated structure resembling a huge box fold with limbs tilted up to the vertical. On the west the syncline is bounded by the Loubad and Zwartkloof anticlines, on the north by the Swaershoekberge anticlinorium and on the south-east by a monoclinal or anticlinal structure in the Rooiberg lavas, which is cut off on the south by post-Karoo faults. A low tectonic saddle in the Swaershoek beds separates the Nylstroom and Loubad synclines. This structure is situated on the north-eastward extension of the Loubad anticline (Jansen, 1982).

A prominent structure along the north-western limb of the Nylstroom syncline (Fig. 5.1), viz. along the southern limb of the Loubad anticline is a fault which bounds the Rooiberg lavas and the Swaershoek beds. The fault is syndepositional and extends to the west into the Bushveld Complex granite and to the east into a flexure in the Waterberg beds (Jansen, 1982). North of Modimolle (Nylstroom) the northern limb of the Nylstroom syncline, viz. the southern limb of the Swaershoekberge anticlinorium, is intersected by strike faults, step faults and also branch and en-echelon faults (Jansen, 1982).

According to Jansen (1982) sub horizontal Swaershoek beds that have been subjected to very gentle folding occupy the core of the Nylstroom syncline, in the area between Modimolle (Nylstroom) and Bela-Bela (Warmbaths). Transverse faults in the core of the Nylstroom syncline are intruded by diabase. Along the southern limb of the Nylstroom syncline the Swaershoek beds are tilted up to the sub vertical and the same applies to the Swaershoek beds on the northern limb in the eastern portion of the syncline. The northern limb has been subjected to flexturing especially where abnormally thick intercalations of argillaceous beds are developed (Jansen, 1982).

Block faulting in the Nylstroom basin took place mainly during deposition of the lower portion of the Swaershoek formation. However, the fault intersecting the Loubad anticline was already active during deposition of the lower portion as is indicated by the distribution of conglomerate beds and by intraformational folding in argillaceous beds (Du Plessis, 1972). Deposition of the sediments in the lowermost beds took place under changing conditions. Several features indicate rapidly alternating erosion and deposition, slumping and drag. The distribution of conglomerates in the upper portion of the Swaershoek formation, which transgresses beyond the Nylstroom protobasin, indicates that contemporaneous block faulting was locally intense (Jansen, 1982).

Although the sediments are partly of local provenance, particularly in areas where block faulting occurred, transport directions indicate that influx of material into the basin was mainly from the north-east (Jansen, 1982). The composition of pebbles and fragments in the arenaceous beds of the Swaershoek Formation and the absence of feldspars indicate that Rooiberg lavas and sedimentary rocks of the Transvaal Group mainly occupied the source areas. Large-scale erosion of the Bushveld granite only started during deposition of the Alma Formation (Jansen, 1982).

A total of 14 sites were sampled in the Swaershoek Formation across the Nylstroom Protobasin as indicated in figure 5.1.

B. Laboratory Results

The bulk magnetic susceptibility, anisotropy of magnetic susceptibility (AMS) and normal remanent magnetization (NRM) of all individual specimens from the Swaershoek Formation were measured using the Digico system as described in Chapter 3. The frequency distribution of all three data sets were not symmetrical, but could be represented by two-parameter or three-parameter log normal distributions as described by Rendu (1981). To calculate the population mean, as well as the associated confidence intervals from this kind of distribution, the Sichel *t* estimator (Sichel, 1966), as described by Clark (1987), was used. The estimated mean for each data set as well as the central 95% confidence interval around each mean are listed in Table 5.1.

Table 5.1: Statistical parameters of the magnetic properties for the Swaershoek Formation

	N	**μ**	**S**	**R**
Magnetic susceptibility ($x10^{-6}$) SI	270	153.74	144.34 – 164.04	33.18 – 4365.07
Intensity of magnetization ($x10^{-3}$) A/m	270	292.98	275.08 – 312.61	4.60 – 28304.26
Degree of anisotropy (An)	270	1.14	1.09 – 1.19	1.0 – 10.37

N = number of specimens; μ = estimated mean for population; S = central 95% confidence limits around estimated mean; R = range.

According to McElhinny (1973) even 20% anisotropy (An=1.20) can be tolerated without significantly deflecting the magnetization direction. From Table 5.1 it is clear that the specimens from the Swaershoek Formation are mainly isotropically distributed (no preferred orientation).

The attitudes (in geographic coordinates) of the susceptibility axes were plotted on stereographic projections. Typical of sedimentary deposits, the minimum susceptibility axes (K3) of most of the sites are moderate to steeply dipping. The average planar bedding ranges between 18.2° and 63.6°. The few sites with steeply dipping bedding planes are situated near indicated lineaments on the geological map or in line with fold axes extensions. As would be expected from isotropic minerals, the maximum susceptibility axes (K1) of the Swaershoek Formation are not clearly grouped. The general palaeocurrent direction for the Swaershoek Formation, as derived from AMS, is ENE-WSW. This is in accordance with the palaeocurrent described by Jansen (1982).

C. Stepwise Alternating Field (AF) and Thermal Demagnetization

Two specimens from site SH1 were subjected to alternating field (AF) demagnetization up to 120mT. Due to the high coercive force of the haematite component in these samples the secondary magnetization could not be delineated with this method. These two specimens were then subjected to progressive thermal demagnetization. Figure 5.3 illustrates how thermal demagnetization was able to delineate specimen SH12A, where AF demagnetization was unable to do so.

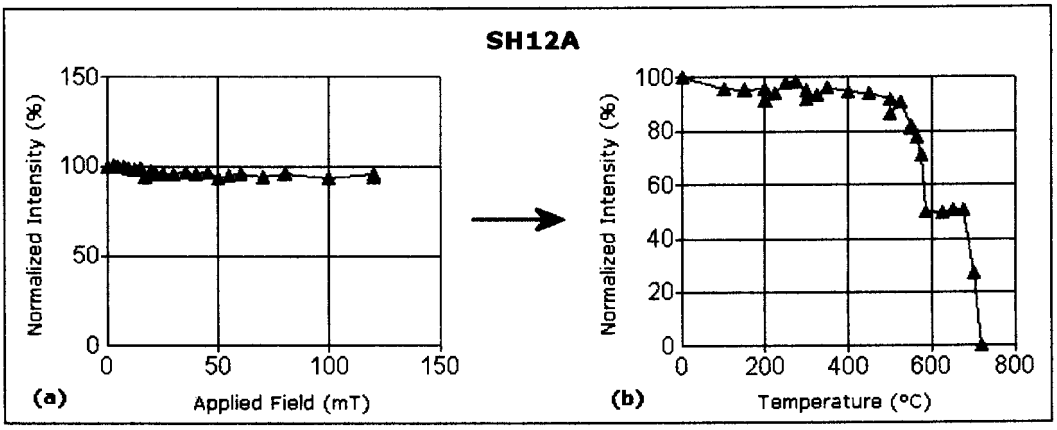

Figure 5.3: Comparison of different demagnetization processes on specimen SH12A. (a) AF demagnetization was unable to delineate the magnetization direction, while (b) thermal demagnetization indicates a blocking temperature of ~700 °C.

A further 138 specimens representing all 14 sites were thermally demagnetized. The advantage of thermal demagnetization is the ability to determine the magnetic components present at each sampling site through the blocking temperatures observed in the samples.

From the variety of thermal demagnetization curves observed, several magnetic components within the Swaershoek Formation can be distinguished. The magnetic components consists mainly of either magnetite with a blocking temperature at ~580 °C (specimen SH86C, Figure 5.4) or haematite with blocking temperature at ~680 °C (specimen SH15E, Figure 5.5). The magnetite and haematite may occur separately (Figures 5.4 and 5.5), but mostly they occur as a combination (specimen SH133B, Figure 5.6).

Reflected light microscopy confirmed that both detrital and post-detrital magnetite and haematite occur in the Swaershoek Formation sediments.

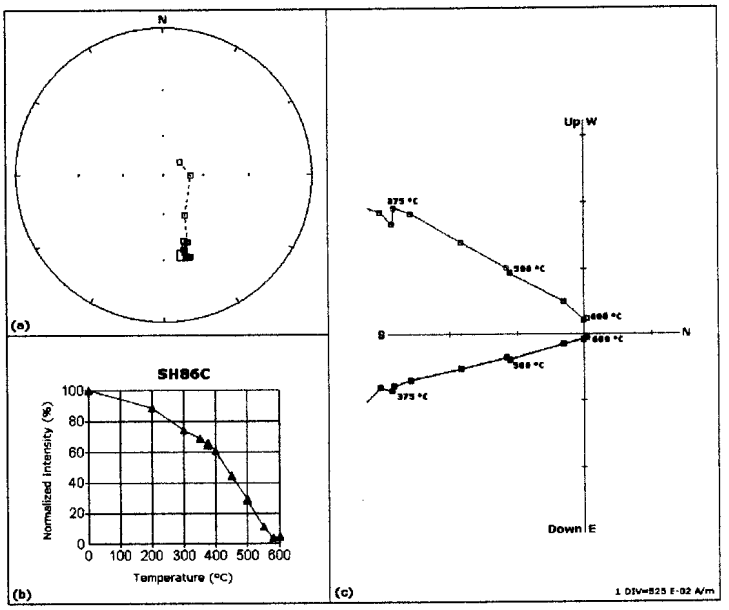

Figure 5.4: Response of specimen SH86C to thermal demagnetization indicating magnetite as main magnetic component (a) Equal-area projection of the change in direction of magnetization; (b) Normalized magnetic intensity curve of progressive demagnetization results indicating a blocking temperature of 580 °C; (c) Zijderveld plot with blue representing the vertical plane and red the horizontal plane; The scale on the axes is in A/m; The distance of each data point from the origin indicates the total NRM intensity.

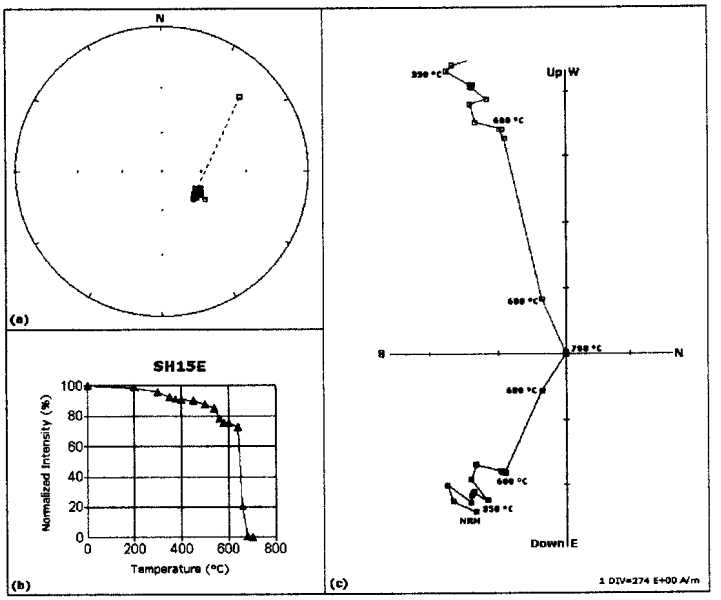

Figure 5.5: Response of specimen SH15E to thermal demagnetization indicating haematite as the carrier of the measured magnetic component (a) Equal-area projection of the change in direction of magnetization; (b) Normalized magnetic intensity curve of progressive demagnetization results indicating a blocking temperature of 680 °C; (c) Zijderveld plot with blue representing the vertical

plane and red the horizontal plane; The scale on the axes is in A/m; The distance of each data point from the origin indicates the total NRM intensity.

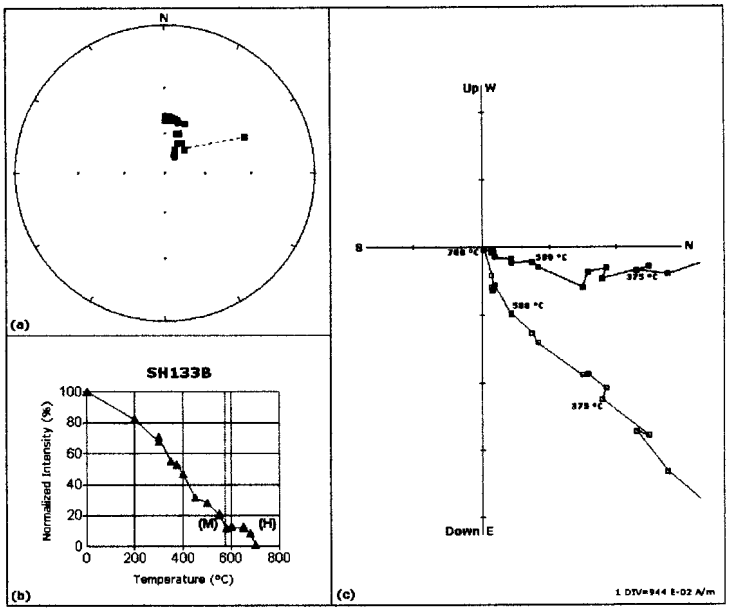

Figure 5.6: Response of specimen SH133B to thermal demagnetization indicating a combination of magnetite (**M**) as well as haematite (**H**) components (a) Equal-area projection of the change in direction of magnetization; (b) Normalized magnetic intensity curve of progressive demagnetization results indicating blocking temperatures of both 580 °C (magnetite) and 680 °C (haematite); (c) Zijderveld plot with blue representing the vertical plane and red the horizontal plane; The scale on the axes is in A/m; The distance of each data point from the origin indicates the total NRM intensity.

Considering the Zijderveld plot of specimen SH133B (Figure 5.6) it is clear that the directions of magnetization of the two components does not differ much from each other. Comparing the electron microscopy results for this site, this could possible be explained due to both minerals originating from the source rock and being orientated parallel to the Earth's field during deposition.

Specimen SH45B (Figure 5.7) demonstrate the presence of another component with lower blocking temperature than magnetite. Titano-magnetite has a large range of blocking temperatures (~300 °C to ~450 °C) depending on the amount of Ti present, and it is suggested this observed blocking temperature is due to the presence of low-stability titano-magnetite.

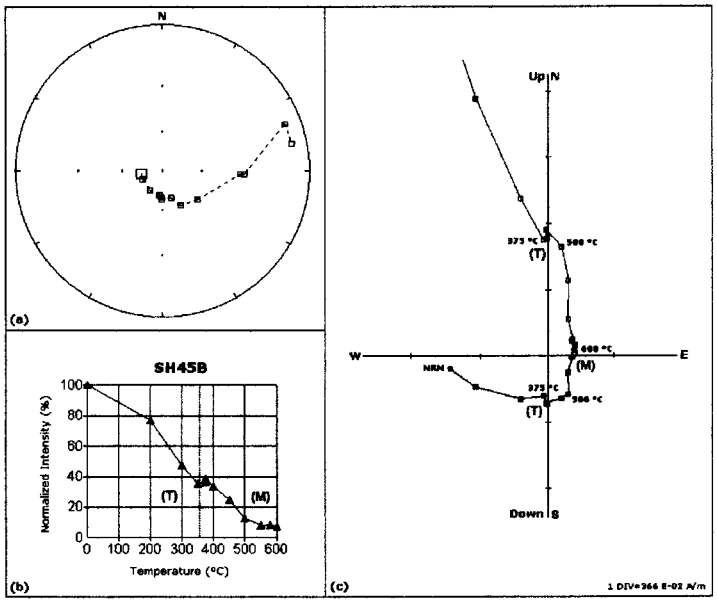

Figure 5.7: Response of specimen SH45B to thermal demagnetization indicating a combination of titano-magnetite (**T**) and magnetite (**M**) components (a) Equal-area projection of the change in direction of magnetization; (b) Normalized magnetic intensity curve of progressive demagnetization results; (c) Zijderveld plot with blue representing the vertical plane and red the horizontal plane; The scale on the axes is in A/m; The distance of each data point from the origin indicates the total NRM intensity.

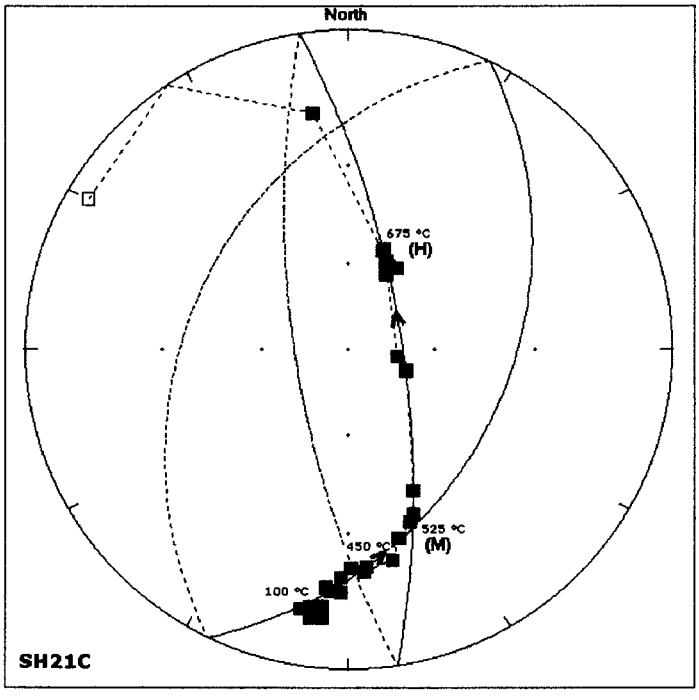

Figure 5.8: Equal-area projection of the change in direction of magnetization of specimen SH21C during thermal demagnetization, demonstrating the partially overlapping coercivity spectra of magnetic minerals magnetite (**M**) and haematite (**H**) within this specimen.

In cases where a combination of magnetic minerals is present, the coercivity spectra yielded remagnetization circles during progressive demagnetization. Figure 5.8 (specimen SH21C) illustrates a case where the overlapping coercivity spectra can still be distinguished from each other.

D. Mineralogy of Opaque Minerals

Polished thin sections were made from 18 specimens of the Swaershoek Formation. One thin section per site was made from selected specimens, with two thin sections from each of sites SH7, SH8 and SH10. The rocks are generally poor to moderately sorted and the grains are subangular to subrounded. The opaque minerals were studied with a reflected light microscope. Both detrital and post-detrital magnetite and haematite were visible under the reflected light microscope, with post-detrital magnetite needles occurring in the thin sections from sites SH7, SH8, SH10 and SH14.

Strong-field thermomagnetic analysis was performed with a Curie balance on four specimens from the Swaershoek Formation. Figure 5.9 shows representative results of strong-field thermomagnetic analysis. A Curie temperature of ~680 °C was observed both on heating and cooling for all four specimens analyzed confirming that the main magnetization component for the Swaershoek Formation is haematite. Figure 5.9 displays actual data, and the noise visible on the curve is due to the very low magnetic intensity of this sample as well as the sensitivity of the instrument.

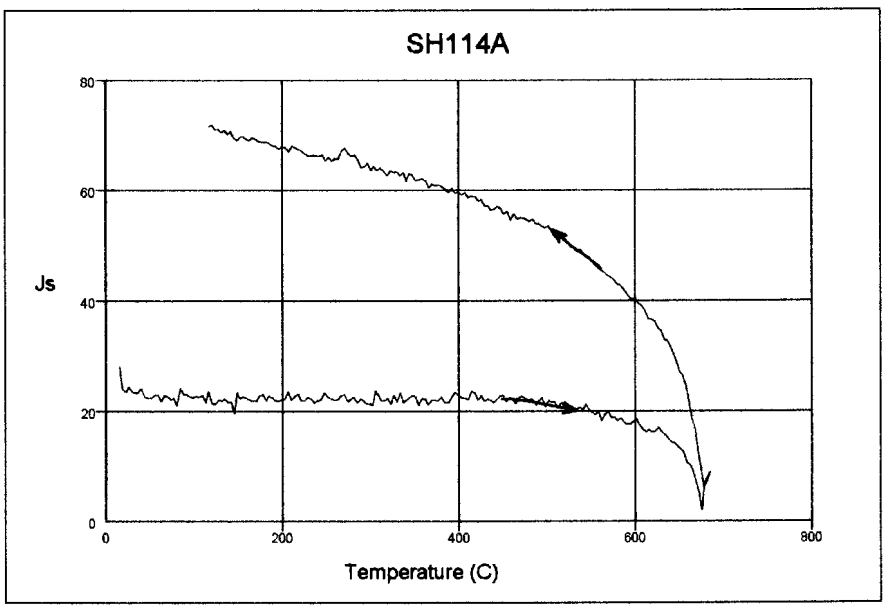

Figure 5.9: Strong-field thermomagnetic behaviour of specimen SH114A. Arrows indicate the direction of temperature change (heating and cooling). Due to the very low magnetic intensity of the sample as well as the sensitivity of the instrument the curves display a lot of noise.

E. Statistical results and palaeomagnetic pole position

Table 5.2 is a summary of the site mean values for the Swaershoek Formation before and after bedding corrections. The site mean results for sites SH3 and SH7 were obtained from the analysis of their remagnetization circles using the IAPD2000 software developed by Torsvik et al. (1996). Figure 5.10 displays the convergence of remagnetization circles from site SH3.

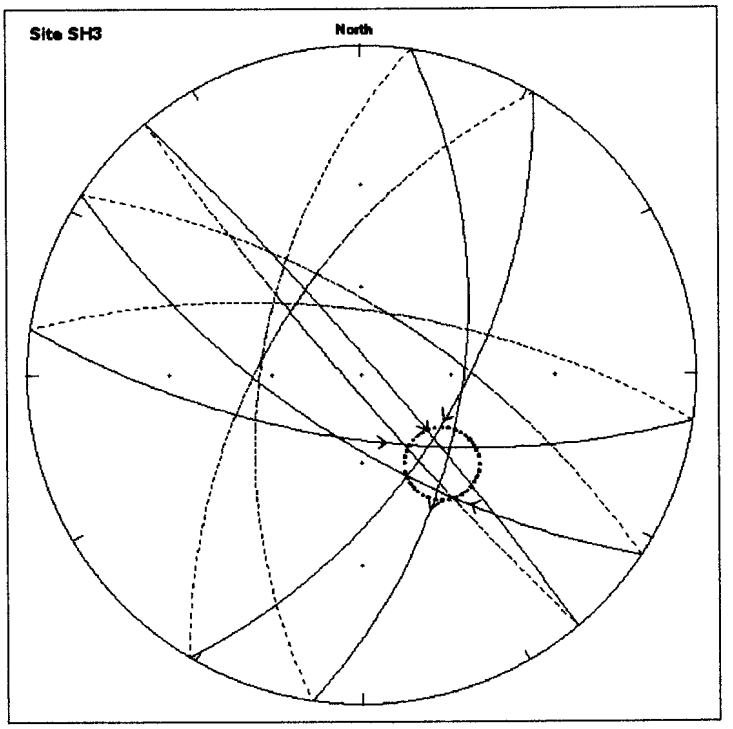

Figure 5.10: Converging remagnetization circles from site SH3 displayed on an equal-area projection.

The mean direction of magnetization for the Swaershoek Formation calculated before the application of bedding corrections is Dec: 152.5°, Inc: -56.8°, α_{95}: 15.5°, N: 9. The mean direction of magnetization calculated after the application of bedding corrections is Dec: 118.9°, Inc: -70.2°, α_{95}: 19.7°, N: 9. Sites excluded from the calculated means are SH2, SH3, SH7, SH9 and SH12. Although the site mean directions of these sites have good precision parameters, they do not converge with the rest of the sites. Figure 5.11 displays the calculated mean directions both before and after bedding-tilt corrections have been applied.

As described by Jansen (1982) and discussed in paragraph A, the Nylstroom protobasin has been subjected to complex folding and faulting both during as well as after deposition. The question thus arises whether the measured magnetization directions were acquired before, during or after these structural processes.

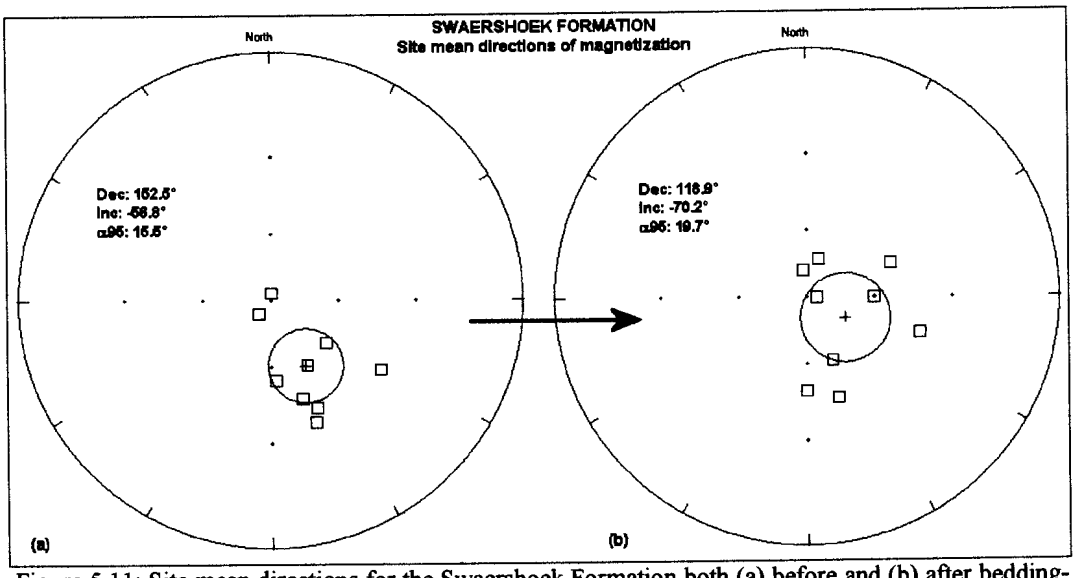

Figure 5.11: Site mean directions for the Swaershoek Formation both (a) before and (b) after bedding-tilt corrections have been applied. Data is plotted on equal-area projections.

According to the fold test (McElhinny, 1964b; McFadden and Jones, 1981), relative timing of acquisition of a magnetic component can be evaluated. If the magnetization was acquired prior to folding/tilting, the directions will converge when the structural correction is made. The magnetization directions are said to "pass the fold test" if clustering increases through application of the structural correction or "fail the fold test" if the directions become more scattered. Bedding-tilt corrections were thus applied to all the sites and the results can be seen in Table 5.2. From the precision parameter (α_{95}) it is clear that the magnetization directions became more scattered, and the data thus failed the test. The result of this test indicates that the direction of magnetization was acquired after (or possibly during) bedding-tilt/folding occurred. This brings the possibility of remagnetization to the foreground. To prove/test this theory, one has to compare the magnetization direction obtained for the Swaershoek Formation with that of the intrusive and volcanic rocks (post-Waterberg diabase as well as the syn-Waterberg trachytic lava) that occur in the area (see chapter VII). The possibility also exists that these structural features only influenced some of the sampling sites, and that a blanket correction might thus not be the correct approach.

A virtual geomagnetic pole position (VGP) for each site-mean was calculated (Table 5.2) and the set of VGPs was then used to find the mean palaeomagnetic pole position by Fisher statistics, treating each VGP as a point on the unit sphere. The mean palaeomagnetic pole position calculated for the Swaershoek Formation is 37.1° S, 175.9° E, with precision parameter α_{95}: 17.4°.

Table 5.2: Site mean demagnetization results for the Swaershoek Formation.

SITE #	NO BEDDING CORRECTIONS										BEDDING CORRECTED									
	DEMAGNETIZATION DATA						VGP				DEMAGNETIZATION DATA						VGP			
	SDEC	SINC	α_{95}	k	N	R	LAT	LONG	DP	DM	SDEC	SINC	α_{95}	k	N	R	LAT	LONG	DP	DM
SH1	151.40	-56.50	6.1	57.0	11	10.82	-22.5	183.9	6.4	8.8	158.10	-59.20	6.1	57.0	11	10.82	-22.1	190.4	6.8	9.10
SH2	114.30	61.60	21.4	8.9	7	6.33	-34.0	82.2	25.5	33.0	127.10	58.50	21.4	8.9	7	6.33	-43.6	86.9	23.5	31.70
SH3*	139.20	50.20	13.0		5		-53.6	99.1	11.7	17.4	155.40	20.90	13.0		5		-62.7	28.5	7.2	13.70
SH4	176.60	-54.00	10.9	23.3	9	8.66	-30.7	205.2	10.7	15.3	91.60	85.30	10.9	23.3	9	8.66	-24.1	18.2	21.4	21.60
SH5	128.10	-58.80	30.2	7.4	5	4.46	-9.6	170.5	33.5	45.0	67.60	-50.40	30.2	7.4	5	4.46	-30.8	321.4	27.2	40.50
SH6	220.00	-81.80	15.3	11.0	10	9.18	12.0	218.9	28.8	29.7	352.20	-77.60	15.3	11.0	10	9.18	48.1	213.1	26.9	28.70
SH7*	315.90	-32.70	13.9		4		48.5	299.1	8.9	15.7	329.60	-5.90	13.9		4		53.6	330.1	7.0	14.00
SH8	160.10	-34.70	37.5	11.9	3	2.83	-42.2	182.6	24.8	43.1	162.90	-44.10	37.5	11.9	3	2.83	-36.9	189.0	29.4	47.00
SH9	176.90	5.50	5.6	116.5	7	6.95	-67.9	200.1	2.8	5.6	176.90	-4.20	5.6	116.5	7	6.95	-63.1	201.5	2.8	5.60
SH10	122.90	-35.20	37.4	7.0	4	3.57	-19.1	151.4	24.9	43.2	107.80	-39.60	37.4	7.0	4	3.57	-5.6	146.2	26.9	44.90
SH11	157.00	-39.60	16.4	17.7	6	5.72	-37.9	181.1	11.8	19.7	180.20	-48.60	16.4	17.7	6	5.72	-35.9	208.5	14.2	21.60
SH12	315.30	48.10	3.9	235.3	7	6.97	-21.3	166.9	3.3	5.1	299.70	35.70	3.9	235.3	7	6.97	-16.5	149.7	2.6	4.50
SH13	8.10	-86.70	20.4	8.3	8	7.16	31.3	207.1	40.4	40.6	17.00	-71.80	20.4	8.3	8	7.16	55.9	191.6	31.6	35.90
SH14	162.50	-44.60	15.1	20.6	6	5.76	-36.2	188.7	12.0	19.0	90.70	-60.00	15.1	20.6	6	5.76	15.5	156.6	17.3	22.80

* Site mean results obtained from remagnetization circles, with the maximum angular deviation (MAD) displayed in the α_{95} columns.

6. THE PALAEOMAGNETISM OF THE WILGE RIVER FORMATION

A. Geology

Jansen (1982) describes the Swaershoek Formation as the basal unit of the Waterberg Group in the Main Basin, and correlates it with the Wilge River Formation in the Middelburg Basin (Fig. 6.1). The Swaershoek Formation as well as its correlate the Wilge River Formation shows a greater similarity in geographic distribution with the Rooiberg Group than with the overlying Waterberg sedimentary rocks (Van Biljon, 1976; Coertze *et al.*, 1977 and Callaghan, 1987). According to relationships established between the Loskop Formation, the Bushveld Complex and the Rooiberg Group, the Loskop Formation is largely or entirely of pre-Bushveld age representing the final stage of the Transvaal cycle of sedimentation (Coertze *et al.*, 1977).

The Wilge River Formation is the only stratigraphic unit within the Middelburg basin and unconformably overlies rocks of the 2100 Ma (Burger and Walraven, 1980) Loskop Formation (Van der Neut and Eriksson, 1999). The Wilge River Formation is lithologically similar to the Swaershoek Formation but in contrast lacks interbedded quartz porphyry and trachyte (Jansen, 1982). It attains a maximum thickness of 2000 m and consists predominantly of a monotonous succession of arenaceous rocks (Visser *et al.*, 1961). The formation's basal rudite has a discordant contact with rocks of the Loskop Formation, Rooiberg Group and the Pretoria Group (Spies, 1951, 1958). The basal contact with the Bushveld granite is an erosive one (Visser *et al.*, 1961 and Coertze *et al.*, 1977). Hence, the relationship between the Wilge River Formation and the older formations is essentially a transgressive one and there is, so far, no evidence of a protobasin comparable with the Nylstroom protobasin.

Coertze *et al.* (1977) correlates the Wilge River Formation with the upper portion of the Swaershoek Formation that displays the same lithological and transgressive features. According to these authors, the scattered occurrences of arenaceous beds in the Springbok Flats other than those near Rust de Winter indicate that the early Waterberg basin in the Nylstroom area and the Cullinan-Middelburg basin were probably linked during deposition of the Wilge River Formation. However, sedimentation probably terminated in the Cullinan-Middelburg basin during deposition of the Alma Formation in the early Waterberg basin (Jansen, 1982). The feldspathic Alma Formation decreases rapidly in thickness from north (Alma) to south (Nylstroom) (Coertze *et al.*, 1977) and there is no evidence of its extension to the south into the Springbok Flats and the Cullinan-Middelburg basin (see Figure 5.2).

Jansen (1982) interpreted the Swaershoek, Wilge River and lower Sterk River Formations as having been deposited in shallow water, possibly with tidal influences. Previous workers consider the Waterberg Group in the Main basin to reflect predominantly alluvial-fluvial braid-plain deposition within a graben setting, with subordinate aeolian and lacustrine or littoral palaeoenvironments (e.g. Vos and Eriksson, 1977; Eriksson and Vos, 1979; Tankard *et al.*, 1982; Callaghan, 1987; Callaghan *et al.*, 1991). Little work has been done within the Middelburg basin, apart from that by Van der Neut *et al.*

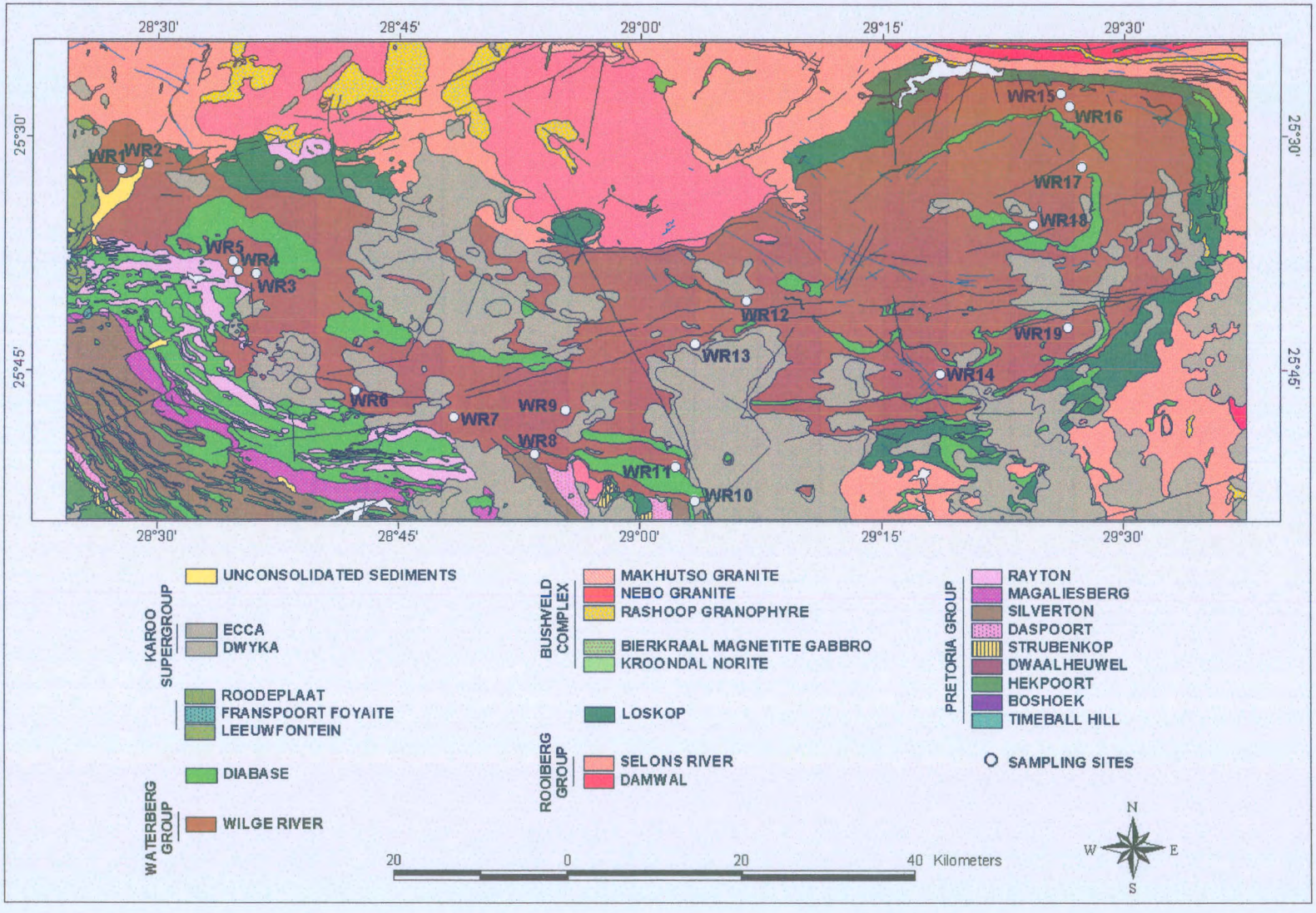

Figure 6.1: Distribution of the lithostratigraphic units in the Middelburg basin indicating the sampling sites in the Wilge River Formation (1:250 000 Geological Series 2528 Pretoria; compiled by Walraven, 1978).

(1991), who propose a distal alluvial-fan braid-plain palaeoenvironmental setting and a graben tectonic framework. A braided-stream model is thus considered to be generally applicable to the Wilge River Formation (Van der Neut and Eriksson, 1997).

Horizontally stratified and cross-bedded sandstones predominate within the Middelburg basin, with subordinate conglomerate beds, particularly in the western portion thereof (Van der Neut and Eriksson, 1999). These strongly red-coloured rocks dip gently towards the centre of the basin at approximately 10°, on average. Maximum dips up to 70° occur on the northeastern margin of the basin, reflecting post-depositional inversion tectonics (Van der Neut and Eriksson, 1999). The Wilge River conglomerates tend to define the bases of upward-fining sandstone successions, capped by thin mudrocks (Eriksson and Vos, 1979; Van der Neut *et al.*, 1991). Sandstone and conglomerate beds exhibit lenticular geometry, with lateral extents up to 850m and thicknesses mostly from 5 to 15m; contacts between the two rock types are commonly gradational tectonics (Van der Neut and Eriksson, 1999).

Hydrological data from the Wilge River Formation (Van der Neut and Eriksson, 1999) reflect a braid-river setting *sensu stricto*, with no evidence of significant suspended load or floodplain influences, and in view of their age, land vegetation was absent and soil-forming biota were not important. These authors inferred that the faulted margins of the Wilge River graben provided a number of smaller drainage areas and that the combination or lack of vegetation and soil biota, as well as aggressive weathering and high erosion rates typical for Precambrian times, promoted formation of sandy detritus close to source areas. High-gradient braided, bedload fluvial systems developed within this framework, and intermittent torrential storms are thought to have played an important role on these braided floodplains.

Van der Neut *et al.* concluded in their 1991 study that the detrital ferromagnesian minerals and limonitic grain coatings in the Wilge River Formation fan sediments were subject to intrastratal, diagenetic alteration, producing haematite stain of both grain cuticles and intergranular material. The Wilge River red beds thus fit Turner's (1980) alluvial red bed environmental setting.

A total of 19 locations in the Middelburg Basin across the Wilge River Formation were sampled. The distribution of these sampling sites is indicated in Figure 6.1.

B. Laboratory Results

The bulk magnetic susceptibility, anisotropy of magnetic susceptibility (AMS) and normal remanent magnetization (NRM) of all individual specimens from the Wilge River Formation were measured and the frequency distribution of all three data sets calculated (Table 6.1).

Table 6.1: Statistical parameters of the magnetic properties for the Wilge River Formation

	N	μ	S	R
Magnetic susceptibility ($x10^{-6}$) SI	399	102.98	100.51 – 105.0	14.45 – 427.13
Intensity of magnetization ($x10^{-3}$) A/m	399	482.24	470.67 – 494.30	2.3 – 11372.75
Degree of anisotropy (An)	399	1.10	1.09 – 1.12	1.0 – 2.44

N = number of specimens; μ = estimated mean for population; S = central 95% confidence limits around estimated mean; R = range.

Similar to the sediments from the Swaershoek Formation the magnetic minerals within the specimens from the Wilge River Formation sediments are mainly isotropically distributed (no preferred orientation).

The minimum susceptibility axes (K3) of most of the sites are moderate to steeply dipping, with the average planar bedding plane for the Wilge River Formation being 34°. Typical of a magnetically isotropic unit the maximum susceptibility axes (K1) of the Swaershoek Formation are not clearly grouped, but roughly indicate an E-W palaeocurrent direction. Vos and Eriksson (1977) and Van der Neut *et al.* (1991) also mentioned lack of preferred facies arrangements, radial palaeocurrent patterns, and combination of streamflow and gravity-flow deposits in these red beds (supporting an alluvial fan palaeoenvironment).

E. Stepwise Alternating Field (AF) and Thermal Demagnetization

Seventeen specimens from sites 1 to 6 were subjected to alternating field (AF) demagnetization up to 100mT. Due to the high coercive force of the haematite component in these samples it was decided to subject all the specimens to progressive thermal demagnetization. Figure 6.2 illustrates how thermal demagnetization was able to delineate specimen WR14B, where AF demagnetization was unable to do so.

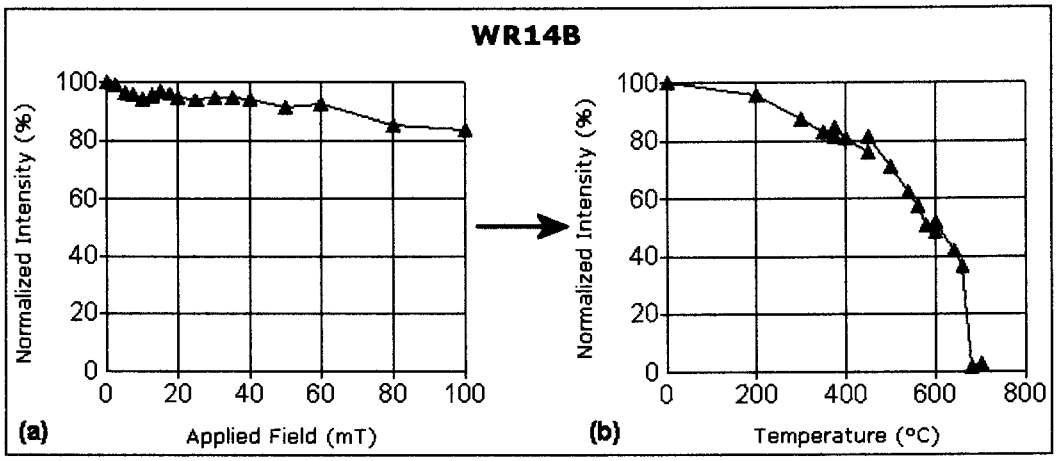

Figure 6.2: Comparison of the effect of different demagnetization processes on specimen WR14B. (a) AF demagnetization was unable to delineate the magnetization direction, while (b) thermal demagnetization indicates a blocking temperature of 680 °C.

A further 197 specimens from 19 sites were thermally demagnetized. Similar to the Swaershoek Formation both magnetite (blocking temperature ~580 °C) and haematite (blocking temperature ~680 °C) were observed as carriers of the Wilge River Formation's remanence. Figures 6.9-6.11 display the progressive demagnetization results of several samples containing either magnetite (**M**), haematite (**H**) or both minerals. A few specimens also revealed lower blocking temperatures that can possibly be associated with the presence of titano-magnetite in the samples.

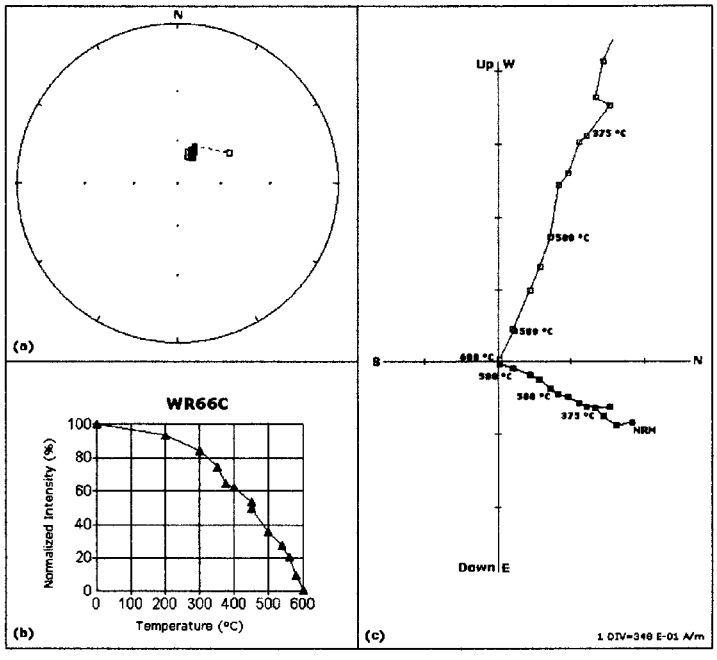

Figure 6.3: Response of specimen WR66C to thermal demagnetization indicating magnetite as main magnetic component (a) Equal-area projection of the change in direction of magnetization; (b) Normalized magnetic intensity curve of progressive demagnetization results indicating a blocking

temperature of 580 °C; (c) Zijderveld plot with blue representing the vertical plane and red the horizontal plane; The scale on the axes is in A/m; The distance of each data point from the origin indicates the total NRM intensity.

Reflected light microscopy revealed several small rounded magnetite grains in the samples from site WR6. These grains occur within defined sediment layers which suggest the magnetite to originate from the source rock.

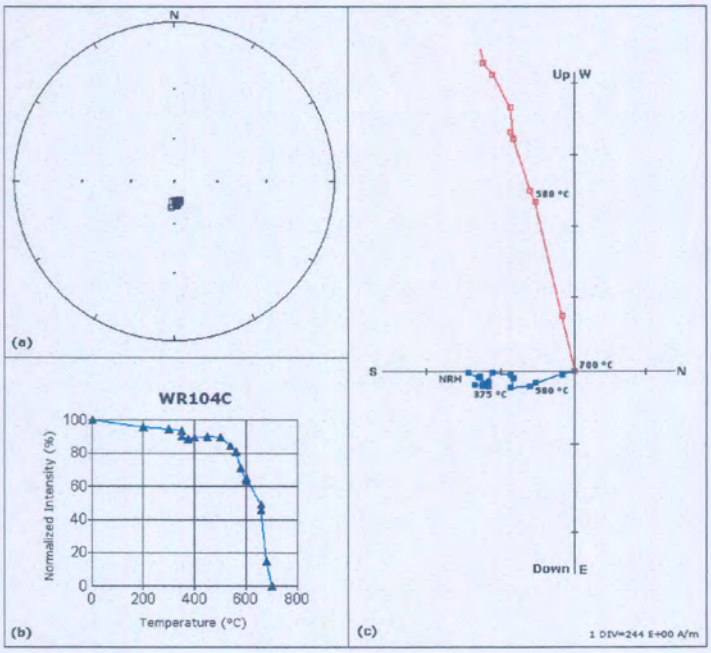

Figure 6.4: Response of specimen WR104C to thermal demagnetization indicating haematite as the carrier of the measured magnetic component (a) Equal-area projection of the change in direction of magnetization; (b) Normalized magnetic intensity curve of progressive demagnetization results indicating a blocking temperature of 680 °C; (c) Zijderveld plot with blue representing the vertical plane and red the horizontal plane; The scale on the axes is in A/m; The distance of each data point from the origin indicates the total NRM intensity.

Similar to site WR6 reflected light microscopy revealed mostly fine grained, rounded opaque minerals which have been rolled along with the current and deposited within well-sorted sedimentary layers. A limited degree of leached haematite occurs within the matrix of the sediment.

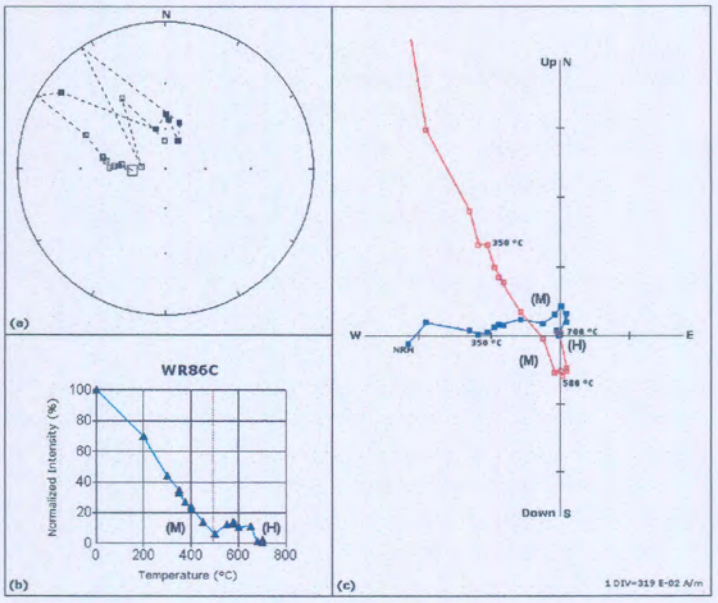

Figure 6.5: Response of specimen WR86C to thermal demagnetization indicating a combination of magnetite (**M**) as well as haematite (**H**) components (a) Equal-area projection of the change in direction of magnetization; (b) Normalized magnetic intensity curve of progressive demagnetization results indicating blocking temperatures of both 580 °C (magnetite) and 680 °C (haematite); (c) Zijderveld plot with blue representing the vertical plane and red the horizontal plane; The scale on the axes is in A/m; The distance of each data point from the origin indicates the total NRM intensity.

The Zijderveld plot of specimen WR86C (Figure 6.5 (c)) displays two distinct components (magnetite and haematite) of which the demagnetization spectra do not overlap. The electron microscopy revealed considerable weathering at this site with both detrital and post-detrital magnetite and haematite present.

During progressive demagnetization specimens containing a combination of magnetic minerals normally yielded remagnetization circles (even combinations of remagnetization circles). Figure 6.6 (specimen WR35C) illustrates a case where the overlapping coercivity spectra could still be distinguished from each other.

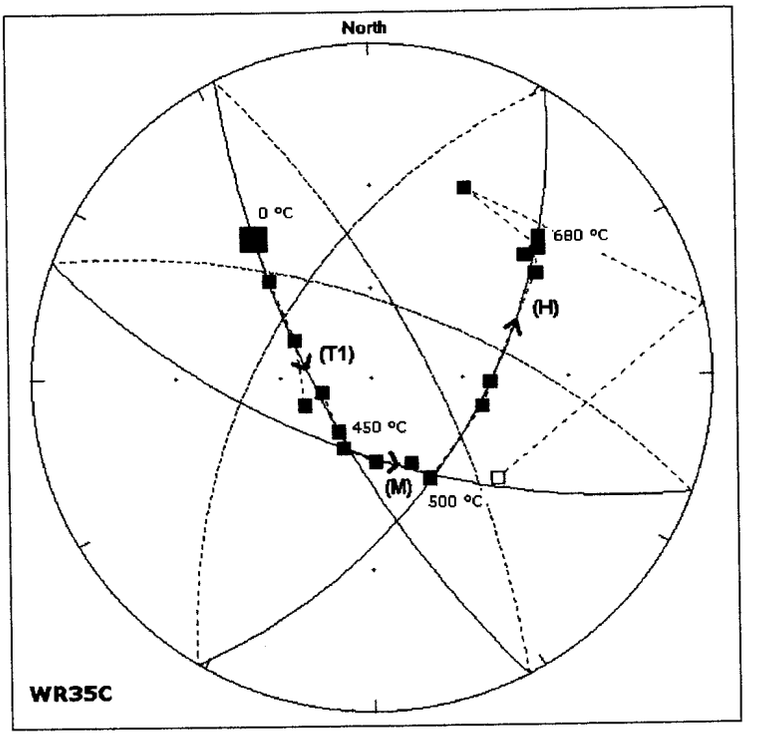

Figure 6.6: Equal-area projection of the change in direction of magnetization of specimen WR35C during progressive thermal demagnetization, demonstrating the partially overlapping coercivity spectra of magnetic minerals within this specimen. The first component represent titano-magnetite (T1), the second a weak overlapped magnetite component (M) with a strong haematite (H) component.

D. Mineralogy of Opaque Minerals

Polished thin sections were made from 38 specimens of the Wilge River Formation (two thin sections per site). The Wilge River Formation covers a very large area with rocks ranging from poorly sorted and coarse-grained to fine-grained and layered. The opaque minerals were studied with reflected light microscope. Both detrital and post-detrital magnetite and haematite were observed.

Strong-field thermomagnetic analysis was performed with a Curie balance on three specimens from the Wilge River Formation. Figure 6.7 shows representative results of strong-field thermomagnetic analysis for specimen WR51A. A Curie temperature of 680 °C was observed both on heating and cooling for all three specimens analyzed, confirming that the main magnetization component for the Wilge River Formation is haematite. Figure 6.7 displays actual data and the noise visible on the curve is due to the very low magnetic intensity of this sample as well as the instrument drift.

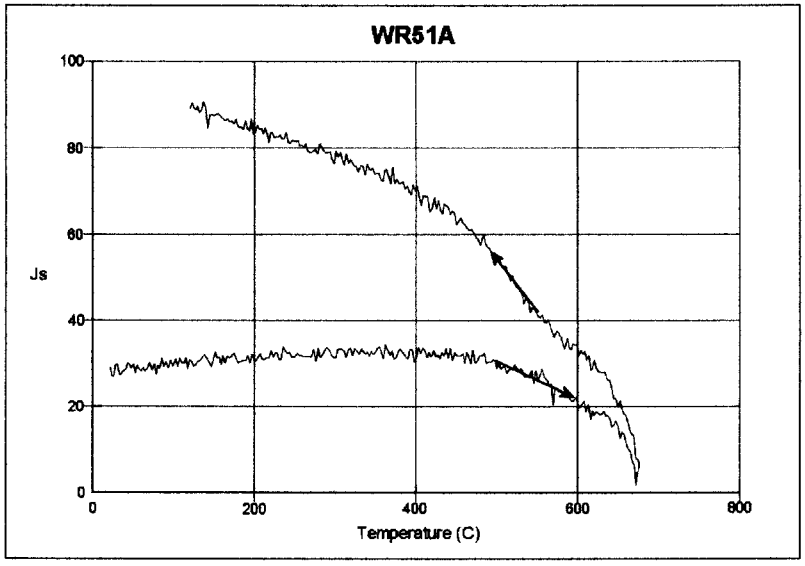

Figure 6.7: Strong-field thermomagnetic behavior of specimen WR51A. Arrows indicate the direction of temperature change (heating and cooling). Due to the very low magnetic intensity of the specimen as well as the sensitivity of the instrument the curves display a lot of noise.

E. Statistical Results and Palaeomagnetic pole position

A great number of sites had to be analyzed using remagnetization circles. In these cases the site means were calculated using the IAPD2000 software developed by Torsvik et al. (1996). Figure 6.8 is an example of converging remagnetization circles.

The calculated site means (both point and great circle data) along with the associated virtual geomagnetic pole positions (VGP) are summarized in Table 6.2. The results were compared both before and after bedding corrections were applied. It was found that although the bedding corrections don't have a significant effect on the results, the precision parameter of the calculated Formation mean does decrease somewhat after the corrections (Figure 6.9). This indicates that the direction of magnetization was acquired after (or possibly during) bedding-tilt occurred. As discussed in chapter 5 this brings the possibility of remagnetization to the foreground. To prove/test this theory, one has to compare the magnetization direction obtained for the Wilge River Formation with that of the intrusive diabase that occurs in the Middelburg basin (see chapter 7). There also exists a possibility that the structural features only influenced some of the sampling sites, and that a blanket correction might thus not be the correct approach.

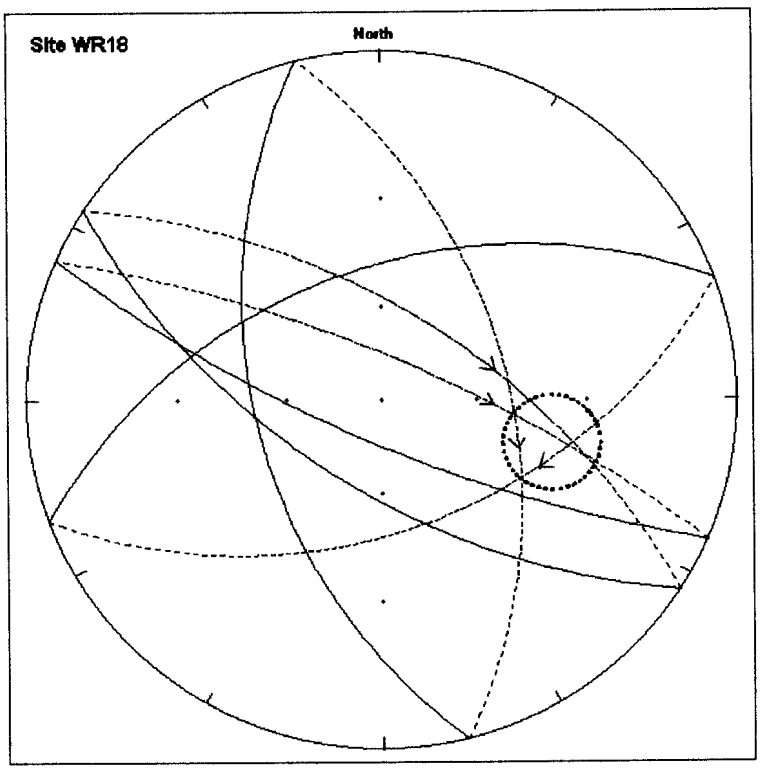

Figure 6.8: Converging remagnetization circles from site WR18 displayed on an equal-area projection.

The calculated mean direction of magnetization for the Wilge River Formation before the application of any bedding corrections is, Dec: 135.6°, Inc: -53.5°, α_{95}: 19.9°, N: 10. The mean direction of magnetization calculated after the application of bedding corrections is Dec: 137.9°, Inc: -50.2°, α_{95}: 21.2°, N: 10.

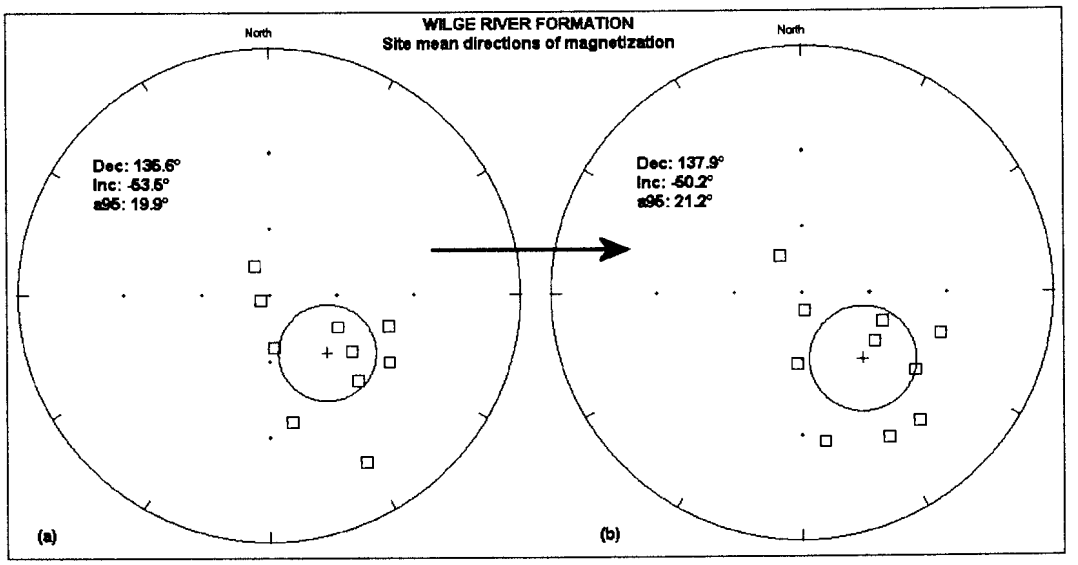

Figure 6.9: Equal-area projections of site mean directions for the Wilge River Formation both (a) before and (b) after bedding-tilt corrections have been applied.

A virtual geomagnetic pole position (VGP) for each site-mean was calculated (Table 6.2) and the set of VGPs was then used to find the mean palaeomagnetic pole position by Fisher statistics, treating each VGP as a point on the unit sphere. The mean palaeomagnetic pole position calculated for the Wilge River Formation is 31.9° S, 172.7° E, with precision parameter α_{95}: 20.5°. The pole position shows poor statistical parameters, which is a problem commonly met when working with older rocks. However, the pole position correlates well with the calculated pole position for the Swaershoek Formation (Chapter 5).

Table 6.2: Site mean results for the Wilge River Formation

SITE #	NO BEDDING CORRECTIONS										BEDDING CORRECTED									
	DEMAGNETIZATION DATA						VGP				DEMAGNETIZATION DATA						VGP			
	SDEC	SINC	α_{95}	K	N	R	LAT	LONG	DP	DM	SDEC	SINC	α_{95}	k	N	R	LAT	LONG	DP	DM
WR1	125.00	-46.30	9.20	44.10	7	6.86	-15.0	159.7	11.8	7.6	110.10	-52.20	9.20	44.10	7	6.86	-1.5	156.3	12.6	8.7
WR2	333.10	-75.20	32.50	8.98	4	3.67	49.2	227.3	59.4	54.4	329.60	-70.30	32.50	8.98	4	3.67	53.5	238.1	56.1	48.5
WR3*	135.90	-37.42	7.01		5		-18.5	263.2	4.8	8.2	231.90	-26.10	7.01		5		-25.9	266.8	4.1	7.6
WR4*	50.07	-30.22	10.15		4		42.6	117.4	6.2	11.1	52.00	-47.10	10.15		4		43.9	134.1	8.5	13.1
WR5	302.50	-57.10	12.00	32.22	6	5.84	40.4	269.7	17.5	12.7	297.10	-68.80	12.00	32.22	6	5.84	36.4	251.3	20.3	17.2
WR6	174.50	-65.70	28.40	4.80	8	6.53	-16.1	204.9	46.3	37.7	183.20	-58.00	28.40	4.80	8	6.53	-25.5	211.5	41.8	30.8
WR7*	123.19	-27.99	8.88		3		-21.4	148.5	5.3	9.7	126.60	-12.50	8.88		3		-29.1	142.9	4.6	9.0
WR8*	183.27	-55.31	8.98		4		-28.2	211.9	9.1	12.8	192.10	-43.40	8.98		4		-37.5	222.7	7.0	11.2
WR9*	146.56	-13.63	15.63		6		-43.9	159.5	8.2	16.0	145.60	-21.10	15.63		6		-40.3	162.2	8.7	16.4
WR10	239.40	-85.30	16.80	11.82	8	7.41	20.9	217.7	33.3	32.9	171.00	-81.60	16.80	11.82	8	7.41	9.6	206.5	32.6	31.6
WR11*	130.94	-59.11	2.26		2		-9.9	173.0	2.5	3.4	143.50	-57.10	2.26		2		-17.8	179.4	2.4	3.3
WR12*	233.42	-54.78	28.11		13		-10.8	251.0	28.1	39.8	229.20	-50.90	28.11		13		-15.9	251.2	25.6	38.0
WR13	181.20	-0.30	16.60	22.30	5	4.82	-64.1	211.8	16.6	8.3	181.10	6.50	16.60	22.30	5	4.82	67.5	31.9	16.7	8.4
WR14	115.70	-56.50	18.50	14.10	6	5.65	-2.9	163.3	26.7	19.3	124.20	-51.40	18.50	14.10	6	5.65	-11.4	163.7	25.1	17.1
WR15	191.70	-6.50	9.40	42.50	7	6.86	-59.1	232.7	9.4	4.7	220.40	-43.20	9.40	42.50	7	6.86	-26.1	250.2	11.7	7.2
WR16	182.30	4.70	4.50	149.20	8	7.95	66.8	35.3	4.5	2.3	182.80	-12.20	4.50	149.20	8	7.95	-58.2	214.8	4.6	2.3
WR17	187.90	34.90	9.70	40.10	7	6.85	80.4	80.2	11.2	6.4	189.80	29.70	9.70	40.10	7	6.85	76.7	74.9	10.7	5.9
WR18*	104.68	-37.53	13.11		4		-3.4	144.7	9.1	15.4	106.80	-30.20	13.11		4		-7.4	141.4	8.1	14.6
WR19*	319.15	-36.51	20.28		5		52.2	299.0	13.8	23.7	314.00	-41.30	20.28		5		48.4	292.0	15.1	24.7

* Site mean results obtained from remagnetization circles, with the maximum angular deviation (MAD) displayed in the α_{95} columns.

7. THE PALAEOMAGNETISM OF THE INTRUSIVE AND VOLCANIC ROCKS IN THE LOWER WATERBERG GROUP

A. Geology

As discussed in previous chapters, Jansen (1982) describes the Swaershoek Formation as the basal unit of the Waterberg Group in the Main Basin (Figure 7.1), and correlates it with the Wilge River Formation in the Middelburg Basin (Figure 7.2). The Swaershoek Formation as well as its correlate the Wilge River Formation show a greater similarity in geographic distribution with the Rooiberg Group than with the overlying Waterberg sedimentary rocks (Van Biljon, 1976; Coertze *et al.*, 1977 and Callaghan, 1987). Both are confined within the limits of the Transvaal Basin (Coertze *et al.*, 1977).

The Swaershoek Formation is a predominantly arenaceous succession consisting of sandstone, locally with interbedded shale, siltstone, pebble and boulder conglomerate and trachytic lavas (Jansen, 1982). The complete Swaershoek succession is only developed in the Nylstroom syncline where it attains a maximum thickness of 2500m (Jansen, 1982). According to Jansen (1970) volcanic activity started immediately with the deposition of the basal Swaershoek beds in which quartz porphyry and trachyte occur. Jansen (1970) further suggests a relatively short time interval between the initial phase of volcanicity and the final Bushveld phase. Flows of quartz porphyry are only developed in the lowermost Swaershoek beds (Jansen, 1982). According to Coertze *et al.* (1977) the trachytic lavas in the Swaershoek Formation represent an extrusive phase with an alkaline character, which followed on the extrusion of the quartz porphyry. In the Swaershoekberge, extrusion of trachytic lavas and block-faulting were contemporaneous events, because the lavas attain greater thickness in the down faulted blocks (Coertze *et al.*, 1977). Coertze *et al.* (1977) further finds that the lavas and overlying beds were in turn subjected to faulting on pre-existing fault-planes. According to Jansen (1982) the trachytic lavas are developed throughout the entire Swaershoek succession with the exception of the lowermost beds. Jansen (1982) found that one persistent flow forms the boundary between the lower and upper Swaershoek portions. According to Coertze *et al.* (1977) the trachytes and andesites in the Soutpansberg trough are associated with basalts and deep faulting, and the source of the trachytic lavas is therefore probably deep seated. Jansen (1982) suggests that the mode of deposition of the volcanic rocks is lava spillage from open fissures with localized eruptions. The trachytic lavas evidently gained access to the surface along fracture and fault zones, most of which must have intersected the Rooiberg lavas and the Bushveld granite (Coertze *et al.*, 1977). According to Coertze *et al.* (1977) this implies that the latter was solidified during the period of extrusion. Coertze *et al.* (1977) continues that this relationship agrees with the fact that the lavas are not developed in the lowermost Swaershoek beds, which are supposed to have been laid down prior to solidification of the Bushveld granite. The trachytic lavas are easily overlooked in the field because they weather more easily than the surrounding arenaceous rocks. In general the lavas have been subjected to intense hydrothermal alteration with the result that their original composition cannot be determined (Jansen 1970, 1982). There is evidence particularly of ferruginization during and immediately after extrusion of the lavas.

The Wilge River Formation is lithologically similar to the Swaershoek Formation but in contrast lacks interbedded quartz porphyry and trachyte. It attains a maximum thickness of 2000 m and consists predominantly of a monotonous succession of arenaceous rocks (Visser *et al.*, 1961). The formation's basal rudite has a discordant contact with rocks of the Loskop Formation, Rooiberg Group and the Pretoria Group (Spies, 1951, 1958). The basal contact with the Bushveld granite is an erosive one (Visser *et al.*, 1961 and Coertze *et al.*, 1977). Hence, the relationship between the Wilge River Formation and the older formations is essentially a transgressive one and there is, so far, no evidence of a protobasin comparable with the Nylstroom protobasin.

According to Jansen (1982) most of the intrusions in the Waterberg area are of post-Waterberg to pre-Karoo age and are represented by dykes and sills of diabase. Extrusive acid rocks of early Waterberg age are represented by quartz-porphyry flows in the lower portion of the Swaershoek Formation. Post-Waterberg diabase dykes intersect all subdivisions of the Waterberg Group, but all were not necessarily emplaced simultaneously (Strauss, 1955). Jansen (1982) reports that most of the post-Waterberg intrusions are dykes, but sills predominate in the Sterk River and Matlabas areas, south of Marken and east and southeast of the Makgabeng plateau. In the Nylstroom syncline this is represented by a large basin-shaped sill.

Core samples for palaeomagnetic analysis were collected from 6 sampling sites across the diabase sill in the Nylstroom protobasin, but due mostly to excessive weathering, only 2 sampling sites could be located on trachytic lava outcrops in the Swaershoek Formation (Figure 7.1). In the Middelburg basin 8 sites were sampled on the diabase occurring in the Wilge River Formation (Figure 7.2). None of these rocks could be found in road cuttings with only one site in the Middelburg basin situated in a streambed. Sampling sites were therefore chosen from outcrops showing minimum weathering.

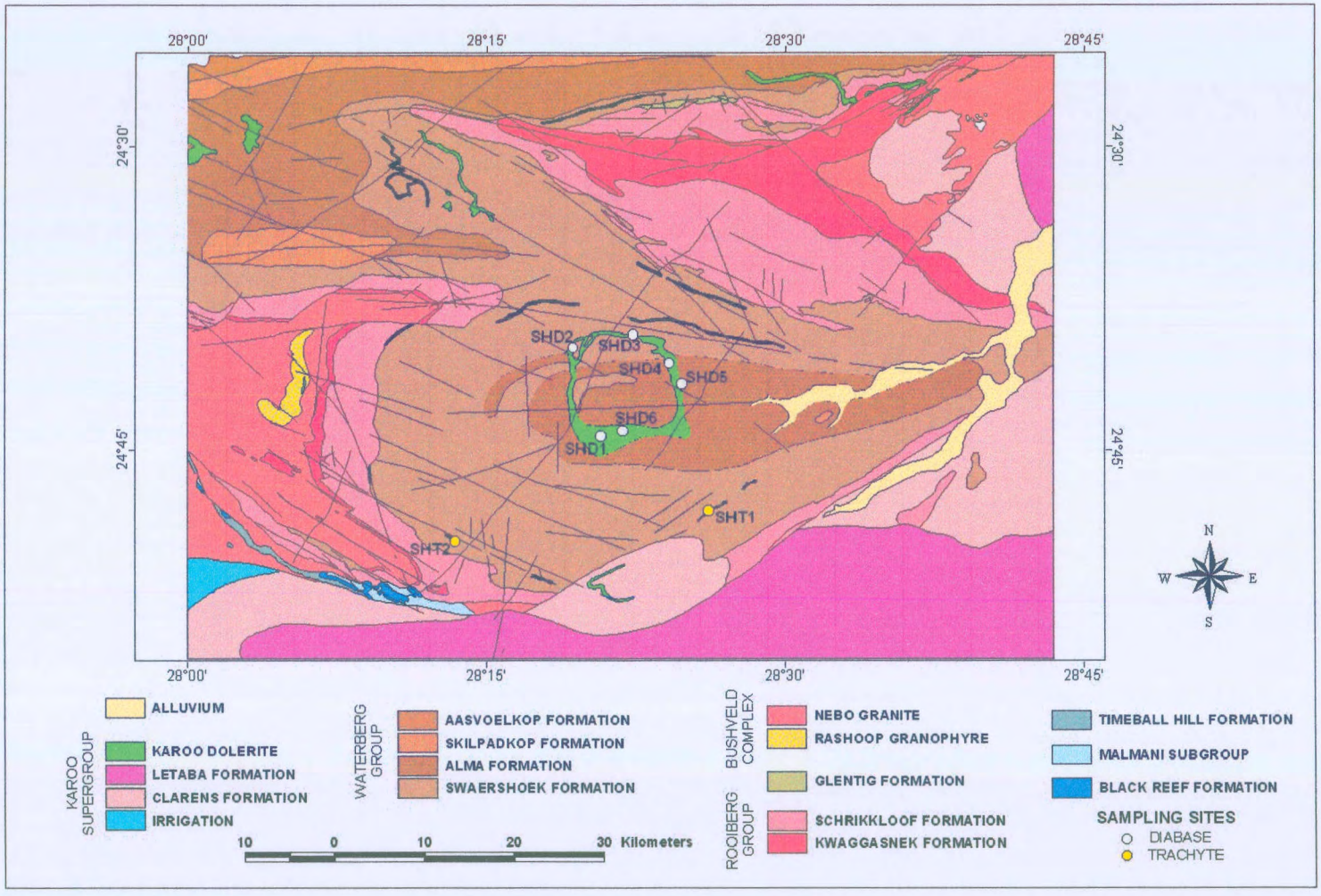

Figure 7.1 : Distribution of the lithostratigraphic units in the Nylstroom basin indicating the sampling sites on the intrusive and volcanic rocks in the Nylstroom Protobasin (1:250 000 Geological Series 2428 Nylstroom, 1978).

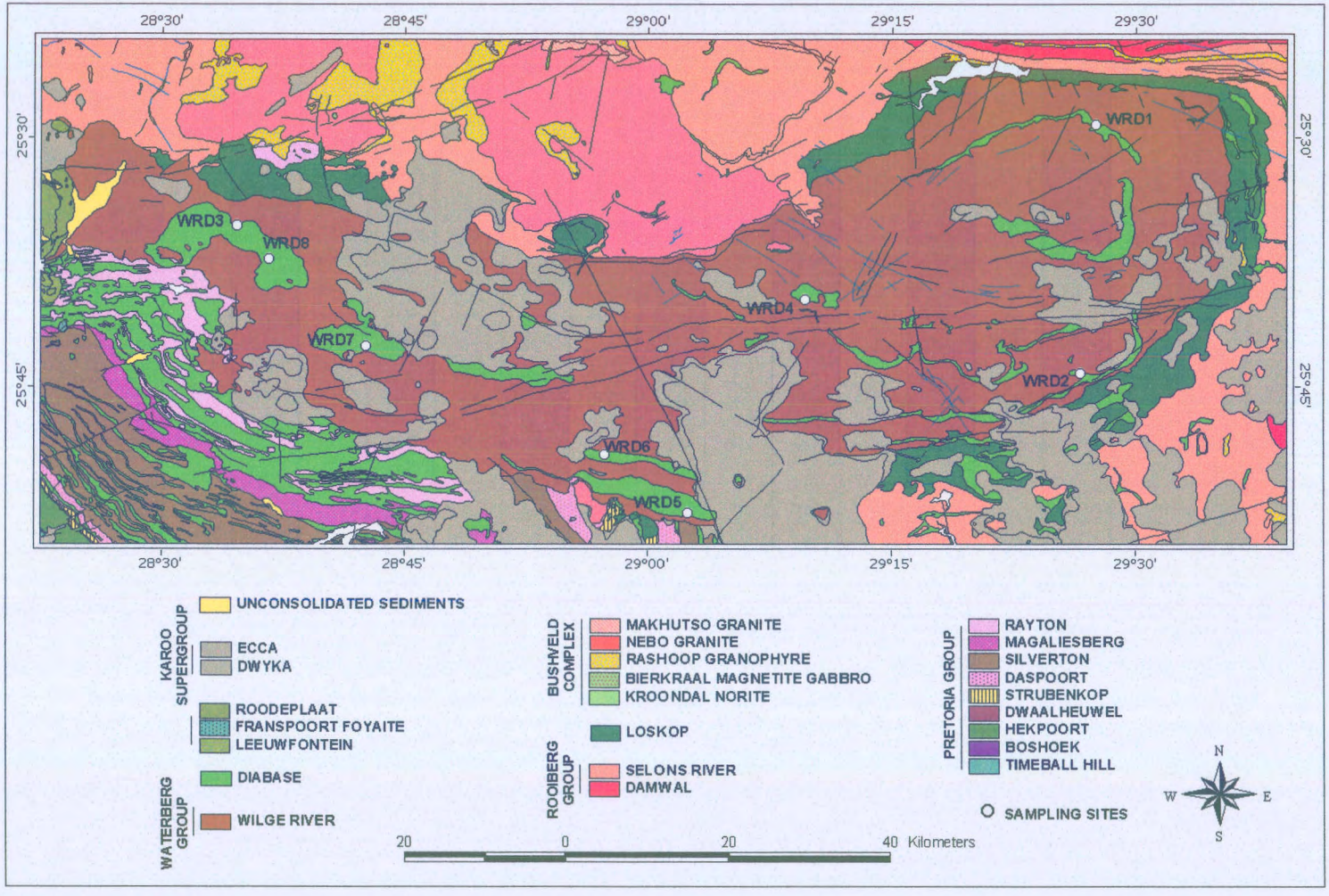

Figure 7.2: Distribution of the lithostratigraphic units in the Middelburg basin indicating the sampling sites on the diabase in the Wilge River Formation (1:250 000 Geological Series 2528 Pretoria, 1978).

B. Laboratory Results

The population means, as well as the associated confidence intervals for the magnetic susceptibility, anisotropy of magnetic susceptibility (AMS) as well as the normal remanent magnetization (NRM) was calculated for all the intrusive and volcanic rocks measured in the lower Waterberg Group. These population means are summarized in Tables 7.1-7.3.

Table 7.1: Statistical parameters of the magnetic susceptibilities from the intrusive and volcanic rocks of the lower Waterberg Group.

	N	μ x10^{-6} SI	S x10^{-6} SI	R x10^{-6} SI
Swaershoek Formation diabase	144	3232.00	3034.14 – 3448.11	56.43 – 18887.76
Wilge River Formation diabase	173	22637.04	21253.91 – 24153.72	6474.70 – 67281.23
Swaershoek Formation trachytic lava	41	194.98	183.07 – 208.04	112.72 – 351.23

N = number of specimens; μ = estimated mean for population; S = central 95% confidence limits around estimated mean; R = range.

Table 7.2: Statistical parameters of the intensities of magnetization (NRM) from the intrusive and volcanic rocks of the lower Waterberg Group.

	N	μ A/m	S A/m	R A/m
Swaershoek Formation diabase	144	177.30	166.47 – 189.18	0.07 – 441.19
Wilge River Formation diabase	173	121.08	113.68 – 129.19	0.00 – 293.20
Swaershoek Formation trachytic lava	41	0.29	0.27 – 0.31	0.01 – 3.22

N = number of specimens; μ = estimated mean for population; S = central 95% confidence limits around estimated mean; R = range.

Table 7.3: Statistical parameters of the degree of anisotropy (An) from the intrusive and volcanic rocks of the lower Waterberg Group.

	N	μ	S	R
Swaershoek Formation diabase	144	1.13	1.06 – 1.21	1.03 – 1.31
Wilge River Formation diabase	173	1.08	1.01 – 1.15	1.02 – 1.19
Swaershoek Formation trachytic lava	41	1.08	1.01 – 1.15	1.00 – 1.21

N = number of specimens; μ = estimated mean for population; S = central 95% confidence limits around estimated mean; R = range.

Nylstroom Basin

As would be expected from a sill structure the magnetic minerals within the diabase in the Swaershoek Formation are mainly oblately orientated (Figure 7.3).

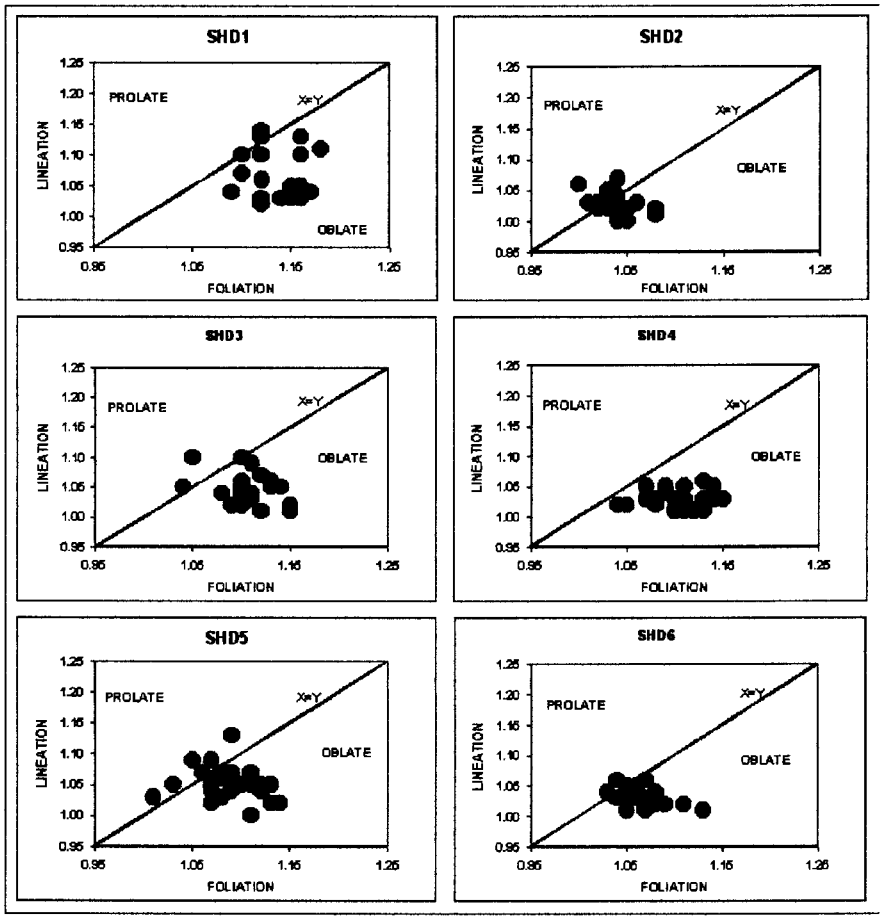

Figure 7.3: Flinn diagrams from diabase sill in the Nylstroom Protobasin indicating the oblate nature of the magnetic minerals.

The magnetic lineation for each site was determined by observing the axial distributions of the principal susceptibilities plotted on a stereonet. These directions were plotted on the geology map to determine the relationship between the magnetic and volcanic fabric (Figure 7.4). It is clear that the magnetic lineations not only indicate the radial flow directions at these sites, but also in several cases the local deformational structures played a major role in the orientation of the magnetic minerals. The mean plane of magnetic foliation for the diabase intrusions is 43.3°, correlating well with a basin-shaped sill. The mean plane of magnetic foliation for the trachyte intrusions it is 37.2°. In both cases the magnetic foliation is steeper than the surrounding sediments into which these rocks intruded.

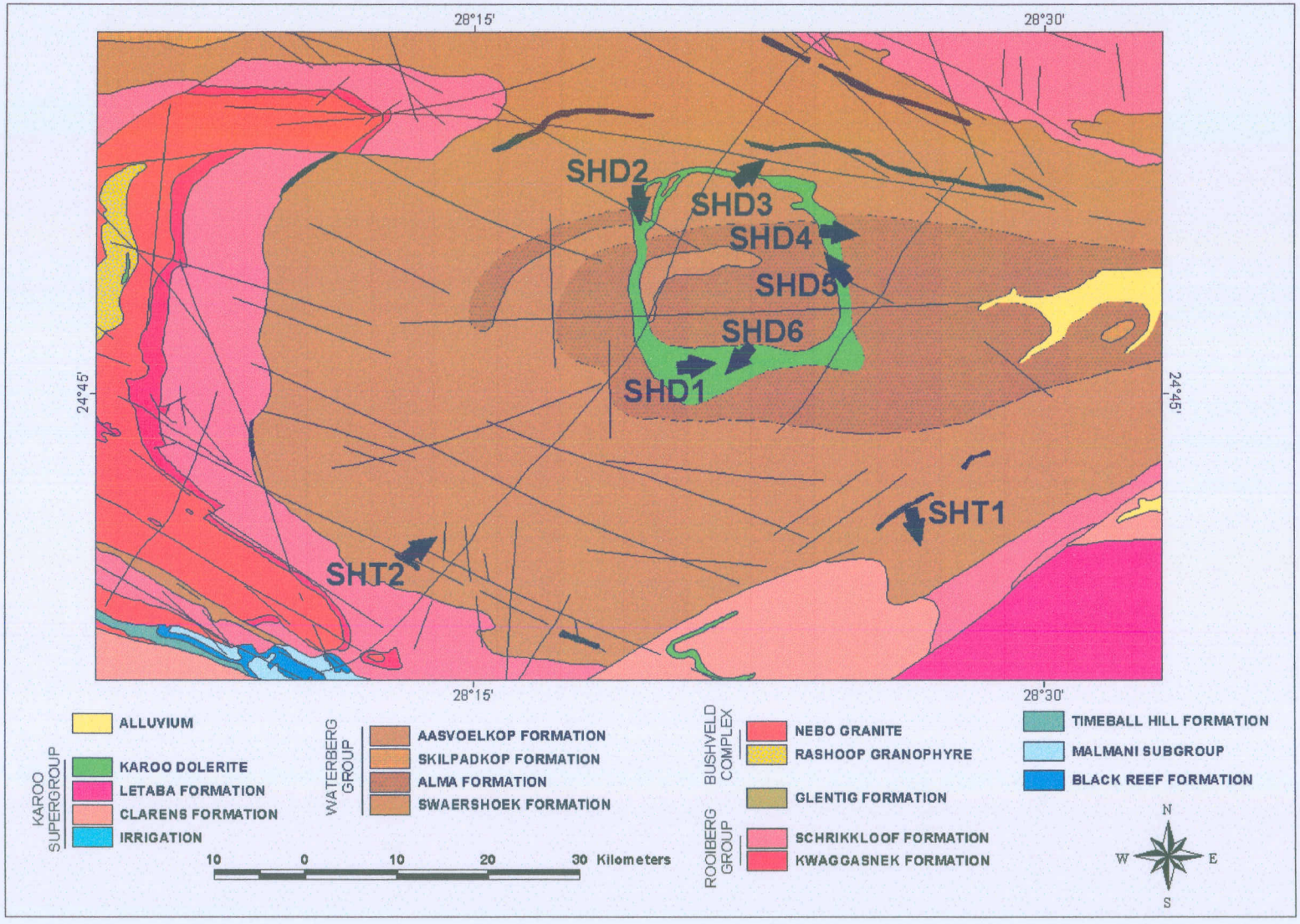

Figure 7.4: Map showing directions of magnetic lineation for the diabase sill and trachytic lava sites in the Nylstroom protobasin.

Middelburg Basin

Even though the degrees of anisotropy for the diabase are virtually isotropic, the Flinn diagrams (Figure 7.5) display the typical oblate orientation of sills. The only exceptions are sites 5 and 6, which display definite prolate orientations of the magnetic minerals. It is suggested that these two sites are situated on diabase dykes rather than sills. This theory is supported by the axial distributions of the principal susceptibilities of site WRD6 plotted on an equal-area projection (Figure 7.6). The magnetic lineation (maximum susceptibility, K_1) for this site indicates that the diabase intruded vertically.

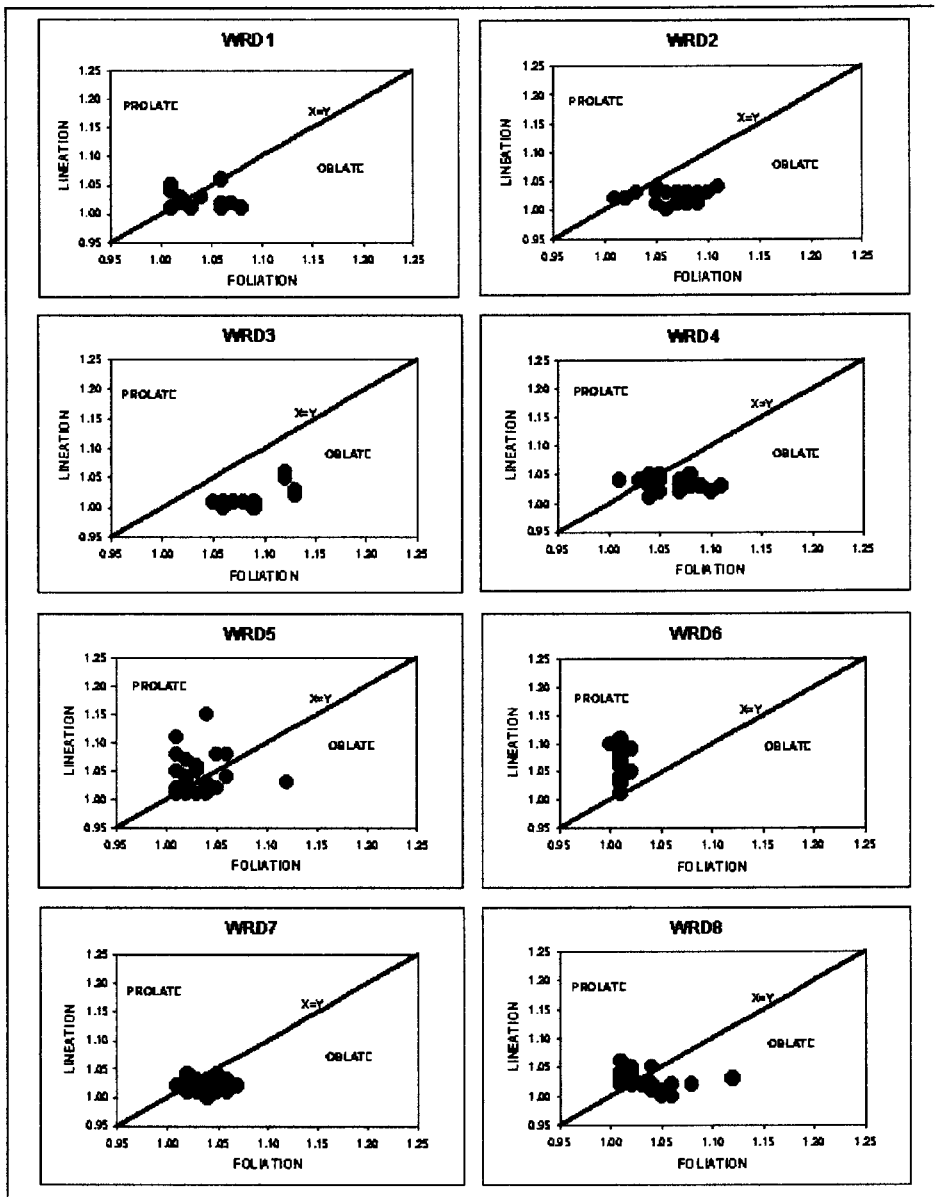

Figure 7.5 : Flinn diagrams from diabase sills situated in the Wilge River Formation.

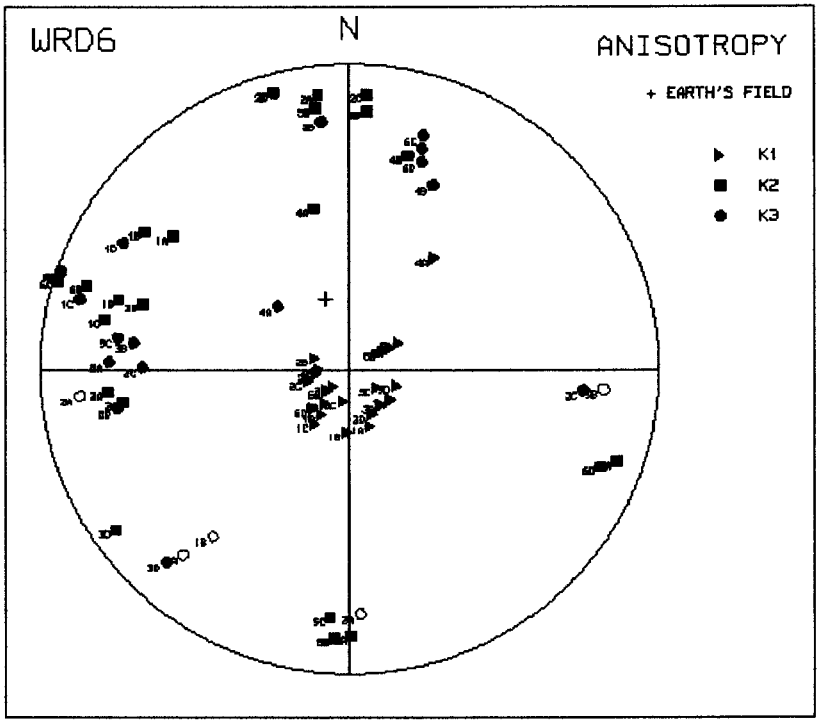

Figure 7.6: Directions of principal susceptibilities for site WRD6. σ=maximum susceptibility direction (K1), ν=intermediate susceptibility direction (K2), λ=minimum susceptibility direction (K3).

The mean plane of magnetic foliation for the diabase intrusions in the Middelburg Basin is relatively shallow, dipping at 25.3°, thereby confirming the intrusions to be sills. As previously discussed the plane of magnetic foliation at site WRD6 is very steep at 79.8° which suggests that this outcrop intruded as a dyke rather than a sill.

C. Stepwise Alternating field (AF) and Thermal Demagnetization

Nylstroom Protobasin

A total of 66 specimens from the 6 sampling sites on the diabase in the Nylstroom protobasin were subjected to alternating field (AF) demagnetization up to a maximum of 100mT. Most of the specimens however were completely demagnetized at 50mT or became unstable at the higher applied fields. One specimen was thermally demagnetized up to 600 °C to confirm magnetite as the primary magnetization component.

All the diabase specimens from the Nylstroom protobasin carried some lightning effect with anomalously high initial NRM intensities that quickly decreased upon AF demagnetization. As the climate in South Africa is conducive to lightning, and with the absence of Pleistocene glaciation and prevailing climatic conditions favourable for chemical weathering (Brink, 1979), IRM is the dominant cause of directional variation of remanent magnetization in surface exposures in southern Africa

(Gough, 1967). This led to the results not always reflecting the primary magnetization components but a combination of different components (Figure 7.7, specimen SHD16B).

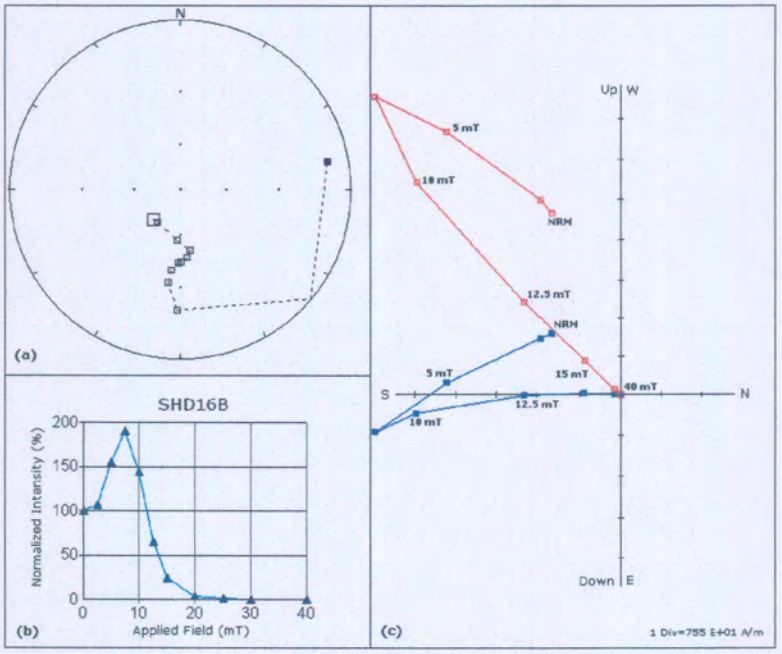

Figure 7.7: Response of specimen SHD16B to AF demagnetization. (a) Equal-area projection of the change in direction of magnetization; (b) Normalized magnetic intensity curve of progressive demagnetization results; (c) Zijderveld plot with blue representing the vertical plane and red the horizontal plane; The scale on the axes is in A/m; The distance of each data point from the origin indicates the total NRM intensity.

Nearly half of the demagnetization curves followed remagnetization circles (Figure 7.8, specimen SHD25C).

Two specimens from the trachytic lava at site SHT1 were subjected to alternating field (AF) demagnetization up to a maximum of 120mT. Due to the high coercive force of the secondary component in these samples the secondary magnetization could not be delineated with this method. It was thus decided to subject the rest of the specimens to progressive thermal demagnetization. Figure 7.9 illustrates how thermal demagnetization was able to delineate specimen SHT13B, where AF demagnetization was unable to do so.

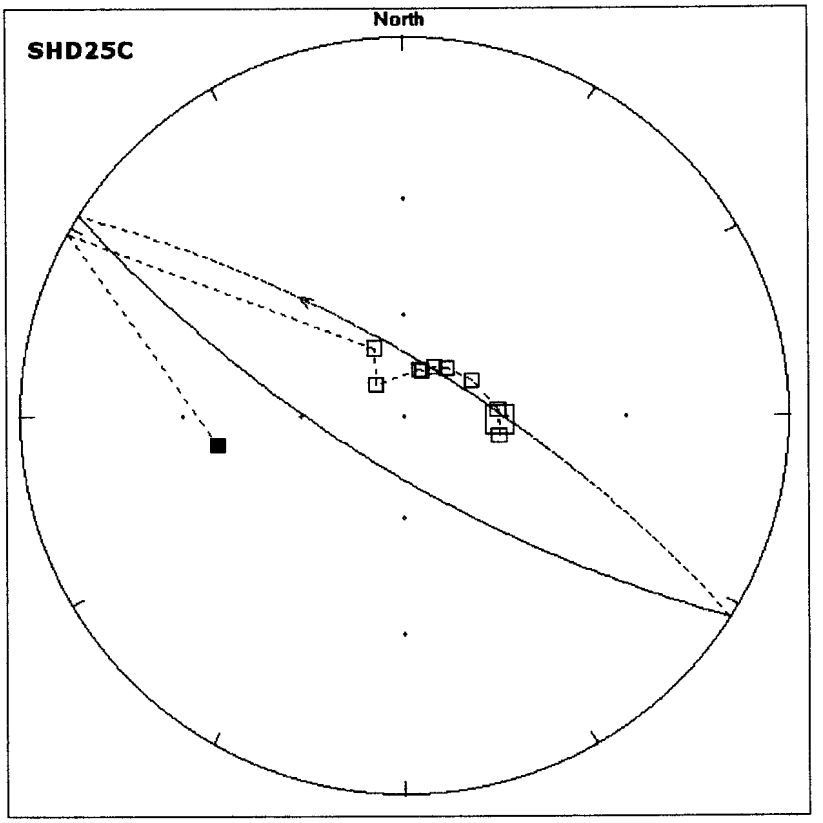

Figure 7.8: Stereographic projection of the change in direction of magnetization of specimen SHD25C during AF demagnetization, illustrating the distribution of progressive demagnetization results along a remagnetization circle.

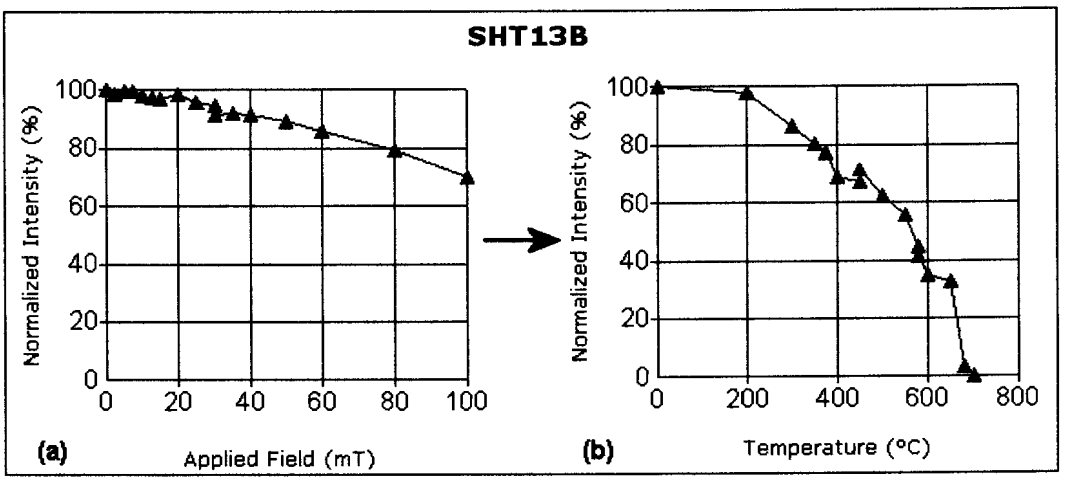

Figure 7.9: Comparison of different demagnetization processes on specimen SHT13B. (a) AF demagnetization was unable to delineate the magnetization, while (b) thermal demagnetization indicating blocking temperature of 680 °C.

A total of 14 specimens from the two sampled trachytic lava sites were thermally demagnetized up to temperatures of 725 °C. Figure 7.10 displays the typical demagnetization curve for the magnetic mineral haematite (blocking temperature at ~680 °C), which is the dominant magnetic component present at site SHT1. Figure 7.11 displays the presence of not only haematite, but also magnetite (blocking temperature at ~580 °C) at site SHT2. This ~580 °C component is interpreted as secondary chemical remanent magnetization (CRM) possibly obtained during hydrothermal alteration as discussed by Jansen (1970; 1982).

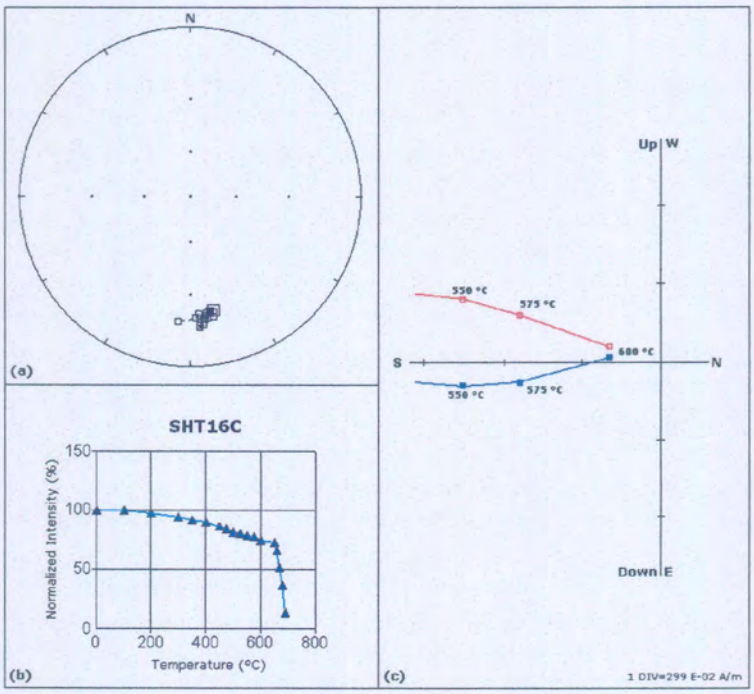

Figure 7.10: Response of the specimen SHT16C to thermal demagnetization. (a) Equal-area projection of the change in direction of magnetization; (b) Normalized magnetic intensity curve of progressive demagnetization results indicating a blocking temperature of 680 °C; (c) Zijderveld plot with blue representing the vertical plane and red the horizontal plane; The scale on the axes is in A/m; The distance of each data point from the origin indicates the total NRM intensity.

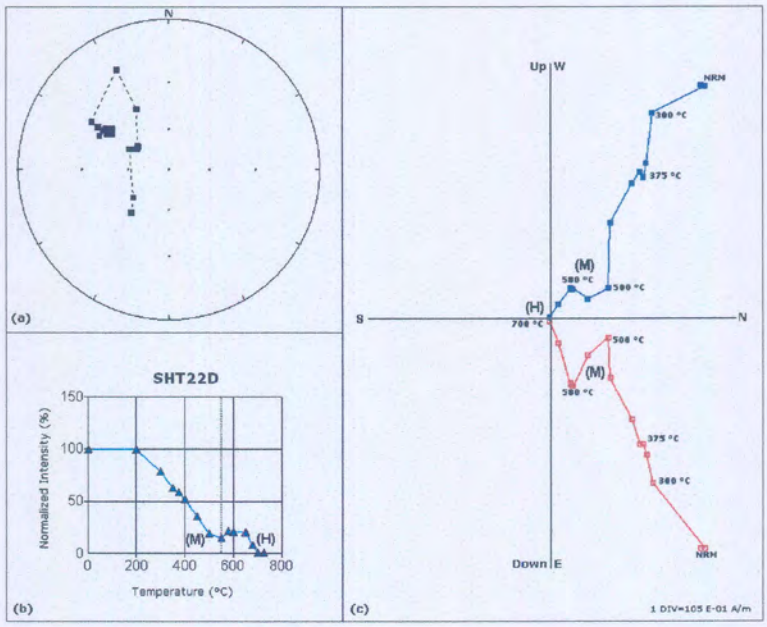

Figure 7.11: Response of specimen SHT22D to thermal demagnetization indicating a combination of the magnetite (**M**) and haematite (**H**) components (a) Equal-area projection of the change in direction of magnetization; (b) Normalized magnetic intensity curve of progressive demagnetization results; (c) Zijderveld plot with blue representing the vertical plane and red the horizontal plane; The scale on the axes is in A/m; The distance of each data point from the origin indicates the total NRM intensity.

Middelburg Basin

A total of 67 specimens from 8 sampling sites on the diabase in the Middelburg basin were subjected to alternating field (AF) demagnetization up to a maximum of 80mT. Most of the specimens however were completely demagnetized at 30mT or became unstable at the higher applied fields. Two specimens were thermally demagnetized up to 600 °C (Figure 7.12) indicating magnetite as the main magnetic component of the diabase.

Similar to the diabase specimens from the Nylstroom Protobasin most of the diabase from the Middelburg basin carried some lightning effect which explains the rapid decrease in magnetic intensity during AF demagnetization (Figure 7.13, specimen WRD53D). Nearly all the demagnetization curves followed remagnetization circles (Figure 7.14, specimen WRD84D) indicating multiple components of NRM with severely overlapping coercivity spectra.

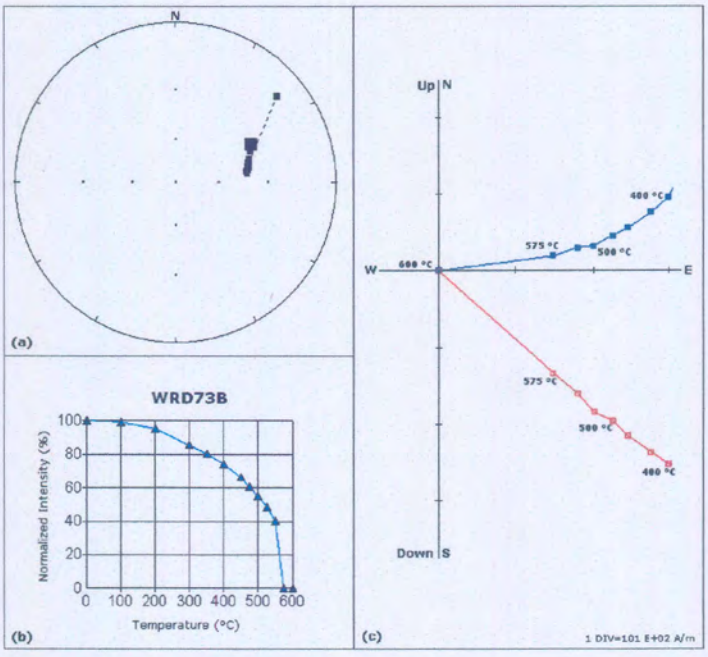

Figure 7.12: Response of specimen WRD73B to thermal demagnetization indicating magnetite as the main magnetic component in the diabase. (a) Equal-area projection of the change in direction of magnetization; (b) Normalized magnetic intensity curve of progressive demagnetization results; (c) Zijderveld plot with blue representing the vertical plane and red the horizontal plane; The scale on the axes is in A/m; The distance of each data point from the origin indicates the total NRM intensity.

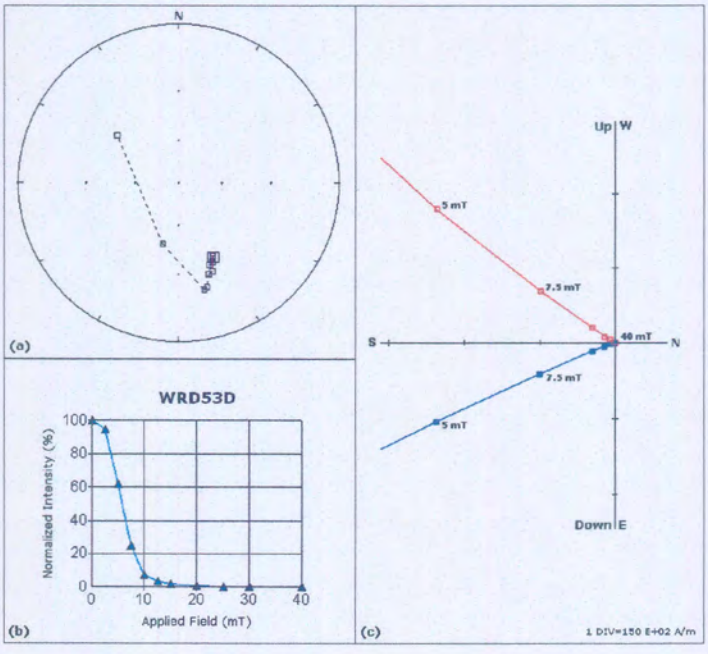

Figure 7.13: Response of specimen WRD53D to AF demagnetization (a) Equal-area projection of the change in direction of magnetization; (b) Normalized magnetic intensity curve of progressive demagnetization results illustrating the rapid decrease in magnetic intensity associated with the removal of a superimposed lightning component.; (c) Zijderveld plot with blue representing the vertical plane

and red the horizontal plane; The scale on the axes is in A/m; The distance of each data point from the origin indicates the total NRM intensity.

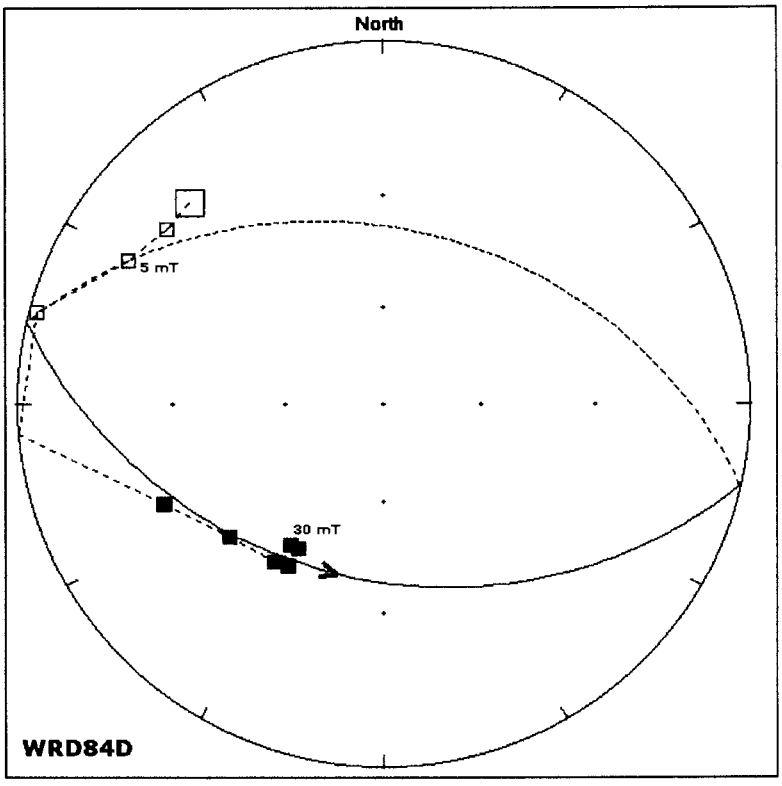

Figure 7.14: Equal-area projection of the change in direction of magnetization of specimen WRD84D during AF demagnetization, illustrating the distribution of progressive demagnetization results along a remagnetization circle.

D. Mineralogy of Opaque Minerals

As discussed in previous chapters the Curie temperatures of ferromagnetic minerals can be determined from strong-field thermomagnetic experiments. Figure 7.15 shows representative results of strong-field thermomagnetic analysis on a diabase specimen from the Nylstroom Protobasin (specimen SHD16C) while Figure 7.16 shows representative results from the Middelburg Basin (specimen WRD61B). A Curie temperature of 580 °C was observed both on heating and cooling confirming that the main magnetization component for the diabase in both basins is magnetite.

Figure 7.17 shows representative results of strong-field thermomagnetic analysis for specimen SHT16C. Due to the very weak intensity of magnetization the specimen nearly immediately acquires a secondary magnetization (steady increase of heating curve). However, a Curie temperature of ~680 °C is observed both on heating and cooling confirming that the main magnetization component for the

trachytic lava in the Swaershoek Formation is haematite. Figure 7.17 displays actual data and the noise visible on the curve is due to the very low magnetic intensity of this sample as well as instrument drift.

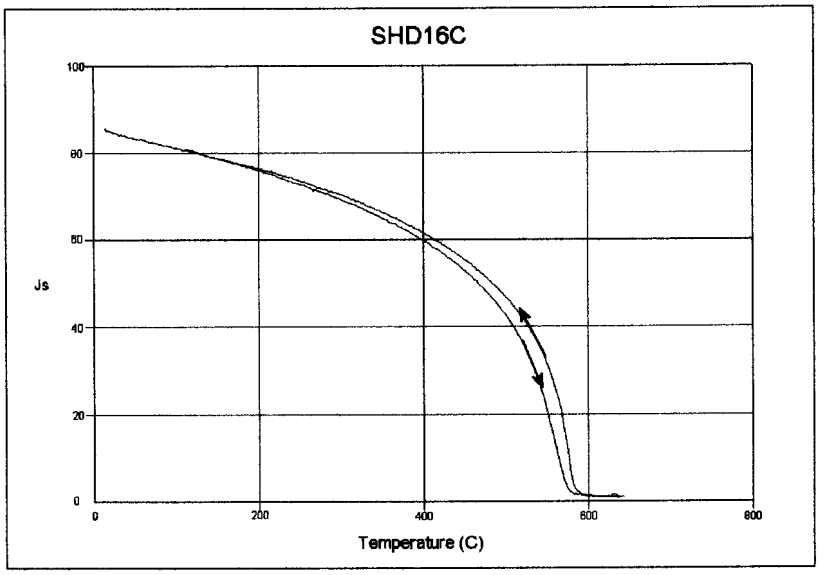

Figure 7.15: Strong-field thermomagnetic behaviour of specimen SHD16C. Arrows indicate the direction of temperature change (heating and cooling). It is clear from the smooth curves that magnetite is the only magnetic component present in this specimen.

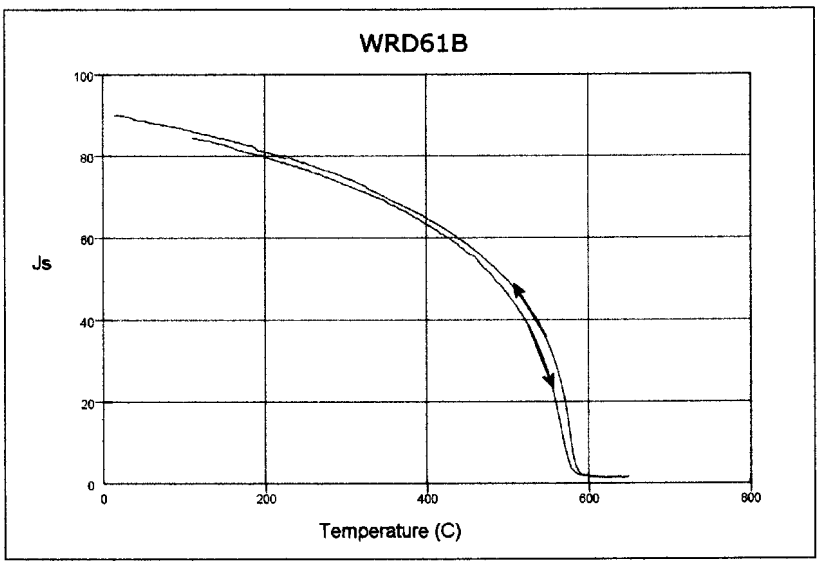

Figure 7.16: Strong-field thermomagnetic behaviour of specimen WRD61B. Arrows indicate the direction of temperature change (heating and cooling). It is clear from the smooth curves that magnetite is the only magnetic component present in this specimen.

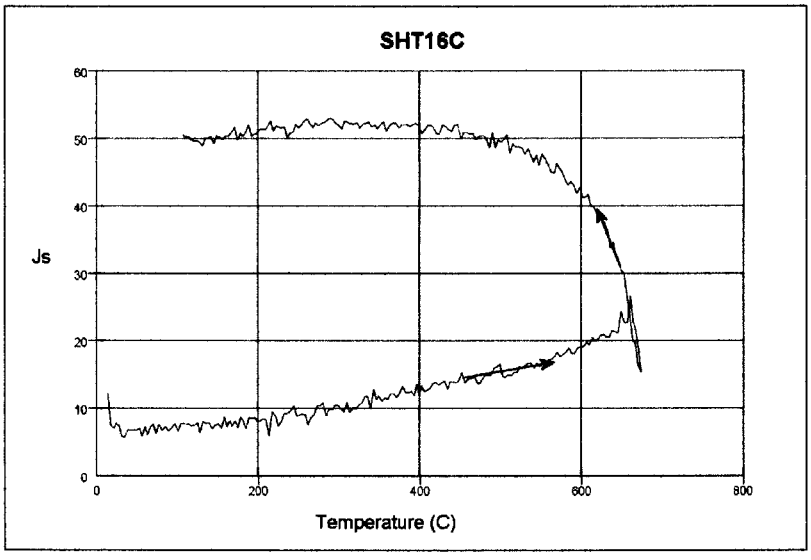

Figure 7.17: Strong-field thermomagnetic behaviour of specimen SHT16C. Arrows indicate the direction of temperature change (heating and cooling). Due to the very low magnetic intensity of the specimen as well as the sensitivity of the instrument the curves display a lot of noise.

E. Statistical results and palaeomagnetic pole positions

Nylstroom protobasin

Due to the widespread lightning effect on the diabase specimens in the Nylstroom protobasin combined with the limited number of sampling sites, good statistical means were difficult to obtain. The site means were calculated from the combined analysis of remagnetization circles and direct observations using software developed by Torsvik et al. (1996). The calculated site means and related virtual geomagnetic pole positions (VGP) are summarized in Table 7.4.

Table 7.4: Summary of results for Swaershoek Formation diabase.

SITE	DEMAGNETIZATION DATA				VGP			
#	SDEC	SINC	MAD	N	LAT	LONG	DP	DM
SHD1	141.66	-60.17	11.00	5	-15.2	179.4	13.0	17.0
SHD2	206.31	15.59	5.00	3	-59.7	269.2	2.0	5.0
SHD3	219.85	40.73	7.00	4	-53.7	304.7	5.0	9.0
SHD4	189.72	-35.46	26.00	5	-44.7	221.3	17.0	30.0
SHD5	169.75	-13.95	30.00	4	-56.7	189.7	16.0	31.0
SHD6	208.01	56.27	10.00	2	-63.2	331.9	10.0	14.0

The directions of magnetization for the diabase in the Nylstroom protobasin don't converge, but are scattered around Dec = 191.48° and Inc = 0.88° (N=6, k=2.73 and α_{95}=50.3°). Similarly the calculated VGPs for the diabase in the Nylstroom protobasin are scattered around a pole position of 63.3° S and 233.2° E, with precision parameter of only A_{95}=35.7° (anti-pole: 63.3° N, 53.2° E).

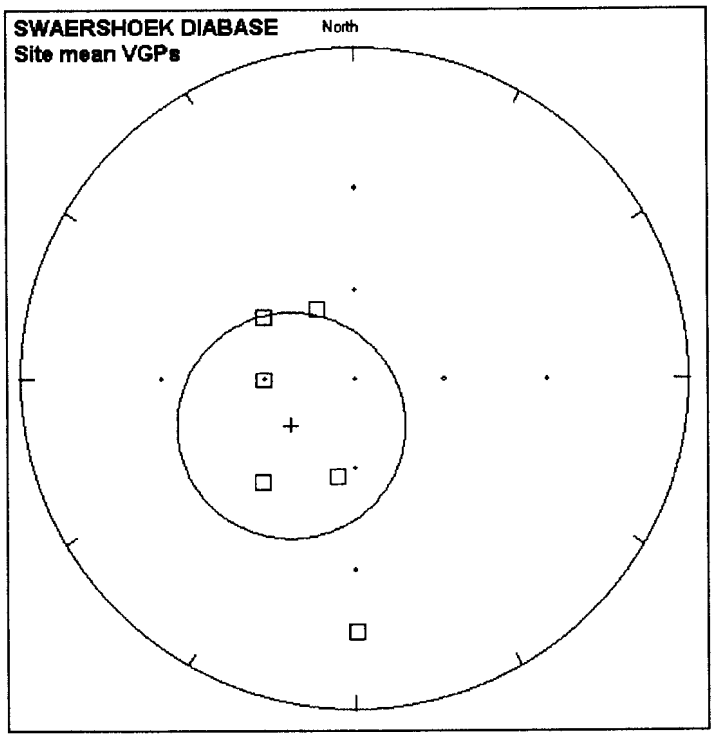

Figure 7.18: Site virtual geomagnetic pole positions (VGP) for the Swaershoek diabase demonstrating poor statistical grouping.

Normally data with a precision parameter >20° will not be considered for further discussion. However, the very weak calculated pole for the Nylstroom diabase does correlate fairly well with published pole positions for the Umkondo diabase by McElhinny and Opdyke (1964) (65.0° N, 42.5° E, A_{95}=6.0°) as well as a result for the post-Waterberg diabase by Jones and McElhinny (1966) (65.0° N, 50.5° E, A_{95}=4.5°).

Due to the fact that most of the trachyte extrusions are hydro-thermally altered and highly weathered (Jansen, 1982), it was not possible to sample from sufficient sites for good statistical analysis. The demagnetization results and associated VGPs for the two trachytic lava sites are presented in Table 7.2.

Table 7.5: Summary of results for the trachytic lava in the Swaershoek Formation.

SITE	DEMAGNETIZATION DATA				VGP			
#	SDEC	SINC	MAD	N	LAT	LONG	DP	DM
SHT1	161.70	-38.20	9.00	5	-40.4	185.9	6.3	10.7
SHT2	155.00	-20.60	0.90	4	-47.0	170.7	0.5	0.9

There is statistically no meaning in a mean for only two points. However, since the two available sites for the trachytic lava correlate so well, a "mean" was calculated for curiosity's sake. The mean direction of magnetization for the two trachytic lava sites is Dec = 158.1° and Inc = -29.4°, N=2, k=38.3 and α_{95}=41.5°. The mean virtual palaeomagnetic pole position (VGP) for the trachytic lava is 43.94° S and 178.72° E, A_{95}=28°.

Middelburg basin

The results from the Middelburg basin are summarized in Table 7.3. Even though there was widespread lightning effect visible from the demagnetization results, good statistical means were obtained. The site means were calculated using remagnetization circles.

Table 7.6: Summary of results for Wilge River Formation diabase.

SITE	DEMAGNETIZATION DATA				VGP			
#	SDEC	SINC	MAD	N	LAT	LONG	DP	DM
WRD1	177.30	-5.10	13.7	6	-61.8	203.7	6.9	13.7
WRD2	142.50	-10.20	16.6	5	-42.3	154.4	8.5	16.8
WRD3	174.00	9.50	6.3	4	-68.4	192.0	3.2	6.4
WRD4	178.10	11.10	8.2	5	-69.9	203.7	4.2	8.3
WRD5	173.90	15.20	15.3	5	-70.9	190.2	8.1	15.7
WRD6	201.70	1.10	33.6	8	-57.2	252.0	16.8	33.6
WRD7	185.10	21.70	22.7	8	-74.8	228.1	12.6	24.0
WRD8	205.50	29.60	16.8	7	-64.3	281.3	10.3	18.6

The mean direction of magnetization for the Middelburg basin diabase is Dec = 179.5° and Inc = 9.6°, N=8, k=12.5 and α_{95}=16.3°. The associated palaeomagnetic pole position was calculated as 69.3° S and 208.5° E, with precision parameter A_{95}=14.2° (anti-pole: 69.3° N, 28.5° E).

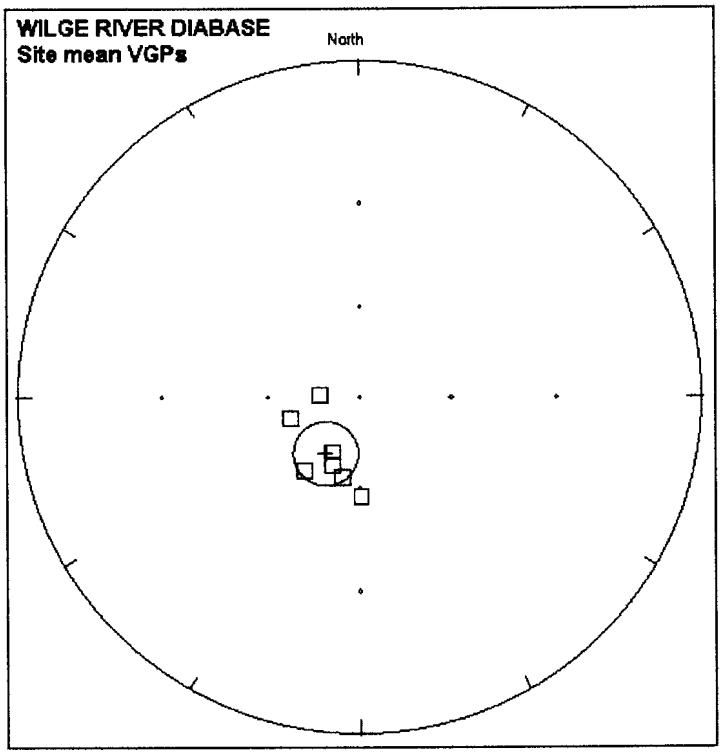

Figure 7.19: Site virtual geomagnetic pole positions (VGP) for the Wilge River diabase demonstrating good statistical grouping.

8. THE PALAEOMAGNETISM OF THE MOGALAKWENA FORMATION

A. Geology

The Mogalakwena Formation is situated in the northeastern and northern reaches of the Main Waterberg Basin (Fig. 8.1). It has a conformable transitional lower boundary with the Makgabeng Formation in most areas. However, in the Blouberg region in the northeast, Bumby (2000) reported that the Mogalakwena Formation overlies the Makgabeng Formation on a disconformity or a slight unconformity. Where the Makgabeng Formation is not developed, the Mogalakwena Formation unconformably overlies pre-Waterberg rocks. In the Blouberg Formation basin, less than 5 km south of the southern strand of the Melinda Fault, the Mogalakwena Formation rests unconformably on the Blouberg Formation, a localised post-Bushveld and pre-Waterberg unit lying on the southern boundary of the Central Zone, Limpopo mobile belt (Bumby *et al.*, 2001a). The upper Mogalakwena boundary is a conformable, transitional contact with the Cleremont Formation (Tickell, 1975). Towards the south and southwest, the formation grades laterally into the Sandriviersberg Formation, but the boundary are poorly defined (Tickell, 1975). The formation is 1250 to 1500m thick.

Recent facies mapping of the Mogalakwena Formation (Bumby, 2000) shows that the unit is conglomeratic at its base, especially in the northeast; coarse sandstone and granulestone beds become predominant higher in the stratigraphy, and in more distal areas towards the south and the west.According to Tickell (1975) the Mogalakwena Formation consists of granule-rich arenites and granule rudite with pebble washes and interbedded pebble rudites. The rudites are subordinate in volume to the arenites. Coarse rudites are common, especially towards the north.

Callaghan (1987), who studied the unit across the Main Waterberg Basin, found that arenites, granule-rich arenites and pebbly granule arenites, which can usually be described as litharenites or sublitharenites, make up the bulk of the Mogalakwena Formation (Callaghan, 1987). They commonly have a red or yellow-red hue. The arenites are generally granule-rich and poorly sorted, with a high percentage of lutaceous matrix. Grains are usually subangular to subrounded and equant. Trough cross-bedding is predominant, although planar cross-bedding may be more abundant locally. The average palaeocurrent direction derived from all structures for the Mogalakwena Formation is 244°; the vector strength is high (69% to 80%). Hence, the Limpopo belt was the main source area (Callaghan, 1987).

Local washes and lenses of small to large pebbles are common in this formation. More extensive rudite beds also occur and are on average 3m thick (Tickell, 1975). There is an increase in the average size of the clasts towards the northern preserved basin edge. In the transition zone with the Sandriviersberg Formation there is, however, no apparent difference in average clast size between the two formations.

Imbrication and length orientation are not well developed, this is probably the result of the equant shape of the clasts. The imbrication direction is at approximately right angles to the clast long axes; this

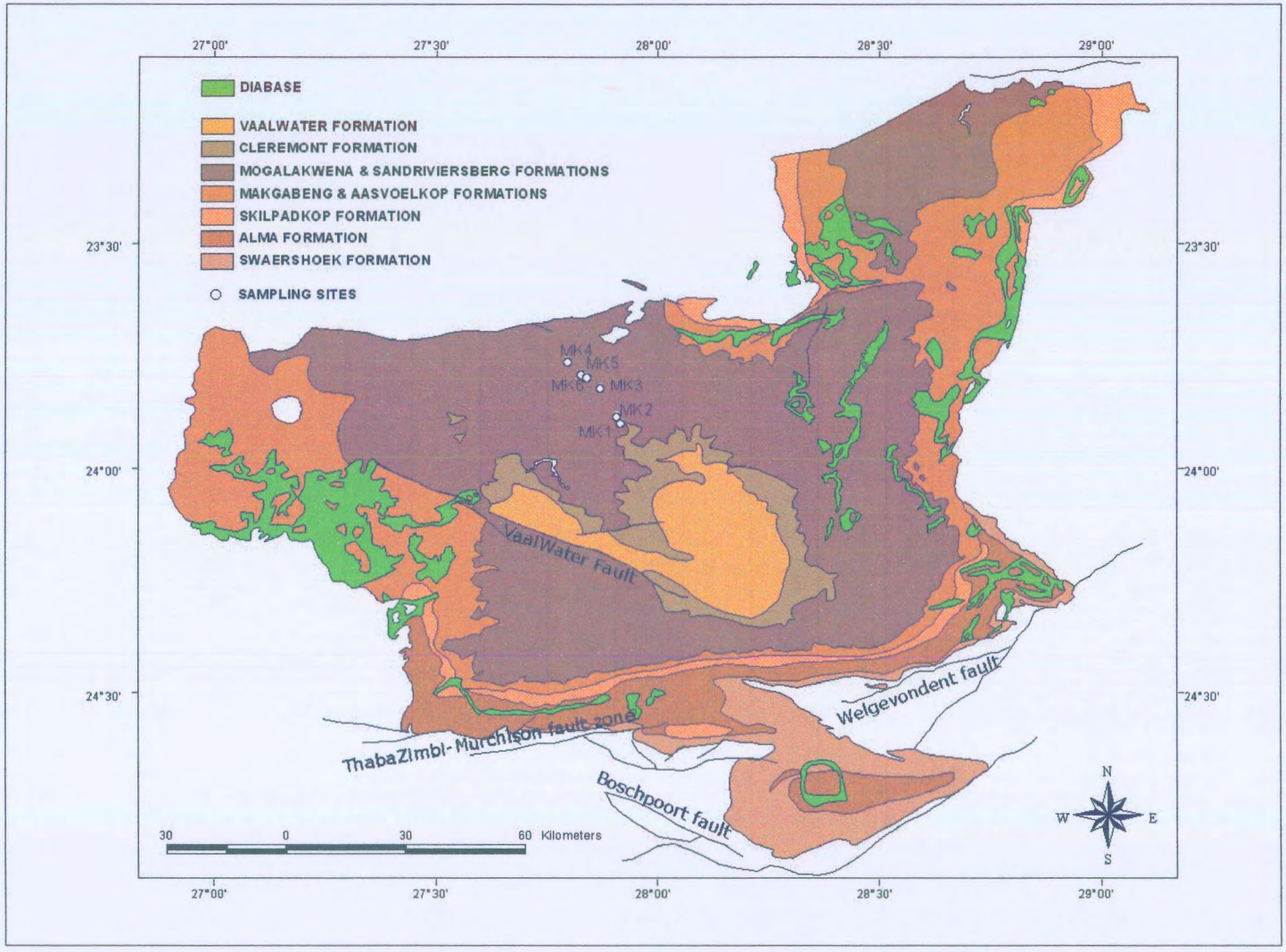

Figure 8.1: Distribution of the lithostratigraphic units within the Waterberg Group (modified from the 1:1 000 000 geological map for the Republic of South Africa and the Kingdoms of Lesotho and Swaziland; compiled by Keyser, 1997). The sampling localities within the Mogalakwena Formation are indicated.

relationship indicates the existence of a-transverse, b-imbricate type cross-bedding, characteristic of normal fluvial processes (Harms *et al.*, 1975). The rudites may be clast- or matrix-supported. Clast types include vein quartz, metaquartzite, felsitic quartzite, arenite, rudite, schist, quartzite, chert, jasper and iron-formation.

Lutites are restricted to clay drapes at the tops of beds and are usually very thin, less than 5mm in thickness.

The Mogalakwena strata, which rest unconformably over the Blouberg Formation, comprise more mature sediments than those of the Blouberg Formation (Bumby *et al.*, 2001a). The contrasting change in Mogalakwena facies from dominantly conglomeratic sheets (with subordinate trough cross-bedded coarse sandstone and granulestone sheets) to dominantly coarse sandstone and granulestone sheets (with subordinate conglomerate, generally confined to basal strata) seems to correlate well with the palaeocurrent direction (Bumby *et al.*, 2001a). According to Bumby *et al.* (2001a) there is a sharp contrast in the thickness of conglomerate facies on either side of the southern strand of the Melinda Fault, and these authors suggested that the Mogalakwena strata onlapped northwards over the denuding fault scarp, as the elevated palaeotopography to the north was peneplained.

Bumby *et al.* (2001a) proposed a provisional model for the tectono-sedimentary evolution of the Blouberg Formation and Waterberg Group. These authors suggested that the Blouberg Formation and Waterberg Group be considered as syn- and post-tectonic successions, respectively, that have been deposited in basins that have formed consecutively, due to reactivation tectonics within the Limpopo Belt along the Palala Shear Zone, accommodated by brittle movement on the Melinda Fault.

Callaghan (1993) proposed that the Sandriviersberg and Mogalakwena Formations be considered to be a single formation because of their lateral stratigraphic equivalence and their great similarity in sedimentary style. The coarser nature of the Mogalakwena Formation, as well as its higher percentage of lutite matrix and clay drapes, suggests that it is less mature than the rocks of the Sandriviersberg Formation and therefore more proximal.

Calculated peak current velocities during sedimentation of the Mogalakwena Formation range up to 5.3 m/s, whereas the maximum current velocities associated with deposition of the Sandriviersberg Formation were in the order of 2 m/s (Callaghan, 1987). These figures relate very well to "typical" flood velocities for rivers, given by Allen (1982).

The Mogalakwena and Sandriviersberg Formations appear to have been deposited during a period when the basin was deepening at a steady rate and during rapid uplift of a mountain mass to the northeast of the basin (Callaghan, 1993). Sedimentation was rapid (coarse-grained and poorly rounded grains), but certainly not chaotic, as indicated by a low occurrence of matrix-supported rudite and relatively consistent palaeocurrent directions. Sediments from the source mountain range built out into

the basin as a large braidplain, overtopping the Letaba-Makoppa rise and possibly continued to a distant ocean (Callaghan, 1987). Coarse rudite accumulated in proximal areas as longitudinal bars, whilst much of the sediment was laid down in channels in which megaripples migrated downstream. Less common lateral bars and sandwaves deposited planar cross-bedded sediments, especially in the more southerly areas. The Mogalakwena Formation was first attributed to braided river deposition by Tickell (1975).

B. Laboratory Results

The bulk magnetic susceptibility, anisotropy of magnetic susceptibility (AMS) and normal remanent magnetization (NRM) of all individual specimens from the Mogalakwena Formation were measured using the Digico system as described in Chapter 3. The frequency distribution of all three data sets were not symmetrical, but could be represented by two-parameter or three-parameter log normal distributions. The estimated mean for each data set as well as the central 95% confidence interval around each mean are listed in Table 8.1.

Table 8.1: Statistical parameters of the magnetic properties for the Mogalakwena Formation

	N	μ	S	R
Magnetic susceptibility ($x10^{-6}$) SI	183	56.95	53.47 – 60.76	19.98 – 287.39
Intensity of magnetization ($x10^{-3}$) A/m	183	22.84	21.44 – 24.37	0.9 – 1982.05
Degree of anisotropy (An)	183	1.18	1.11 – 1.26	1.01 – 2.70

N = number of specimens; μ = estimated mean for population; S = central 95% confidence limits around estimated mean; R = range.

Considering the degree of anisotropy for individual sites it was found that sites 1-3 have the highest values. These three sites might have experienced some deflection of their magnetization directions. Upon inspection of the geology map it was determined that these sites occur either on or near structural lineaments inferred from aerial photographs (mapped by S.J. Tickell during 1972-1973; 2326 Ellisras 1:250 000 sheet compiled and partly revised by G. Brandl, 1993). The Flinn diagrams indicate that sites 1-4 have predominantly oblate magnetic fabric (figure 8.4), while sites 5-6 tend to be more isotropic.

According to Hrouda (1982), if the ferromagnetic fraction is represented by a magnetically isotropic mineral of the magnetite type, the magnetic lineation (maximum susceptibility axes) is usually parallel to the current direction and plunges slightly against the current. Exceptionally, if the current is strong, the magnetic lineation may be perpendicular to the current owing to the rolling effect. If the carrier of

rock magnetism is haematite (as is the case for the Mogalakwena Formation), the intermediate susceptibility axes is parallel to the water current (Hrouda, 1982).

When comparing the current directions derived from AMS with that derived from the geological analysis, however, one needs to consider the sampling density of the two methods. In the case of the geologically derived average current direction, these directions are composed of both the sedimentary external structures (sole markings, flute casts, groove casts) as well as the internal structures (cross-bedding, current ripple lamination, symmetric and asymmetric ripples, imbricated pebble beds). In the case of AMS, sampling is dependent on the availability of fresh outcrops and as a rule, for normal palaeomagnetic studies (as is the case of this study), conglomerates or pebble beds are not sampled due to the reworking of the original magnetization directions. Further, due to the size of the samples it is not always possible to get a representative sample population of all the sedimentary structures needed to obtain a global current direction.

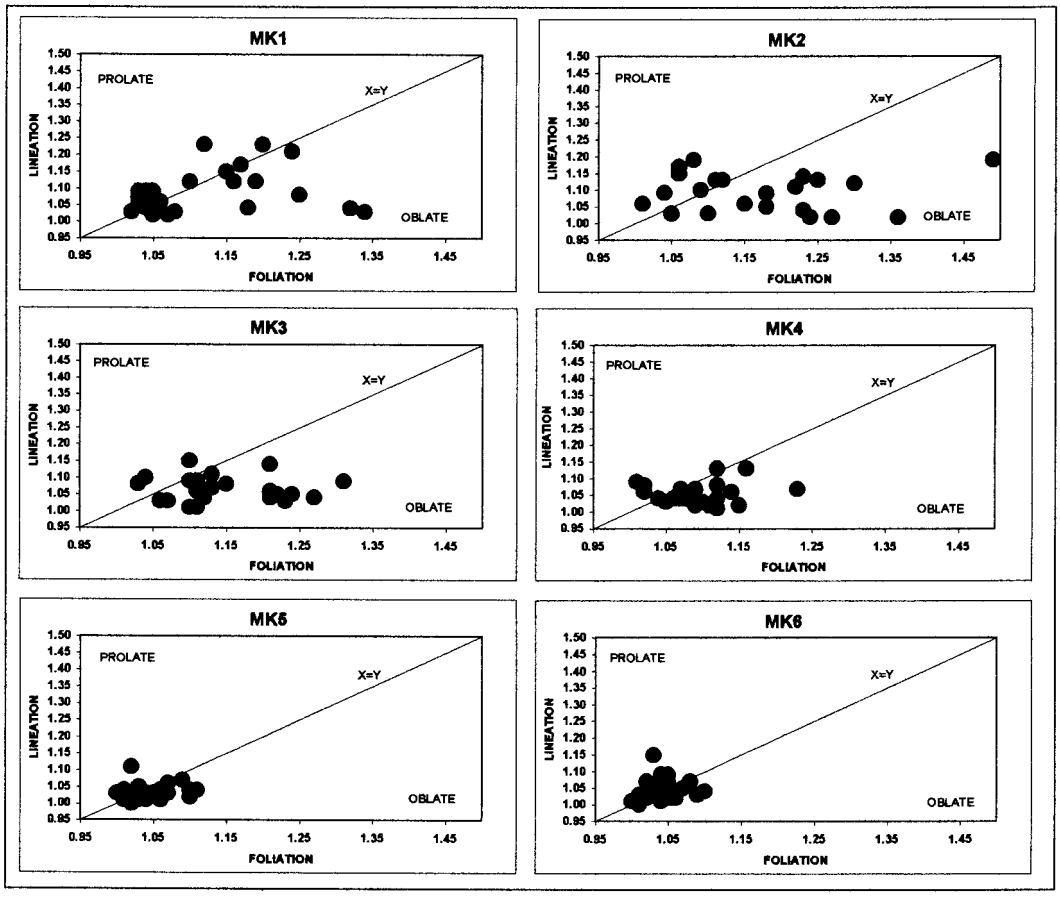

Figure 8.2: Flinn diagrams from the Mogalakwena Formation indicating the mainly oblate nature of the magnetic minerals within the sedimentary group.

The attitudes (in geographic coordinates) of the susceptibility axes were plotted on stereographic projections. Typical for sedimentary deposits, the minimum susceptibility axes of all the sites are

steeply dipping to near vertical and thus perpendicular to the bedding plane. According to these results the planar bedding planes range between 16.7° and 37.6°. The intermediate susceptibility axes of the Mogalakwena Formation are generally not clearly grouped, and indicate local deviations from the palaeocurrent described by Callaghan (1987, 1993). This might be explained by locally developed cross-bedding as well as insufficient sampling. Figure 8.5 displays the water current directions for each site, as indicated by the intermediate susceptibility axes.

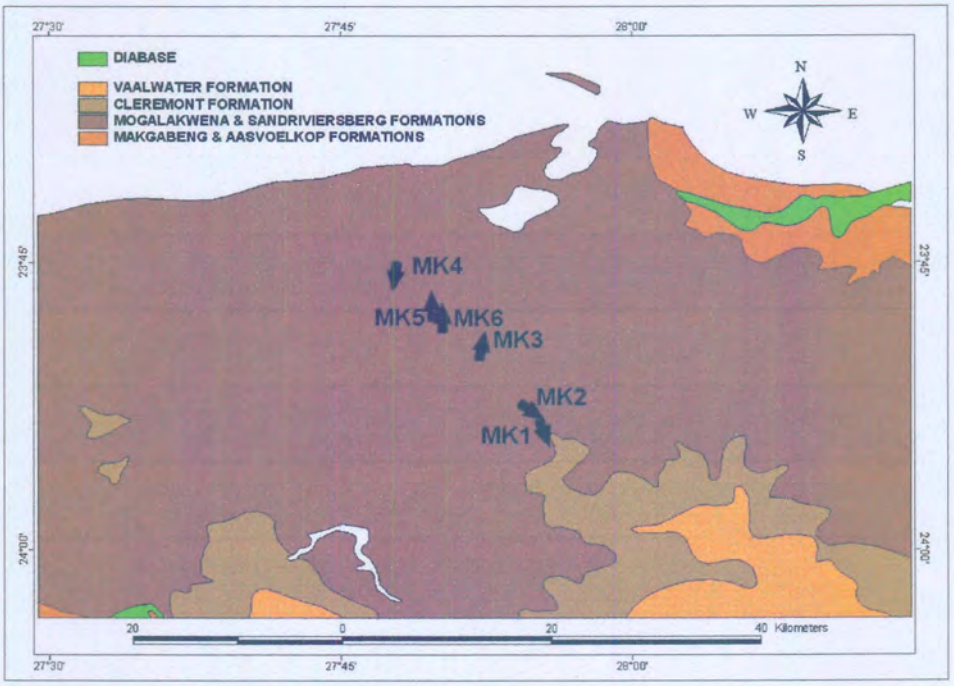

Figure 8.3: Current directions at sampling sites as derived from the intermediate susceptibility axes.

C. Stepwise Alternating Field (AF) and Thermal Demagnetization

Two specimens where subjected to AF demagnetization, but this method was unable to successfully demagnetize the specimens even up to applied fields of 120 mT. As discussed in Butler (1991) the haematite-bearing rocks usually carry high coercive force but small volume. Grains with these properties can carry secondary magnetization components, but would not be erased by AF demagnetization since their coercive force could easily exceed the maximum available field. Therefore, in rocks with haematite as the dominant ferromagnetic mineral, thermal demagnetization is required to remove the secondary magnetization. The rest of the specimens from the Mogalakwena Formation were thus demagnetized by means of thermal demagnetization. Figure 8.4 illustrates how thermal demagnetization was able to delineate specimen MK34E where AF demagnetization was unable to do so.

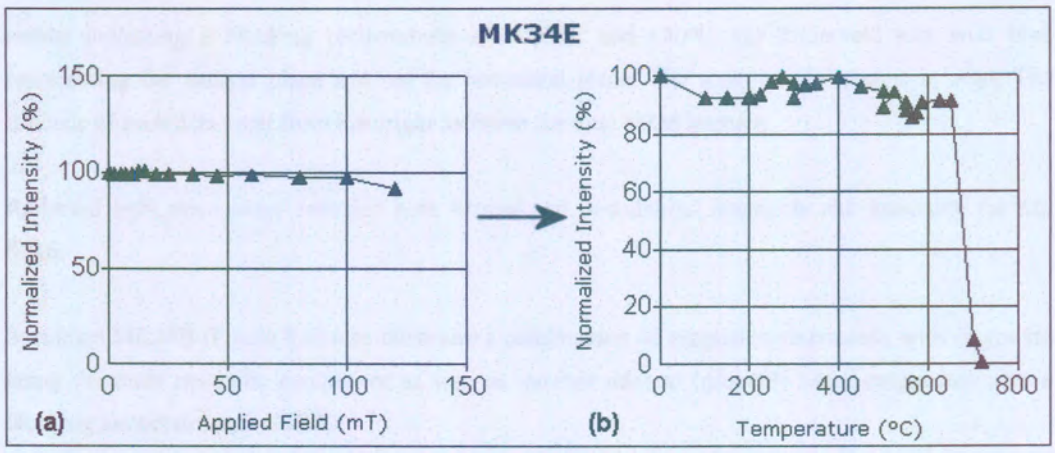

Figure 8.4: Comparison of different demagnetization processes on specimen MK34E. (a) AF demagnetization was unable to delineate the magnetization, while (b) thermal demagnetization indicating blocking temperature of ~680 °C

A total of 66 specimens was progressively thermally demagnetized up to temperatures of 725 °C. Figures 8.4 to 8.6 illustrate the typical responses of specimens from the Mogalakwena Formation to thermal demagnetization. The normalized intensity plot of specimen MK34E (Figure 8.4(b)) illustrates a typical response where haematite is the main magnetic component present (blocking temperature of ~680 °C). Specimen MK65A (Figure 8.5) illustrates a combination of magnetic components with overlapping coercivity spectra, with magnetite (blocking temperature of ~580 °C) as well as haematite (blocking temperature ~680 °C).

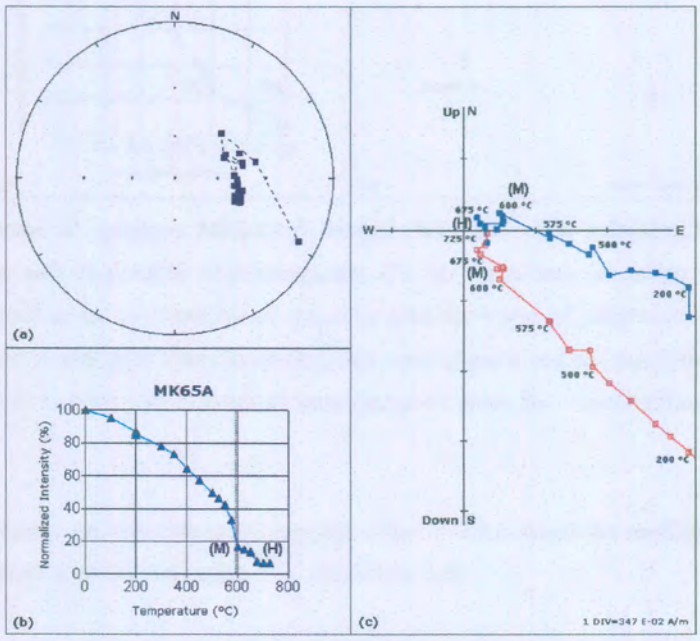

Figure 8.5: Response of specimen MK65A to thermal demagnetization indicating a combination of magnetite (M) as well as haematite (H) components. (a) Equal-area projection of the change in direction of magnetization; (b) Normalized magnetic intensity curve of progressive demagnetization

results indicating a blocking temperatures of 600 °C and 680°C; (c) Zijderveld plot with blue representing the vertical plane and red the horizontal plane; The scale on the axes is in A/m; The distance of each data point from the origin indicates the total NRM intensity

Reflected light microscopy revealed both detrital and post-detrital magnetite and haematite for site MK6.

Specimen MK24B (Figure 8.6) also illustrates a combination of magnetic components, with magnetite being the main magnetic component as well as another mineral (probably titano-magnetite) with a blocking temperature of ~375 °C.

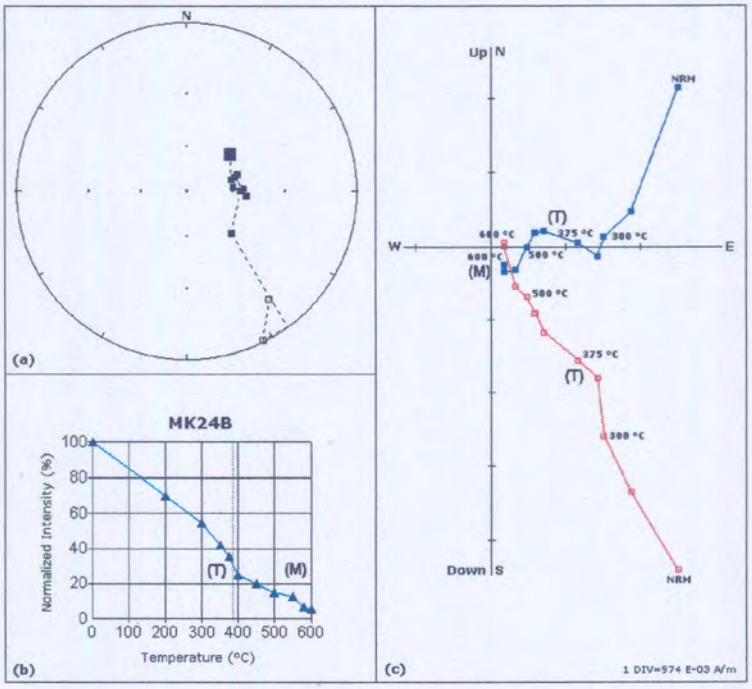

Figure 8.6: Response of specimen MK24B to thermal demagnetization indicating a combination of magnetite (M) as well as possibly titano-magnetite (T). (a) Equal-area projection of the change in direction of magnetization; (b) Normalized magnetic intensity curve of progressive demagnetization results; (c) Zijderveld plot with blue representing the vertical plane and red the horizontal plane; The scale on the axes is in A/m; The distance of each data point from the origin indicates the total NRM intensity.

Reflected light microscopy indicates radial growths of post-detrital magnetite needles as well as a few well rounded magnetite grains originating from the source rock.

In cases where a combination of magnetic minerals is present, the coercivity spectra yield a remagnetization circle during progressive demagnetization (Figure 8.7, specimen MK26D).

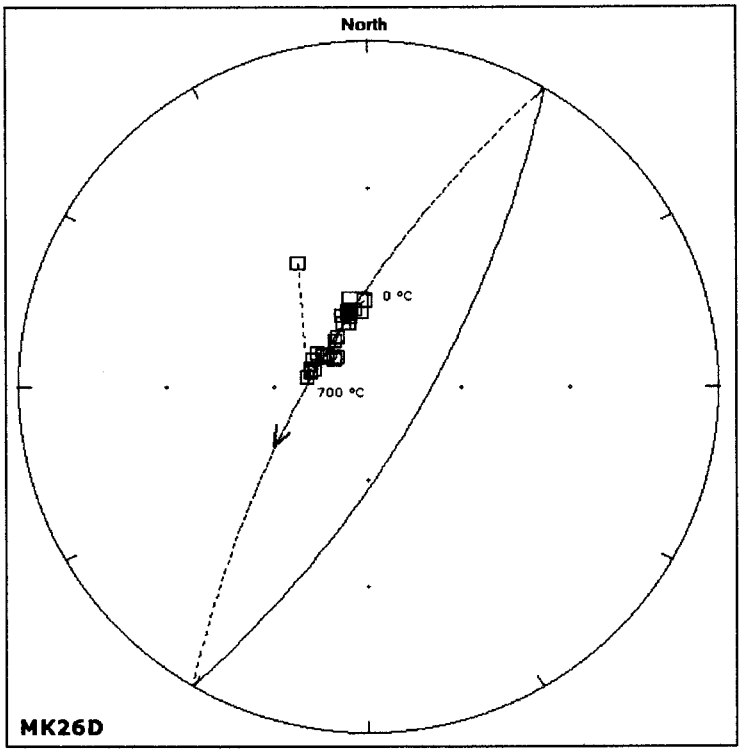

Figure 8.7: Equal-angle projection of the change in direction of magnetization of specimen MK26D to thermal demagnetization, demonstrating the overlapping coercivity spectra of magnetic minerals within this specimen.

D. Mineralogy of Opaque Minerals

Polished thin sections were made from 7 specimens of the Mogalakwena Formation. With the exception of site MK4, one polished thin section was made for each sampling site. The rocks are generally poorly to moderately sorted and the grains are sub-angular to sub-rounded. The opaque minerals were studied with reflected light microscopy.

The opaque minerals at both sites MK2 and MK3 consist predominantly of magnetite needles in the matrix. These needles have no preferred orientation but often occur as radial growths in the matrix. Both polished thin sections from site MK4 indicated little to no post-depositional magnetite growth in the matrix. These two thin-sections contained unsorted, but well-rounded magnetite grains with haematite exsolution lamellae. The rounded grains indicate that they originate from the parent rock, while the unsorted nature as well as the limited post-depositional magnetite in the matrix explains why no mean magnetization direction could be obtained for this site.

Strong-field thermomagnetic analysis was performed with a Curie balance on one sample from the Mogalakwena Formation (MK13A, Fig. 8.8). Although the magnetic intensity was very weak, a Curie temperature of ~680 °C is observed both on heating and cooling confirming that the main

magnetization component for site MK13 is haematite. Figure 8.8 displays actual data and the noise visible on the curve is due to the very low magnetic intensity of this sample as well as the sensitivity of the instrument.

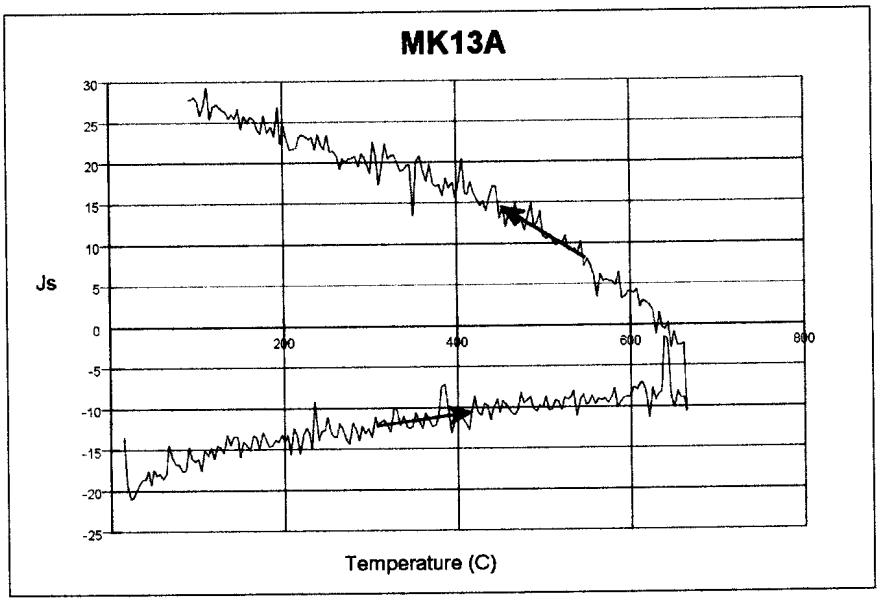

Figure 8.8: Strong-field thermomagnetic behaviour of specimen MK13A. Arrows indicate the direction of temperature change (heating and cooling). Due to the very low magnetic intensity of the sample as well as the sensitivity of the instrument the curves display a lot of noise.

E. Statistical results and palaeomagnetic pole position

The site mean results before and after bedding corrections are summarized in Table 8.2. The specimens from site MK4 produced completely random demagnetization directions. This can be explained, as discussed in paragraph D of this chapter, by the unsorted deposition of primary magnetite and haematite grains from the source rock, with very little to no post-depositional detrital growth in the matrix. The result from this site was thus not considered further during statistical analysis.

The site mean directions of sites MK1, MK2 and MK6 were calculated from remagnetization circles, while site MK5 were calculated from a combination of remagnetization circles and point data. Figure 8.9 displays the converging remagnetization circles from site MK6.

The mean direction of magnetization for the Mogalakwena Formation, calculated before bedding corrections, is Dec = 193.3° and Inc = -43.1°, N=5 and α_{95}=27.4°. After bedding corrections the mean direction of magnetization does not change much, Dec = 193.6° and Inc = -48.4°, N=5 and α_{95}=27.3°. The precision parameters for the Mogalakwena Formation are poor. This is not only due to the limited number of sites from this Formation, but is also common problem encountered with older rocks.

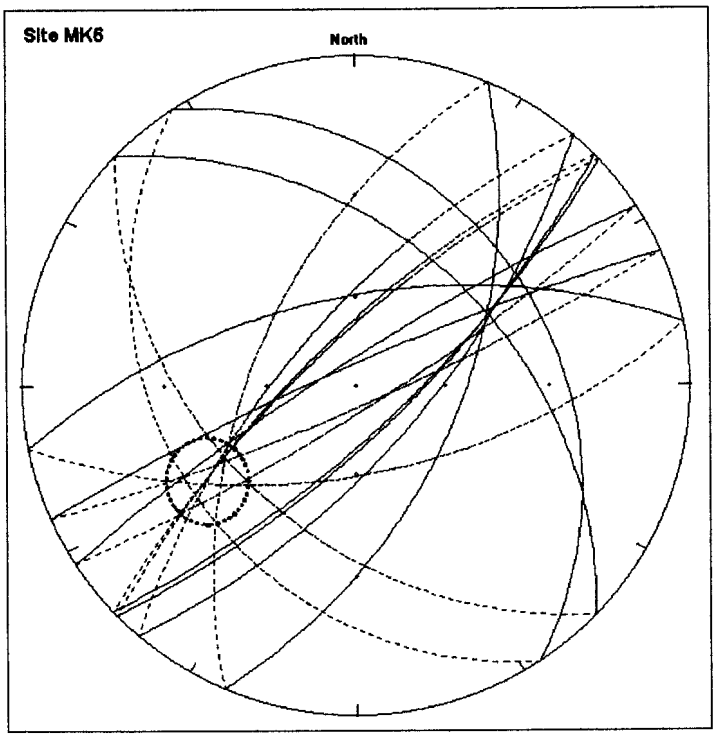

Figure 8.9: Converging remagnetization circles from site MK6 displayed on an equal-area projection.

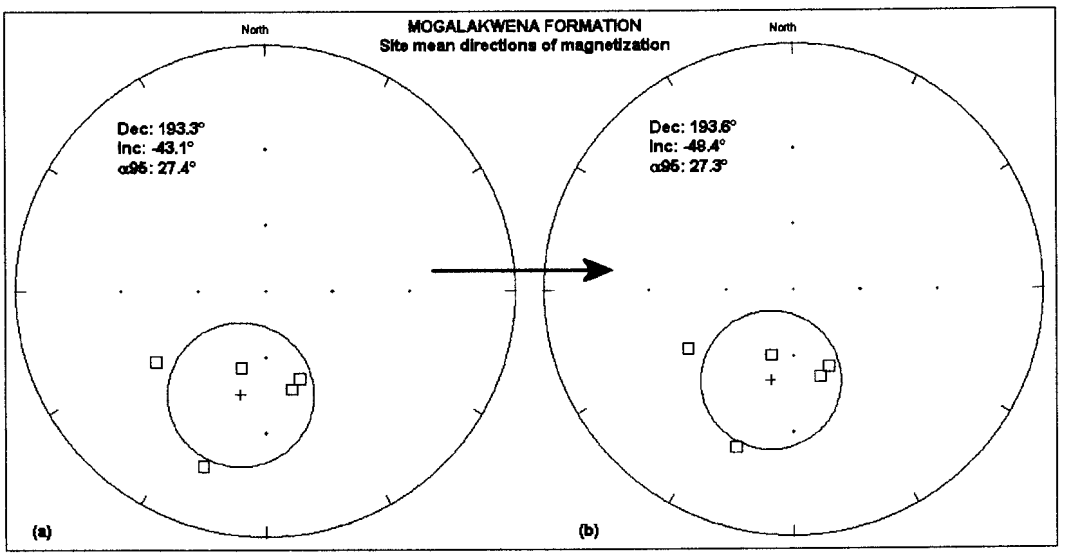

Figure 8.10: Equal-area projection of site mean directions for the Mogalakwena Formation both (a) before and (b) after bedding-tilt corrections have been applied. Clearly there no significant change is observed.

The virtual palaeomagnetic pole positions (VGP) of the individual sites are also summarized in Table 8.2. The mean palaeomagnetic pole position for the Mogalakwena Formation was calculated after bedding-tilt corrections as 36.1° S, 207.3° E, N=4 and α_{95}=27.6° (anti-pole: 36.1° N, 27.3° E).

Table 8.2: Site mean demagnetization results for the Mogalakwena Formation

SITE #	NO BEDDING CORRECTIONS										BEDDING CORRECTED									
	DEMAGNETIZATION DATA						VGP				DEMAGNETIZATION DATA						VGP			
	SDEC	SINC	α_{95}	k	N	R	LAT	LONG	DP	DM	SDEC	SINC	α_{95}	k	N	R	LAT	LONG	DP	DM
MK1*	165.40	-45.10	13.7		6		-37.5	191.4	11.0	17.3	162.90	-49.50	13.7		6		-33.3	190.3	12.1	18.20
MK2*	197.30	-53.80	22.2		4		-29.5	224.3	21.7	31.0	198.00	-58.80	22.2		4		-24.4	223.1	24.6	33.00
MK3	158.90	-48.20	16.4	17.6	6	5.72	-33.2	185.8	14.1	21.5	155.50	-52.30	16.4	17.6	6	5.72	-28.7	184.5	15.5	22.50
MK4	105.20	-13.40	33.2	6.3	5	4.36	-11.0	130.3	17.3	33.9	103.70	-14.30	33.2	6.3	5	4.36	-9.4	130.1	17.4	34.00
MK5**	199.20	-15.90	34.2	8.2	4	3.63	-53.0	240.6	18.1	35.2	199.70	-21.70	34.2	8.2	4	3.63	-50.0	238.8	19.1	36.10
MK6*	236.80	-34.70	12.8		9		-20.0	265.1	8.5	14.7	240.30	-38.40	12.8		9		-15.8	264.9	9.0	15.20

* Site mean results obtained from demagnetization circles, with maximum angular deviation (MAD) displayed in the α_{95} columns.

** Site mean results obtained from a combination of point data and demagnetization circles.

9. DISCUSSION OF RESULTS AND ASSOCIATED TECTONIC IMPLICATIONS

A. Correlation between the lower Waterberg Group and the associated diabase intrusions

The calculated palaeomagnetic anti-pole for the Swaershoek Formation sediments is 37.1° N, 4.1° W, A_{95}=17.4° (chapter 5), while that for the Wilge River Formation sediments was calculated as 31.9° N, 7.3° W, A_{95}=20.5° (chapter 6).

The palaeomagnetic results from the diabase in the Nylstroom syncline (chapter 7) indicate considerable variations due to lightning effect and the virtual geomagnetic pole positions from the individual sites (VGPs) are weakly scattered around the anti-pole of 63.3° N, 53.2° E (A_{95}=35.7°). The very poor statistical parameter for the diabase is unfortunately a problem commonly encountered with older rocks. However, the direction correlates well with the results from the diabase in the Middelburg Basin. The palaeomagnetic results from the diabase in the Middelburg basin converged to an anti-pole of 69.3° N, 28.5° E (A_{95}=14.2°) (chapter 7). Both these poles correlate well with the published result for the Umkondo diabase by McElhinny and Opdyke (1964) (65.0° N, 42.5° E and A_{95}=6.0°), as well as the post-Waterberg diabase result by Jones and McElhinny (1966) (65.0° N, 50.5° E and A_{95}=4.5°).

The 'mean' virtual palaeomagnetic anti-pole position for the trachytic lava in the Nylstroom protobasin is 43.94° N, 1.28° W and A_{95}=28° (chapter 7). The "mean" VGP of the trachytic lava should not be considered for comparison with any other results due to the considerable alterations these lavas underwent. Only two sites were sampled which is also statistically insufficient for calculating a mean. It is however noteworthy that this calculated pole position correlates fairly well with that of the Swaershoek Formation sediments, which should be expected considering the lava was extruded contemporaneously with the upper Swaershoek beds (Jansen, 1982)

Figure 9.1 displays the calculated pole positions for the Wilge River **(WR)** and Swaershoek Formations **(SH)** in red, as well as the associated diabase intrusions **(WRD** and **SHD)** in yellow. From Figure 9.1 it is clear that the pole positions from the Wilge River and Swaershoek Formation sediments are situated sufficiently displaced from the pole positions of the post-Waterberg diabase to conclude that the lower Waterberg Group as a whole was not remagnetised by these intrusive events.

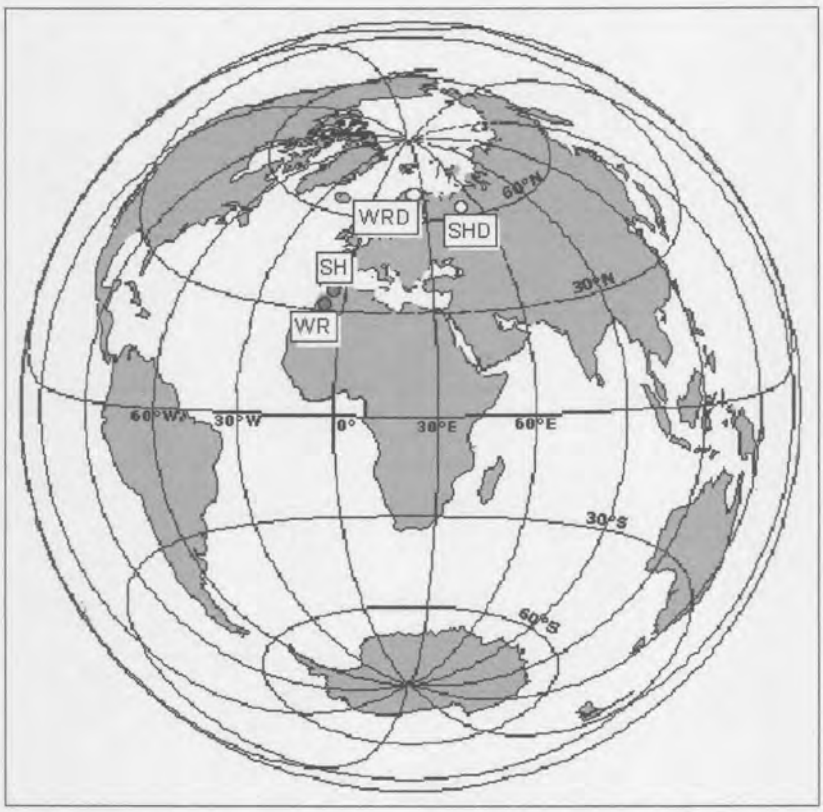

Figure 9.1: Relative palaeomagnetic anti-pole positions of the Swaershoek Formation (**SH**), Wilge River Formation (**WR**), and the diabase intrusions within the Swaershoek (**SHD**) and Wilge River (**WRD**) Formations respectively. All poles are south poles.

B. Comparison of results with previous studies

In 1967 Jones and McElhinny published the results from a joint palaeomagnetic study on the Waterberg red beds. The authors (Jones and McElhinny, 1967) postulated that these results represent a pattern of polar wandering that occurred during the deposition and consolidation of the Waterberg Group (Figure 9.2).

After demagnetization the authors (Jones and McElhinny, 1967) grouped the sites into three stratigraphic groups according to their pole positions: Sites J, K and M form the base of the succession as group 1. Sites F, G, L and I formed group 2. Sites A and H were grouped together as group 3.

In a later publication McElhinny (1968) regrouped the results into five groups (Table 9.1). Sites A and H formed group 1, sites B and C formed group 2, while sites F, G, L and I form group 3. McElhinny gave the samples from site D unit weight and calculated a pole position for this single site, and regarded it as group 4. Sites J, K and M were grouped together to form group 5.

Figure 9.2: APWP with virtual pole positions A-M from previous Waterberg Group study (modified after Jones and McElhinny, 1967).

Table 9.1: Results for the Waterberg Group as described by McElhinny (1968)

GROUPS	SITE #	DEC	INC	N	K	A95	PLAT	PLON	DP	DM
Group1	A, H	186	4	9	21		67	44		
Group 2	B, C	182	-45	9	97.8	25.5	41	33	20.4	32.3
Group 3	F, G, L, I	109.6	-47.9	22	33.5	16.1	3.2	333.4	13.7	21
Group 4	D	145.5	-69.5	5	11.2	24	8.3	10	35.1	41
Group 5	J, K, M	16.8	45.1	15	41.4	19.4	35.6	47.5	15.6	24.6

Figure 9.3 displays the pole positions as suggested by McElhinny (1968) as well as the calculated poles from the current study. Allsopp *et al.* (1989) suggested that the pole positions indicated by both the studies of Jones and McElhinny (1967) and McElhinny (1968) show that deposition of the Waterberg Group commenced during emplacement of the acid rocks of the Bushveld Complex (at ca. 2.05 Ga). These authors further suggested that the Waterberg Group deposition continued intermittently through numerous tectonic events in the Transvaal basin until close to the onset of the Umkondo thermal event (at ca. 1.1 Ga).

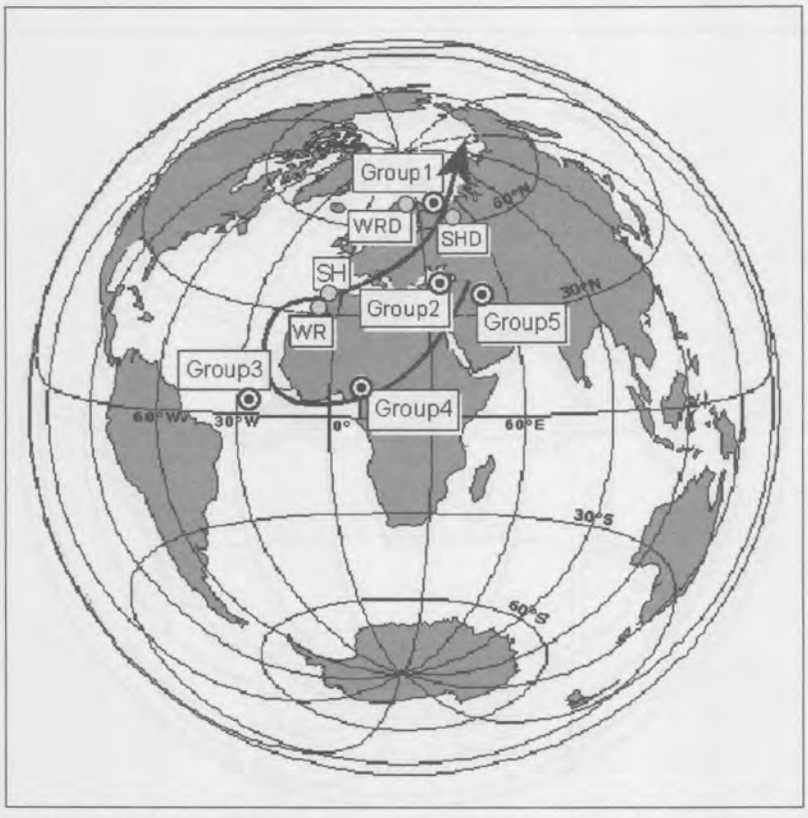

Figure 9.3: APWP with pole positions as suggested by McElhinny (1968) in yellow, as well as poles from the current study in red.

The pole position from the Mogalakwena Formation (**MK**) correlates fairly well with group 2 of McElhinny (1968). McElhinny grouped the results from sites B and C from a previous study (Jones and McElhinny, 1967) into group 2. These sites (B and C) were sampled in the Wyllies Poort Formation, Soutpansberg Group. Bumby *et al.* (2001b) have indicated that the Wyllies Poort Formation is stratigraphically younger than the Mogalakwena Formation (chapter 9, paragraph F), which fits in with the locations of the two poles (**MK** and **Group2**) on the APWP in figure 9.3. Considering the weak statistics of the pole position for the Mogalakwena Formation, it would be difficult to determine from these poles exactly how much older the latter is than the Wyllies Poort Formation.

The pole positions for the Swaershoek (SH) and Wilge River Formations (WR) do not correlate well with any of McElhinny's groups. However considering the paucity of sampling sites from the Jones and McElhinny (1967) study, as well as the cross formational groupings by McElhinny (1968), the results should only be compared with great caution.

C. Apparent Polar Wandering Path (APWP) with regards to the Waterberg Group

The calculated palaeomagnetic anti-pole positions for selected formations in the Waterberg Group as well as the associated diabase intrusions are summarized in Table 9.2.

Table 9.2: Results for the Waterberg Group as calculated from the current study.

LITHOLOGY	PALEO-LATITUDE	PALEO-LONGITUDE	A_{95}
Swaershoek Formation (SH)	37.1° N	355.9° E	17.4°
Wilge River Formation (WR)	31.9° N	352.7° E	20.5°
Mogalakwena Formation (MK)	36.1° N	027.3° E	27.6°
Swaershoek diabase (SHD)	63.3° N	053.2° E	35.7°
Wilge River diabase (WRD)	69.3° N	028.5° E	14.2°

As discussed in paragraph A of this chapter, the palaeomagnetic anti-pole positions for the lower Waterberg Group (Swaershoek and Wilge River Formations) correlates well as can be seen from the close grouping on the APWP for Africa (Figure 9.4). The Mogalakwena Formation occurs higher up in the lithostratigraphy of the Waterberg Group and is thus relatively younger than the above mentioned Formations. This is also reflected in its relative position on the APWP. The calculated palaeomagnetic anti-pole position for the Mogalakwena Formation correlates fairly well with group 2 of McElhinny (1968). It is the opinion of the current author that the latter reflects a pole position for the Wyllies Poort Formation (Soutpansberg Group).

Figure 9.4 displays the APWP for Africa with selected pole positions shown from Southern Africa for the ca. 2070-1070 Ma period. The poles calculated in the current study for selected Formations in the Waterberg Group as well as the poles from the diabase sills in the lower Waterberg Group (Table 9.2) were added in grey.

Figure 9.5 is a repeat of the data from Figure 9.4 but plotted with plate boundaries as opposed to continent boundaries and including A_{95} circles. This diagram was created using the GMAP2002 standard edition © software developed by Torsvik and Smethurst (1999).

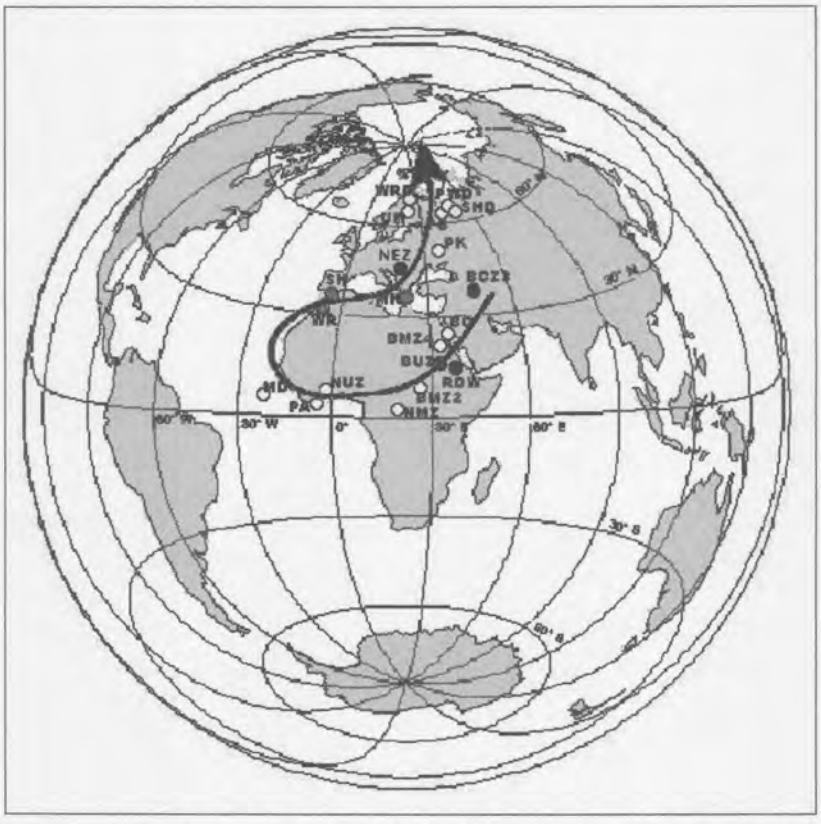

Figure 9.4: The apparent polar wandering path (APWP) for Southern Africa for ca. 2070-1070 Ma Solid circles, south poles; open circles, north poles. The pole positions are as follows: **BC** (2050 Ma) – Bushveld Complex (Gough and Van Niekerk, 1959); **BMZ2** – Subzone B, Main Zone (Hattingh, 1986b); **BMZ4** – Subzone C, Main Zone (Hattingh, 1986b); **BCZ3** – Critical Zone, Bushveld Complex (Hattingh, 1986a); **BUZ** – Bushveld Complex Upper Zone (Hattingh, 1989); **NMZ** – Northern Bushveld Complex, Main Zone (Hattingh and Pauls, 1994); **NUZ** – Northern Bushveld Complex, Upper Zone (Hattingh and Pauls, 1994); **RDW** (2025 Ma) –Rust de Winter Formation (Morgan and Briden, 1981 and Walraven, 1981); **PA** – Phalaborwa syenite and dolerites (Morgan and Briden, 1981); **MD** (1830 Ma) – Mashonaland dolerites (McElhinny and Opdyke, 1964; Bates and Jones, 1996). Rock age from Morgan and Briden (1981); **SH** – Swaershoek Formation (this study); **WR** – Wilge River Formation (this study); **MK** – Mogalakwena Formation (this study); **NEZ** (1240 Ma) – Namaqua Eastern Zone (Evans *et al.*, 2002); **PK** – Premier Mine Kimberlite (Jones, 1968); **PWD** (1090 Ma) – Post-Waterberg dolerite (Jones and McElhinny, 1966, Allsopp *et al.*, 1967, 1989); **UM** (1080 Ma) – Umkondo igneous events (Hargraves, Hattingh and Onstott, 1994, Allsopp *et al.*, 1989); **TG** (1072 Ma) – Timbavati gabbro (Hargraves, Hattingh and Onstott, 1994); **SHD** – Swaershoek Formation Diabase (this study); **WRD** – Wilge River Formation Diabase (this study).

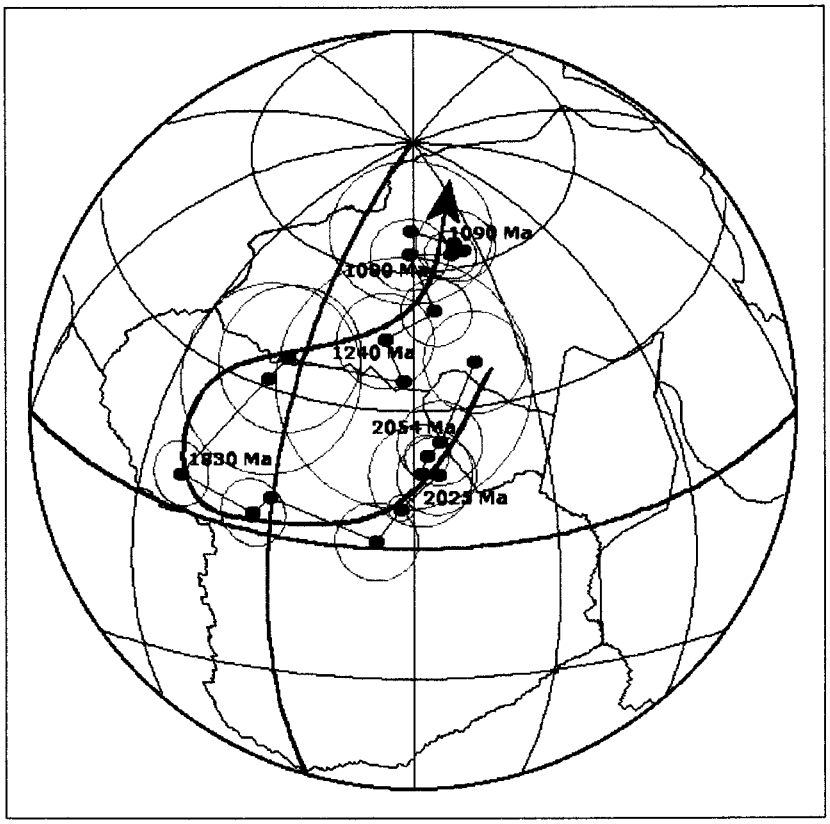

Figure 9.5: The apparent polar wandering path (APWP) for Southern Africa for ca. 2070-1070 Ma with A_{95} circles indicated. Diagram created using the GMAP2002 standard edition © software developed by Torsvik and Smethurst (1999).

D. Correlation of the Swaershoek and Wilge River Formations

Jansen (1982) describes the Swaershoek Formation as the basal unit of the Waterberg Group in the Nylstroom Protobasin, and correlates it with the Wilge River Formation in the Middelburg Basin. As discussed in Chapter 5, both the Swaershoek as well as the Wilge River Formations are confined within the limits of the preserved Transvaal Basin (Coertze *et al.*, 1977). The composition of pebbles and fragments in the arenaceous beds of both the Swaershoek and Wilge River Formations indicates the Transvaal Supergroup as the main source area (Jansen, 1982 and Visser *et al.*, 1961).

The genesis of the Nylstroom basin has been interpreted as being due to upper crustal warping (Jansen, 1975 and Coertze *et al.*, 1977). The differences in thickness at many localities, the presence of local sedimentary unconformities and the large number of conglomerate bands of rather small extent, indicate that the basal portion of the Swaershoek Formation represents rapid sedimentation upon a locally highly irregular topography. Although the sediments are partly of local provenance, particularly in areas where block faulting occurred, transport directions indicate that influx of material into the basin was mainly from the north-east (Jansen, 1982).

Spies (1952, 1954) has described the Wilge River Formation as a large gentle synclinal basin-fill. Vos and Eriksson (1977) and Van der Neut *et al.* (1991) interpreted the Wilge River Formation as a distal wet fan setting, with fan-deltas forming where alluvial lobes prograded into a shallow lacutrine basin, where weak tides reworked the sediments. This shallow synformal basin derived most of its detritus from Transvaal lithologies lying to the west (Van der Neut, in prep.). Waterberg palaeoclimatic conditions are generally accepted by most workers as having been semi-arid (e.g., Callaghan *et al.*, 1991; Simpson *et al.*, 2002, in press a and b). This observation is compatible with the approximately 30° palaeolatitude determined in this study.

The good correlation between the palaeomagnetic pole positions from the Swaershoek and Wilge River Formations (this study) confirms the theory that these formations must have been deposited contemporaneously.

Coertze *et al.* (1977) suggested that the scattered occurrences of arenaceous beds in the Springbok Flats region are lithologically similar to both the Swaershoek and Wilge River Formations. Coertze *et al.* (1977) therefore suggested that the early Waterberg basin in the Nylstroom area and the Middelburg basin were probably linked during deposition of the Wilge River Formation. Morgan and Briden (1981) published a palaeomagnetic pole position for red sediments at Rust de Winter (see RDW, Fig. 9.2). The authors correlated the Rust de Winter sediments with the lower Waterberg Group on the basis that their calculated palaeomagnetic pole position falls mid-way between McElhinny's two oldest Waterberg poles (groups 4 and 5, 1968). These sediments have however been stratigraphically reclassified as the Rust de Winter Formation, Transvaal Supergroup (Walraven, 1981). Walraven (1981) correlates the Rust de Winter Formation with the Loskop and Glentig Formations by combining all available field evidence with geochronological results and chemical and lithological data. The age of the Rust de Winter Formation is ~2096 Ma, which supports the idea that these sediments are older than the Bushveld Complex at ~2054 Ma (Walraven *et al.*, 1993). Walraven (1981) published a minimum age for the interbedded rhyolite of the Rust de Winter Formation at ~2025 Ma This additional information therefore explains the positioning of the palaeomagnetic pole position (RDW) by Morgan and Briden (1981) on the APWP in figure 9.4

E. Relationship between the Bushveld Complex and the Waterberg Group.

According to Coertze *et al.* (1977) field relationships and composition of the sedimentary rocks (e.g. pebbles in conglomerates) indicate that the Bushveld granite was not yet subjected to erosion during deposition of the lower Swaershoek Formation. Coertze *et al.* (1977) continues that a 3000m thick succession of Rooiberg lavas invariably intervenes between the granite and the lower Swaershoek beds. Hence, the Bushveld granite was still roofed during the initial phase of Waterberg sedimentation. Coertze *et al.* (1977) further suggests that erosion of the Bushveld granite only commenced during

deposition of the uppermost Swaershoek beds near Sterkrivier Dam and took place on a large scale during deposition of the Alma Formation in the Alma trough.

The relationship between the Bushveld granite and the oldest Waterberg beds can also be deduced from structural data. According to Coertze *et al.* (1977) a large fault-zone intersects the core of the Loubad anticline including the Bushveld granite. This indicates that the latter was already solidified during deposition of the lower portion of the Swaershoek Formation. The above evidence puts a big question mark on the results of group 5 from McElhinny (1968) which suggested that the Waterberg sedimentation commenced during emplacement of the acid rocks of the Bushveld Complex.

However, Du Plessis (1972) suggested that features such as parallelism between all contacts in the Loubad area, tilting of the basal Swaershoek beds during deposition and the extrusion of quartz porphyry flows in the lowermost beds, can be attributed to late magmatic updoming. In that case Coertze *et al.* (1977) suggested that the acid Bushveld magma had not been completely solidified under its still existing thick roof of Rooiberg lavas (see above). Faulting probably started near the Rooiberg-Waterberg contact and subsequently extended downward into the Bushveld granite after solidification of the latter (Coertze *et al.*, 1977). Coertze *et al.* (1977) continues that early faulting in the roof prior to solidification is also suggested by the distribution of the ignimbrite sheet (on the contact) and of the quartz porphyry flows, both immediately south of the fault-zone. The possibility is, therefore, not excluded that deposition of the lowermost Waterberg beds, the extrusion of quartz porphyry and the emplacement of the bulk of the acid Bushveld magma were contemporaneous events (Coertze *et al.*, 1977).

The Wilge River Formation overlies the Bushveld granite with an erosional contact (Coertze *et al.*, 1977). According to Coertze *et al.* (1977) this can be illustrated by areas where prominent pegmatite veins in the granite immediately below the contact do not extend into the overlying sedimentary rocks. This indicates that the granite was deroofed prior to deposition of the Wilge River beds. Similar erosional contacts have been described between the granite at Balmoral and the overlying Wilge River Formation (Daly and Molengraaff, 1924).

F. Age constraint on the Waterberg Group

At the start of this project one of the aims was to constrain the time of deposition of the Waterberg Group. The idea was to obtain this constraint by comparing the palaeomagnetic pole positions obtained from the lower Waterberg Group with that from the Mogalakwena Formation, which forms part of the upper Kransberg Subgroup.

The calculated palaeomagnetic pole position for the Mogalakwena Formation indicates a younger age than the Swaershoek and Wilge River Formations (Figs. 9.3 and 9.4). This is in accordance with the

stratigraphic positioning of these Formations in the Waterberg Group. As discussed in paragraph B (this chapter), the statistically weak pole position for the Mogalakwena Formation correlates fairly well with group 2 of McElhinny (1968). McElhinny's group 2 consists of the results from sites B and C from a previous study (Jones and McElhinny, 1967), which were sampled in the Wyllies Poort Formation, Soutpansberg Group. In a recent study by Bumby *et al.* (2001b) it was determined, both by field and geochemical data from the Blouberg area, that the Mogalakwena Formation pre-dates the Wyllies Poort Formation. The study by Bumby *et al.* (2001b) demonstrates that the Sibasa Formation, Soutpansberg Group also post-dates the Mogalakwena Formation. The Sibasa Formation has been dated by Cheney *et al.* (1990) as between 1974-1800 Ma (Rb-Sr whole rock). Depending on the accuracy of such dates, this work suggests that the Waterberg Group may be older than previously thought. As indicated in paragraph B above, the Bushveld granites yield the lower limiting age for the Waterberg Group, and were dated at 2054.4 +/- 1.8 Ma by Walraven *et al.* (1993). The deposition of the Waterberg Group is thus constrained between Bushveld (2050 Ma) and Sibasa (1800 Ma) ages (Bumby *et al.*, 2001b).

G. Conclusions

The palaeomagnetic data (Table 9.2, Figs. 9.4 and 9.5) suggest that Waterberg sedimentation began much closer to the late crystallisation of the Bushveld acid magmas (at ca. 2054 Ma, Walraven *et al.*, 1993) than the generally inferred upper age limit of ca. 1.9 Ga (e.g., SACS, 1980; Jansen, 1982). This is in agreement with the work of Martini (1998) who found that the Loskop Formation, a direct correlate of the Rust de Winter Formation (e.g., SACS, 1980), was deposited synchronously with the Rustenburg Suite of the Bushveld Complex. The Loskop sedimentary rocks were intruded very soon after this episode by Nebo granites. The preserved Rust de Winter sedimentary lithologies between the Nylstroom Protobasin and the Middelberg Basin may thus be viewed as the proto-Waterberg deposits.

The new palaeomagnetic data from the Swaershoek and Wilge River Formations support the onset of earliest Waterberg alluvial sedimentation during final cooling of the acid rocks of the Bushveld Complex. Waterberg semi-arid alluvial-fluvial and localised erg deposits are also compatible with the approximately 30° palaeolatitude determined in this study. These mineralogically and texturally relatively immature deposits may thus be viewed as two molasse basins resulting from the paroxysm and dynamic palaeotopography that originated from the Bushveld superplume event.

The new palaeomagnetic data from the Mogalakwena Formation, together with its good correlation with the palaeomagnetic data from the Wyllies Poort Formation (group2 from McElhinny, 1968), and the recent results from the Sibasa Formation suggest that the deposition of the Waterberg Group is thus constrained between Bushveld (2050 Ma) and Sibasa (1800 Ma) ages (Bumby *et al.*, 2001b).

ACKNOWLEDGEMENTS

The author would like to express her gratitude to the Chief Director of the Council for Geoscience for the use of the palaeomagnetic laboratory at the Council for Geoscience, as well as acknowledge the financial support from the Council for Geoscience in the form of a bursary.

She wishes to thank her technical assistants in the palaeomagnetic laboratory over the years, Miss B.C. Oosthuizen, Mr L.R. Tabane and Mr. M.E. Hauger, as well as all her colleagues and friends for their interest and stimulating discussions and suggestions.

The author would like to express a special word of thanks to Prof. T. H. Torsvik from the Norwegian Geological Survey for showing her the ropes with his software (both IAPD2000 and GMAP2001) as well as for running strong-field thermomagnetic analysis on several of the Waterberg samples. His useful comments and educational discussions was a great asset to the author.

A word of thanks to Prof. P.J. Hattingh who initiated the study and who was the original supervisor until illness forced him into early retirement, as well as to Dr. Laurent Ameglio whom took over the task of supervisor from Prof. Hattingh.

The author would like to thank Prof. P.G. Eriksson who agreed to act as co-supervisor and for his contribution and advise on the geology of the Waterberg Group as well as for his enlightening discussions and suggestions towards the tectonic implications of the results.

Lastly, but not the least, I would like to express my sincerest gratitude to my husband for his patience and encouragement over the long years of study.

REFERENCES

Allen, J.R.L. (1982). Sedimentary structures, their character and physical basis, 1. Elsevier, Amsterdam. 593p.

Allsopp, H.L., Burger, A.J. and Van Zyl, C. (1967). A minimum age for the Premier kimberlite yielded by biotic Rb-Sr measurements with related galena isotopic data. Earth and Planetary Science Letters, 3, 161-166.

Allsopp, H.L., Kramers, J.D., Jones, D.L. and Erlank, A.J. (1989). The age of the Umkondo Group, eastern Zimbabwe, and implications for palaeomagnetic correlations. South African Journal of Geology, 92(1), 11-19.

Bailey, R.C. and Halls, H.C. (1984). Estimate of confidence in palaeomagnetic directions derived from mixed remagnetization circle and direct observational data. Journal of Geophysics, 54, 174-182.

Balsley, J.R. and Buddington, A.F. (1960). Magnetic susceptibility anisotropy and fabric of some Adirondack granites and orthogneisses. American Journal of Science, 258A, 6-20.

Barton, J.M. and McCourt, S. (1983). Rb-Sr age for the Palala granite, Limpopo Mobile belt. Special Publication of the Geological Society of South Africa, 8, 45-46.

Bates, M.P. and Jones, D.L. (1996). A palaeomagnetic investigation of the Mashonaland dolerites, north-east Zimbabwe. Geophysical Journal Int., 126, 513-524.

Bingham, C. (1964). Distributions on the sphere and on the projective plane. Ph.D. Thesis, Yale University, New Haven.

Borradaile G.J. (1988). Magnetic susceptibility, petrofabrics and strain. Tectonophysics, 156, 1-20.

Brandl, G. (1993). Map 2326 Ellisras 1:250 000 geological series. Council for Geoscience, Government Printer, Pretoria.

Brink, A.B.A. (1979). Engineering geology of Southern Africa. Building Publications, Pretoria, 319pp.

Bumby, A.J. (2000). The geology of the Blouberg Formation, Waterberg and Soutpansberg Groups in the area of Blouberg mountain, Northern Province, South Africa. Ph.D. Thesis, University of Pretoria (unpublished).

Bumby, A.J., Eriksson, P.G., Van der Merwe, R. and Brümmer, J.J. (2001a). Shear-zone controlled basins in the Blouberg area, Northern Province, South Africa: syn- and post-tectonic sedimentation relating to ca. 2.0 Ga reactivation of the Limpopo Belt. African Earth Sciences, 33, 445-461.

Bumby, A.J., Eriksson, P.G., Van der Merwe, R. and Maier, W.D. (2001b). The stratigraphic relationship between the Waterberg and Soutpansberg Groups in Northern Province, South Africa: Evidence from the Blouberg area. South African Journal of Geology, 104, 205-216.

Burger, A.J. and Walraven, F.J. (1974). Radiometric age measurements on rocks from southern Africa to the end of 1971. Bulletin of the Geological Survey of South Africa, 58.

Burger, A.J. and Walraven, F.J. (1980). Summary of age determinations carried out during the period April 1978 to March 1979. Annuals of the Geological Survey of South Africa, 14, 109-118.

Butler, R.F. (1992). Palaeomagnetism. Blackwell Scientific Publications, Boston, 319pp.

Callaghan, C.C. (1987). The geology of the Waterberg Group in the southern portion of the Waterberg basin. Unpublished M.Sc. Thesis University of Pretoria, 164pp.

Callaghan, C.C. (1993). The geology of the Waterberg Group in the southern portion of the Waterberg basin. Bulletin of the Geological Survey of South Africa, 104.

Callaghan, C.C., Eriksson, P.G. and Snyman, C.P. (1991). The sedimentology of the Waterberg Group in the Transvaal, South Africa: an overview. Journal of African Earth Sciences, 13(1), 121-139.

Cheney, E.S. and Twist, D. (1986). The Waterberg "Basin" – A reappraisal. Transactions of the geological society of South Africa, 89, 353-360.

Cheney, E.S., Barton, J.M., Jr. and Brandl, G. (1990). Extent and age of the Soutpansberg sequences of southern Africa. South African Journal of Geology, 93, 664-675.

Clark, I (1987). Turning the tables – an interactive approach to the traditional estimation of reserves. Journal of the South African Institute for Mining and Metallurgy, 87(10), 293-306.

Coertze, F.J., Jansen, H. and Walraven, F. (1977). The transition from the Transvaal Sequence to the Waterberg Group. Transactions of the Geological Society of South Africa, 80(3), 145-156.

Collinson, D.W. (1965a). The remanent magnetism and magnetic properties of red sediments. Geophysical Journal of the Royal Astronomical Society, 10, 105-126.

Collinson, D.W. (1965b). Depositional remanent magnetization in sediments. Journal of Geophysical Research, 70, 4663-4668.

Cox, A. (1961). Anomolous remanent magnetization of basalt. US Geological survey, Bulletin, 1083(E), 131-160.

Creer, K.M., Hedley, I.G. and O'Reilly, W. (1975). Magnetic oxides in geomagnetism. *In:* Craik, D.J. (ed.) Magnetic Oxides Part 2. 649-688, John Wiley & Sons, London, 798pp.

Creer, K.M. and Sanver, M. (1967). The use of the sun compass, 11-16. In: Methods in Palaeomagnetism: Developments in solid Earth Geophysics, 3, Elsevier Publishing Company, Amsterdam.

Daly, R.A. and Molengraaff, G.A.F. (1924). Structural relations of the Bushveld Igneous Complex, Transvaal. Journal of Geology, 32, 1-35.

De Vries, W.C.P. (1970). The geology of the southern portion of the Waterberg area, north eastern Transvaal. Report from the Geological Survey of South Africa. (unpublished), no. 1970-0062.

Du Plessis, M.D. (1972). The relationship between the Bushveld Complex and the Waterberg system in the area between Loubad and Warmbad. Annals of the Geological Survey of South Africa, 9, 85-88.

Du Plessis, M.D. (1978). Map 2428 Nylstroom 1:250 000 geological series. Council for Geoscience, Government Printer, Pretoria.

Evans, D.A.D., Beukes, N.J. and Kirschvink, J.L. (2002). Paleomagnetism of a lateritic paleoweathering horizon and overlying Paleoproterozoic red beds from South Africa: Implications for the Kaapvaal apparent polar wander path and a confirmation of atmospheric oxygen enrichment. Journal of Geophysical Research, 107(B12), 2-1 - 2-22

Fisher, R.A. (1953). Dispersion on a sphere. Procedures of the Royal Society of London, A217, 295-305.

Flinn, D. (1962). On folding during three-dimentional progressive deformation. Quarterly Journal of the Geological Society of London, 118, 385-433.

Fuller, M.D. (1967). The A.C. bridge method. In Collinson, D.W., Creer, K.M. and Runcorn, S.K. (eds.). Methods in palaeomagnetism. Developments in Solid Earth geophysics, 3, Elsevier Publication Company, Amsterdam, 403-408.

Gough, D.I. (1956). A study of the palaeomagnetism of the Pilanesberg dykes. Montly Notes of the Royal Astronomical Society, Geophysical Suppliments, 7, 196-213.

Gough, D.I. (1967). Notes on rock sampling for palaeomagnetic research, 3-7. In: Collinson, D.W., Creer, K.M. and Runcorn, S.K. (eds). Methods in Palaeomagnetism: Developments in solid Earth geophysics, 3, Elsevier Publishing Company, Amsterdam.

Gough, D.I. and Van Niekerk, C.B. (1959). A study of the palaeomagnetism of the Bushveld Gabbro. Philosophical Magazine, 4, 126-136.

Graham, J.W. (1954). Magnetic susceptibility, an unexploited element of petrofabric. Geological Society of America, Bulletin, 65, 1257-1258.

Graham, K.W. and Hales, A.L. (1957). Palaeomagnetic measurements on Karoo dolerites. Philosophical Magazine, Supplement for Advanced Physics, 6, 149-167.

Griffiths, D.H., King, R.F., Rees, A.I. and Wright, A.E. (1960). The remanent magnetization of some recent varved sediments. Procedures of the Royal Society of London, A256, 359-383.

Halls, H.C. (1975). Shock-induced remanent magnetization in Late Precambrian rocks from Lake Superior. Nature, 225, 692-695.

Halls, H.C. (1976). A least-squares method to find a remanence direction from converging remagnetization circles. Geophysical Journal of the Royal Astronomical Society, 45, 297-304.

Halls, H.C. (1977). Reply to P.L. McFadden's comment. Geophysical Journal of the Royal Astronomical Society, 48, 551-552.

Halls, H.C. (1978). The use of converging remagnetization circles in paleomagnetism. Physics of the Earth and Planetary Interiors, 16, 1-11.

Hamilton, N. and Loveland, P.J. (1967). Some preliminary susceptibility anisotropy measurements on greywackes from the Trinity Penunsula Series ofGraham Land. British Antrarctica Survey, Bulletin 11, 59-71.

Hamilton, N. Owens, W.H. and Rees, A.I. (1968). Laboratory experiments on the production of grain orientation in shearing sand. Journal of Geology, 76, 465-472.

Hargraves R.B., Johnson D. and Chan C.Y. (1991). Distribution Anisotropy : The cause of AMS in igneous rocks? Geophysical Reseach Letters, 18, 2193-2196.

Hargraves, R.B., Hattingh, P.J. and Onstott, T.C. (1994). Palaeomagnetic results from the Timbavati Gabbros in the Kruger National Park, South Africa. South African Journal of Geology, 97(2), 114-118.

Harms, J.C., Southard, J., Spearing, D.R. amd Walecer, R.G. (1975). Depositional environments as interpreted from primary sedimentary structures and stratification sequences. Lecture notes, Society of Economic Paleontologists and Mineralogists, Short course 2, Dallas, 161p.

Hattingh, P.J. (1986a). The palaeomagnetism of the Merensky Reef footwall rocks of the Bushveld Complex. Transactions of the Geological Society of South Africa, 89, 1-8.

Hattingh, P.J. (1986b). The palaeomagnetism of the main zone of the eastern Bushveld Complex. Tectonophysics, 124, 271-295.

Hattingh, P.J. (1989). Paleomagnetism of the upper zone of the Bushveld Complex. Tectonophysics, 165, 131-142.

Hattingh, P.J. and Pauls, N.D. (1994). New palaeomagnetic results from the northern Bushveld Complex of South Africa. Precambrian Research, 69, 229-240.

Hrouda, F (1982). Magnetic Anisotropy of Rocks and its Application in Geology and Geophysics. Geophysical Surveys, 5, 37-82.

Hrouda, F. and Janak, F. (1971). A study of the Hematite fabric of some red sediments on the basis of their magnetic susceptibility anisotropy. Sedimentary Geology, 6, 187-199.

Hrouda, F. and Janak, F. (1976). The changes in shape of the magnetic susceptibility ellipsoid during progressive metamorphism and deformation. Tectonophysics, 34, 135-148.

Irving, E. (1964). Palaeomagnetism and its application to geological and geophysical problems. John Wiley and Sons, New York, 399p.

Irving, E. and Major, A. (1964). Post-depositional detrital remanent magnetization in a synthetic sediment. Sedimentology, 3, 135-143.

Jansen, H. (1970). The structural evolution of the southern part of the Waterberg basin. Annals of the geological Survey of South Africa, 7(2), 57-62.

Jansen, H. (1975). Precambrian basins on the Transvaal craton and their sedimentological and structural features. Transactions of the geological survey of South Africa, 78/1, 25-33.

Jansen, H. (1976). The Waterberg and Soutpansberg Groups in the Blouberg area, northern Transvaal. Transactions of the geological survey of South Africa, 79, 281-291.

Jansen, H. (1982). The geology of the Waterberg Basin in the Transvaal, Republic of South Africa. Memoires of the Geological Survey of South Africa, 71, 98pp.

Johnson, E.A., Murphy, T. and Torrenson, O.W. (1948). Prehisory of the Earth's magnetic field. Journal of Terrestrial Magnetism and Atmospheric Electricity, 53, 349-372.

Jones, D.L. (1968). Paleomagnetism of the Premier Mine kimberlite. Journal of Geophysical Research, 73, 6937-6944.

Jones, D.L. and McElhinny, M.W. (1966). Paleomagnetic correlation of basic intrusions in the Precambrian of Southern Africa. Journal of Geophysical Research, 71, 543-552.

Jones, D.L. and McElhinny, M.W. (1967). Stratigraphic interpretation of paleomagnetic measurements on the Waterberg Red Beds of South Africa. Journal of Geophysical Research. 72(16), 4171-4179.

Kent, J.T., Briden, J.C. and Mardia, K.V. (1983). Linear and planar structure in ordered multivariate data as applied to progressive demagnetization of palaeomagnetic remanence. Geophysical Journal of the Royal Astronomical Society, 75, 593-621.

Keyser, N. (1997). Map: 1:1 000 000 geological map of the Republic of South Africa and the Kingdoms of Lesotho and Swaziland. Council for Geoscience, Government Printer, Pretoria.

King, R.F. (1955). The remanent magnetism of artificially deposited sediments. Monthly Notes of the Royal Astronomical Society, Geophysical Supplement, 7, 115-134.

King, R.F. and Rees, A.I. (1966). Detrital magnetism in sediments: An examination of some theoretical models. Journal of geophysical Research, 71, 561-571.

Kirschvink J.L. (1980). The least-squares line and plane and the analysis of palaeomagnetic data. Geophysical Journal of the Royal Astronomical Society, 62, 699-718.

Martini, J.E.J. (1998). The Loskop Formation and its relationship to the Bushveld Complex, South Africa. Journal of African Earth Sciences 27, 193-222.

McElhinny, M.W. (1964a). An improved method for demagnetising rocks in alternating magnetic fields. Geophysical Journal of the Royal Astronomical Society, 10, 369-374.

McElhinny, M.W. (1964b). Statistical significance of the fold test in palaeomagnetism. Geophysical Journal of the Royal Astronomical Society, 8, 338-340.

McElhinny, M.W. (1968). Palaeomagnetic directions and pole positions - IX. Geophysical Journal of the Royal Astronomical Society, 16, 207-224.

McElhinny, M.W. (1973). Palaeomagnetism and plate tectonics. Cambridge Earth Science Series. Cambridge University Press, Great Britain, 358pp.

McElhinny, M.W. and Opdyke, N.D. (1964). The palaeomagnetism of the Precambrian dolerites of eastern South Rhodesia. An example of geologic correlation by rock magnetism. Journal of Geophysical Research, 69, 2465-2475.

McFadden, P.L. (1977). Comments on "A least-squares method to find a remanence direction from converging remagnetization circles" by H.C. Halls. Geophysical Journal of the Royal Astronomical Society, 48, 549-550.

McFadden, P.L. and Jones D.L. (1981). The fold test in palaeomagnetism. Geophysical Journal of the Royal Astronomical Society, 67, 53-58.

Meinster, B. (1970). Deformed crossbedding in the Swaershoek stage; Waterberg system. Annals of the geological Survey of South Africa, 2, 63-68.

Meinster, B. (1971). The geology of the south-eastern portion of the Waterberg Basin between, Heuningfontein and the Makapansberge (Sheet 2428). Unpublished report of the Geological Survey of South Africa, 38p.

Meinster, B. (1975). Thrusting and block-faulting around Gatkop east of Thabazimbi, Transvaal. Annals of the Geological Survey of South Africa, 10, 57-72.

Morgan, G.E. and Briden, J.C. (1981). Aspects of Precambrian palaeomagnetism, with new data from the Limpopo mobile belt and Kaapvaal Craton in Southern Africa. Phylosophical Earth and Planetary Interiors, 24, 142-168.

Nagata, T. (1961). Rock magnetism. Maruzen, Tokyo (2nd edn.).

Nye, J.F. (1957). Physical Properties of Crystals. Clarendon Press, Oxford (Russian translation, Moscow, 1960).

Onstott, T.C. (1980). Application of the Bingham distribution function in paleomagnetic studies. Journal of Geophysical Research, 85(B3), 1500-1510.

O'Reilly, W. (1984). Rock and Mineral Magnetism. Blackie, USA: Chapman and Hall, New York, 220pp.

Owens W.H. (1974). Mathematical model studies of factors affecting the magnetic anisotropy of deformed rocks. Tectonophysics, 24, 115-131.

Park, J.K., Tanczyk E.I. and Desbarats A. (1988). Magnetic fabric and its sifnificance in the 1400 Ma Mealy Diabase Dykes of Labrador, Canada. Journal of Geophysical Research, 93, 13689-13704.

Patton, B.J. and Fitch, J.L. (1962). Anhysteretic remanent magnetization in small steady fields. Journal of Geophysical Research, 67, 307-311.

Rathore, J.S. (1975). Studies of magnetic susceptibility anisotropy in rocks. Ph.D. Thesis, University of Newcastle upon Tyne.

Rees, A.I. (1966). The effects of depositional slopes on the anisotropy of magnetic susceptibility of laboratory deposited sands. Journal of Geology, 74, 856-867.

Rees, A.I. (1968). The production of preferred orientation in a concentrated dispersion of elongated and flattened grains. Journal of Geology, 76, 457-465.

Rees, A.I. (1971). The magnetic fabric of a sedimentary rock deposited on a slope. Journal of Sedimentary Petrology, 41, 307-309.

Rees, A.I., and Woodall, W.A. (1975). The magnetic fabric of some laboratory-deposited sediments. Earth and Planetary Science Letters, 25, 121-130.

Rendu, J.M. (1981). An introduction to geostatistical methods of mineral evaluation. South African institute of mining and metallurgy. Geostatistics, 2, 84pp.

SACS (South African Committee for Stratigraphy), (1980). Stratigraphy of South Africa Part 1 (Comp. L.E. Kent). Lithostratigraphy of the Republic of South Africa, South West Africa/Namibia, and the Republics of Boputhatswana, Transkei and Venda. Geological Survey of South Africa, 8.

Sharpe, M.R., Everson, N.M. and Naldrett, A.J. (1986). Sm/Nd and Rb/St isotopic evidence from liquid mixing, magma generation and contamination in the eastern Bushveld Complex. Extende Abstracts, Geocongress '86, Geological Society of South Africa, 621-624.

Sichel, H.S. (1966). The estimation of means and associated confidence limits for small samples from lognormal populations. Presented at the Symposium on Mathematical Statistics and Computer Applications in Ore Valuation. Johannesburg, The South African Institute of Mining and Metallurgy, 106-122.

Spies, J.J. (1952). Die geologie van die gebied noord en noordwes van Middelburg, Transvaal. Report Geological Survey of South Africa, 1951-0044, 54p. (Unpublished).

Spies, J.J. (1958). Die geologie van die gebied suid en wes van baknoral, Distrik Pretoria. Report Geological Survey of South Africa, 1958-0037, 29p. (Unpublished).

Stacey F.D. (1960). Magnetic anisotropy of igneous rocks. Journal of Geophysical Research, 65, 2429-2442.

Stacey, F.D. (1963). The physical theory of rock magnetism. Philosophical Magazine, Supplement of Advanced Physics, 12, 46-133.

Strauss, C.A. (1955). Die geologie en mineraalafsettings van die Potgietersrustinvelde. Memoirs of the Geological Survey of South Africa, 46.

Tankard, A.J., Jackson, M.P.A., Erikson, K.A., Hobday, K.A., Hunter, D.R. and Minter, W.E.L. (1982). Crustal evolution of Southern Africa: 3,8 billion years of earth history: with a contribution by S.C. Eriksson. 532p, 182 Figs. Springer-Verlag New York.

Tarling, D.H. (1971). Principles and applications of palaeomagnetism. Chapman and Hall, London, 164p.

Tauxe, L. (2002). Paleomagnetic principles and practice. Kluwer Academic Publishers, Dordrecht, 299p.

Tickell, S.J. (1975). Braided river deposits in the Waterberg supergroup. Transactions of the Geological society of South Africa, 78(1), 83-88.

Torsvik, T.H., Briden, J.C. and Smethurst, M.A. (1996). Super-IAPD and updated IAPD2000 software packages using 'Linefind rountines' after Kent, Briden and Mardia, (1983). Software available as freeware on http://www.geodynamics.no.

Torsvik, T.H. and Smethurst, M.A. (1998). Plate tectonic modelling: virtual reality with GMAP*. Computers and Geosciences, 25, 395-402. GMAP2001 standard edition software available as freeware on http://www.geodynamics.no.

Turner, P. (1980). Continental red beds. Elsevier, Amsterdam, Holland.

Van Biljon, W.J. (1976). Goud is nie waar dit gevind word nie. 'n Oorsig van die struktuur, gesteentes en ertsafsettings van die Transvaal. Transactions of the Geological Society of South Africa, 79, 155-167.

Van der Neut, M. and Eriksson, P.G. (1999). Palaeohydrological parameters of a Proterozoic braided fluvial system (Wilgeriver Formation, Waterberg Group, South Africa) compared with a Phanerozoic example. Special Publications of the international Association of Sedimentology, 28, 381-392.

Van der Neut, M., Eriksson, P.G., and Callaghan, C.C. (1991). Distal alluvial fan sediments in early Proterozoic red beds of the Wilgeriver Formation, Waterberg Group, South Africa. Journal of African Earth Sciences, 12 (4), 537-547.

Van Eeden, O.R. (1972). The geology of the Republic of South Africa. An explanation of the 1:1 000 000 Map, 1970 edition. Special Publication of the Geological Survey of South Africa, 18, 85pp.

Van den Ende, C. (1975). On the origin of anisotropy of magnetic susceptibility in Permian red beds from the western part of the Dome de Barrot (S. France), in Borradaile et al. (eds.), Progress in Geodynamics. North-Holland Publications Corporation, 176-189.

Visser, H.N., Spies, J.J., Fourie, C.P., Viljoen, J.J., Söhnge, A.P.G. and Venter, F.A. (1961). Die geologie van die gebied tussen Middelburg en Cullinan, Transvaal. Explanatory sheet 2528D (Bronkhorstspruit) and 2529C (Witbank), Geological Survey of South Africa.

Vos, R.G. and Eriksson, K.A. (1977). An embayment model for tidal and wave-swash deposits occurring within a fluvial dominated Proterozoic sequence in South Africa. Sedimentary Geology, 18, 161-173.

Walraven, F. (1978). Map 2528 Pretoria 1:250 000 geological series. Council for Geoscience, Government Printer, Pretoria.

Walraven, F. (1981). The stratigraphic position of the post-Rooiberg sediments at Rust de Winter. Annals of the Geological Survey of South Africa, 15/2, 37-41.

Walraven, F., Burger, A.J., and Allsopp, H.L. (1983). Summary of age determinations carried out during the period 1980 to March 1981. Annals of the Geological Survey of South Africa, 16, 107-114.

Walraven, F. and Hattingh, E. (1993). Geochronology of the Nebo granite, Bushveld Complex. South African Journal of Geology, 96(1/2), 31-41.

Watson, G.S.A. (1956). A test for randomness of directions. Monthly Notes of the Royal Astronomical Society, Geophysical Supplement, 7, 153-159.

Zijderveld, J.D.A. (1967). A.C. demagnetization of rocks: Analysis of results. In.Collinson, D.W., Creer, K.M. and Runcorn, S.K. (eds.), Methods in Palaeomagnetism, 254-286, Elsevier, Amsterdam.

APPENDIX: FIELD DATA

APPENDIX : FIELD DATA

Sample numbers were chosen to indicate lithology, site, core and specimen numbers. The first few characters indicate the formation e.g. "SH" = Swaershoek, "WR" = Wilge River and "MK" = Mogalakwena, with a "D" added to indicate the diabase associated to the prefixed formation or "T" to indicate trachytic lava. The next number (or two if there are more than 9) indicate the site number, while the last number indicate the core number. To identify the individual specimens cut from each core, another character is added at the end of the sample number. This letter is added in sequence (A-E) from top to bottom of the core.

Tables A.1 – A.6 summarize the field data for each lithological unit.

Table A.1: Field data for the Swaershoek Formation.

SITE	SITE LOCATION		BEDDING ORIENTATION		CORE ORIENTATION		
#	LAT	LONG	STRIKE	DIP	#	AZIMUTH	HADE
SH1	-24.78	28.36	188.00	-5.0	1	122.18	55.0
					2	120.47	68.0
					3	130.12	56.0
					4	116.31	61.0
					5	119.07	49.0
					6	170.86	20.0
SH2	-24.79	28.35	97.50	8.0	1	45.27	17.5
					2	63.11	13.0
					3	351.19	22.5
					4	29.80	18.0
					5	359.30	14.5
SH3	-24.67	28.47	94.50	36.0	1	200.71	48.5
					2	223.89	60.0
					3	217.03	40.0
					4	179.77	51.5
					5	227.32	62.0
					6	222.51	63.5
SH4	-24.66	28.48	94.50	36.0	1	8.67	22.0
					2	27.51	23.0
					3	91.89	8.0
					4	41.24	28.0
					5	11.06	39.0
					6	28.82	28.0

SITE	SITE LOCATION		BEDDING ORIENTATION		CORE ORIENTATION		
#	LAT	LONG	STRIKE	DIP	#	AZIMUTH	HADE
SH5	-24.64	28.48	108.00	40.0	1	335.87	26.0
					2	348.49	28.0
					3	339.28	31.0
					4	359.94	27.0
					5	336.39	20.0
SH6	-24.66	28.45	101.00	19.0	1	15.56	11.5
					2	312.33	16.0
					3	0.92	39.5
					4	20.69	41.0
					5	1.86	19.5
					6	5.55	24.5
SH7	-24.64	28.44	108.00	45.0	1	277.64	5.5
					2	6.17	52.5
					3	18.42	11.5
					4	359.75	35.5
					5	2.04	44.5
					6	1.59	43.5
SH8	-24.59	28.33	232.00	-10.0	1	355.94	14.0
					2	205.55	9.0
					3	295.66	13.5
					4	20.35	25.5
					5	54.47	15.0
					6	342.73	9.0
SH9	-24.65	28.31	72.00	10.0	1	344.45	22.0
					2	271.13	22.5
					3	220.61	19.0
					4	282.13	19.0
					5	290.26	18.0
SH10	-24.64	28.33	103.00	20.0	1	35.60	33.5
					2	45.60	80.5
					3	27.60	21.0
					4	28.60	69.5
					5	43.10	43.5
					6	34.60	42.0

SITE	SITE LOCATION		BEDDING ORIENTATION		CORE ORIENTATION		
#	LAT	LONG	STRIKE	DIP	#	AZIMUTH	HADE
SH11	-24.58	28.30	189.00	-25.0	1	359.10	60.5
					2	336.10	45.5
					3	304.10	39.5
					4	344.10	29.5
					5	335.60	59.0
					6	344.10	64.5
SH12	-24.49	28.19	163.00	-21.0	1	194.70	22.5
					2	226.70	44.0
					3	203.70	61.5
					4	195.20	48.0
					5	324.20	29.5
SH13	-24.82	28.22	289.00	15.0	1	96.90	70.5
					2	19.90	35.5
					3	35.40	48.5
					4	76.40	30.0
					5	140.40	33.5
					6	104.40	29.5
SH14	-24.83	28.23	293.00	50.0	1	354.40	57.0
					2	11.90	53.0
					3	356.40	53.0
					4	72.40	40.0
					5	23.40	49.0
					6	59.40	40.0

Table A.2: Field data for the Wilge River Formation.

SITE	SITE LOCATION		BEDDING ORIENTATION		CORE ORIENTATION		
#	LAT	LONG	STRIKE	DIP	#	AZIMUTH	HADE
WR1	-25.54	28.44	93.00	14.0	1	130.14	51.0
					2	168.98	44.5
					3	191.12	58.0
					4	116.90	49.0
					5	114.55	86.5
					6	186.51	74.5
					7	165.44	82.5
					8	167.70	53.0
WR2	-25.53	28.46	49.00	5.0	1	159.93	30.0
					2	160.28	42.0
					3	143.76	34.0
					4	181.05	24.5
					5	133.29	39.0
					6	119.15	11.5
WR3	-25.65	28.59	294.00	13.0	1	321.96	14.0
					2	127.88	12.0
					3	33.57	11.0
					4	282.76	40.0
					5	269.10	11.5
					6	8.62	22.5
WR4	-25.64	28.56	313.00	17.0	1	281.36	12.0
					2	254.65	11.0
					3	285.62	19.0
					4	291.05	17.0
					5	343.44	17.0
					6	12.82	8.0
WR5	-25.63	28.56	223.00	12.0	1	269.53	5.0
					2	266.23	21.0
					3	302.95	17.0
					4	328.01	9.0
					5	278.79	12.0
					6	268.89	9.5

SITE	SITE LOCATION		BEDDING ORIENTATION		CORE ORIENTATION		
#	LAT	LONG	STRIKE	DIP	#	AZIMUTH	HADE
WR6	-25.77	28.69	300.00	9.0	1	284.93	80.0
					2	286.66	7.0
					3	148.08	7.0
					4	243.16	8.0
					5	189.27	21.0
					6	189.67	15.0
WR7	-25.80	28.81	246.00	18.0	1	180.66	15.0
					2	157.47	40.0
					3	178.21	13.0
					4	159.49	16.0
					5	184.60	16.0
					6	180.26	20.0
WR8	-25.84	28.89	310.00	14.0	1	339.50	50.0
					2	330.70	50.0
					3	209.73	17.0
					4	16.56	34.0
					5	52.42	19.0
					6	67.16	18.0
WR9	-25.79	28.92	78.00	8.0	1	88.02	17.0
					2	153.08	6.0
					3	202.33	7.0
					4	171.09	14.0
					5	327.61	7.0
					6	14.38	10.0
WR10	-25.89	29.06	228.00	8.0	1	171.91	5.0
					2	333.74	37.0
					3	171.29	10.0
					4	240.80	12.0
					5	224.49	29.5
					6	337.15	33.5

SITE	SITE LOCATION		BEDDING ORIENTATION		CORE ORIENTATION		
#	LAT	LONG	STRIKE	DIP	#	AZIMUTH	HADE
WR11	-25.86	29.04	303.00	8.0	1	4.95	8.0
					2	34.79	9.0
					3	18.61	43.0
					4	336.42	47.0
					5	21.21	12.0
					6	333.16	17.0
					7	8.90	15.0
WR12	-25.68	29.11	282.00	5.0	1	340.05	17.0
					2	176.49	11.0
					3	355.84	26.0
					4	345.63	11.0
					5	214.46	6.0
					6	348.55	4.0
					7	83.06	10.0
WR13	-25.73	29.06	284.00	7.0	1	210.91	19.0
					2	47.65	4.0
					3	248.73	18.0
					4	118.52	12.0
					5	6.77	14.0
					6	172.64	19.0
WR14	-25.75	29.33	260.00	8.0	1	328.20	69.0
					2	333.20	73.0
					3	318.20	74.0
					4	321.20	71.0
					5	323.20	79.0
					6	299.20	45.0
WR15	-25.46	29.46	237.00	64.0	1	161.84	62.0
					2	80.49	60.0
					3	154.99	46.0
					4	164.89	48.0
					5	118.77	59.0
					6	139.77	63.5
					7	89.77	24.0
					8	98.02	55.0
					9	90.75	60.0

SITE	SITE LOCATION		BEDDING ORIENTATION		CORE ORIENTATION		
#	LAT	LONG	STRIKE	DIP	#	AZIMUTH	HADE
WR16	-25.47	29.46	72.00	18.0	1	90.42	67.0
					2	100.11	74.0
					3	117.24	74.0
					4	128.37	78.0
					5	100.95	70.0
					6	164.21	71.0
WR17	-25.54	29.48	129.00	6.0	1	252.42	53.0
					2	298.60	75.0
					3	292.46	73.0
					4	296.14	37.0
					5	64.69	6.0
					6	331.36	93.0
					7	295.15	71.0
WR18	-25.59	29.42	219.00	8.0	1	322.87	10.0
					2	357.28	13.0
					3	320.35	11.0
					4	171.96	7.0
					5	105.24	8.0
					6	131.87	7.0
WR19	-25.70	29.46	280.00	8.0	1	123.52	19.0
					2	161.08	29.0
					3	84.35	17.0
					4	71.93	15.0
					5	131.52	17.0
					6	108.90	18.5

Table A.3: Field data for the Mogalakwena Formation.

SITE	SITE LOCATION		BEDDING ORIENTATION		CORE ORIENTATION		
#	LAT	LONG	STRIKE	DIP	#	AZIMUTH	HADE
MK1	-23.91	27.93	96.00	5.0	1	20.51	45.0
					2	37.06	64.0
					3	83.57	34.0
					4	85.87	41.0
					5	29.25	27.0
					6	41.95	30.0
MK2	-23.88	27.91	99.00	5.0	1	72.15	59.0
					2	66.35	20.0
					3	53.92	36.0
					4	56.21	48.0
					5	56.13	68.0
					6	85.49	11.0
MK3	-23.82	27.87	97.00	5.0	1	62.72	38.0
					2	52.45	51.0
					3	51.25	27.5
					4	23.50	40.0
					5	52.32	39.0
					6	54.74	46.0
MK4	-23.77	27.80	89.00	5.0	1	262.48	51.0
					2	160.58	48.0
					3	248.30	41.5
					4	241.74	55.0
					5	237.00	41.0
					6	239.36	64.0
MK5	-23.80	27.84	82.00	6.0	1	212.85	40.0
					2	213.32	50.0
					3	219.06	45.0
					4	223.02	52.0
					5	227.97	53.0
					6	286.70	52.0

SITE	SITE LOCATION		BEDDING ORIENTATION		CORE ORIENTATION		
#	LAT	LONG	STRIKE	DIP	#	AZIMUTH	HADE
MK6	-23.80	27.85	90.00	6.0	1	254.98	45.0
					2	228.17	14.0
					3	268.17	29.0
					4	246.9	23.0
					5	208.04	30.0
					6	210.09	45.0

Table A.4: Field data for the diabase intrusion in the Nylstroom Protobasin.

SITE	SITE LOCATION		BEDDING ORIENTATION		CORE ORIENTATION		
#	LAT	LONG	STRIKE	DIP	#	AZIMUTH	HADE
SHD1	-24.75	28.35			1	83.85	38.0
					2	1.26	14.0
					3	70.03	15.0
					4	113.68	29.0
					5	44.45	8.0
					6	135.23	36.0
					7	75.00	18.0
SHD2	-24.67	28.32			1	256.10	11.5
					2	341.33	14.0
					3	305.82	18.5
					4	258.93	14.5
					5	268.43	16.5
					6	73.44	4.5
SHD3	-24.65	28.38			1	146.36	14.5
					2	321.82	11.0
					3	46.42	23.0
					4	118.73	8.5
					5	48.75	21.5
					6	116.65	15.0

SITE	SITE LOCATION		BEDDING ORIENTATION		CORE ORIENTATION		
#	LAT	LONG	STRIKE	DIP	#	AZIMUTH	HADE
SHD4	-24.69	28.40			1	77.92	9.0
					2	265.03	18.0
					3	307.11	8.5
					4	259.96	18.0
					5	1.82	29.5
					6	305.31	16.5
SHD5	-24.70	28.42			1	103.67	20.5
					2	96.14	16.0
					3	118.93	26.5
					4	18.37	12.5
					5	331.82	12.5
					6	122.61	21.5
SHD6	-24.73	28.37			1	71.68	20.5
					2	78.10	9.5
					3	100.52	7.5
					4	132.07	33.5
					5	160.73	19.5
					6	205.29	20.5

Table A.5: Field data for the trachytic lava in the Nylstroom Protobasin.

SITE	SITE LOCATION		BEDDING ORIENTATION		CORE ORIENTATION		
#	LAT	LONG	STRIKE	DIP	#	AZIMUTH	HADE
SHT1	-24.80	28.44			1	251.53	48.0
					2	269.03	50.0
					3	253.51	44.0
					4	174.13	18.0
					5	200.86	29.0
					6	296.56	54.0
					7	353.62	5.0
SHT2	-24.83	28.22			1	230.12	15.0
					2	271.52	25.0
					3	130.41	8.0
					4	172.24	25.0
					5	277.94	22.0
					6	324.27	18.0

Table A.6: Field data for the diabase intrusions in the Middelburg Basin.

SITE	SITE LOCATION		BEDDING ORIENTATION		CORE ORIENTATION		
#	LAT	LONG	STRIKE	DIP	#	AZIMUTH	HADE
WRD1	-25.49	29.46			1	191.18	11.0
					2	210.31	6.0
					3	231.41	2.0
					4	224.13	5.0
					5	71.85	12.0
					6	208.22	22.0
WRD2	-25.74	29.45			1	271.51	13.0
					2	164.53	16.0
					3	40.10	12.0
					4	27.93	22.0
					5	357.02	14.0
					6	247.40	11.0
WRD3	-25.59	28.58			1	133.14	13.0
					2	40.71	11.0
					3	355.27	20.0
					4	174.71	18.0
					5	146.71	20.0
					6	288.88	28.0
WRD4	-25.66	29.16			1	290.98	19.0
					2	338.09	15.0
					3	310.42	21.0
					4	52.58	17.0
					5	46.17	11.0
					6	143.45	9.0
WRD5	-25.88	29.03			1	7.42	14.0
					2	275.56	24.0
					3	309.68	12.0
					4	197.10	18.0
					5	321.92	23.0
					6	294.53	13.0

SITE	SITE LOCATION		BEDDING ORIENTATION		CORE ORIENTATION		
#	LAT	LONG	STRIKE	DIP	#	AZIMUTH	HADE
WRD6	-25.82	28.95			1	188.07	23.0
					2	248.52	13.0
					3	133.27	20.0
					4	212.76	13.0
					5	89.83	14.0
					6	196.89	11.0
WRD7	-25.71	28.71			1	84.57	11.0
					2	121.76	22.0
					3	123.68	27.0
					4	52.88	19.0
					5	154.79	15.0
					6	116.77	8.0
WRD8	-25.62	28.61			1	290.74	9.0
					2	248.08	13.0
					3	323.21	8.0
					4	357.14	17.0
					5	302.31	9.0
					6	61.78	12.0